ACOUSTIC BIOMICROSCOPY

an *in vitro* tool for development of ultrasonic tissue characterization

TON VAN DER STEEN

ACOUSTIC BIOMICROSCOPY

Akoestische biomicroscopie

Een *in vitro* hulpmiddel voor de ontwikkeling van weefselidentificatie met ultrageluid.

Een wetenschappelijke proeve op het gebied van de Medische Wetenschappen.

Proefschrift

ter verkrijging van de graad van doctor aan de Katholieke Universiteit Nijmegen, volgens besluit van het College van Decanen in het openbaar te verdedigen op vrijdag 4 februari 1994 des namiddags te 1.30 precies

door

Antonius Franciscus Wilhelmus van der Steen

geboren op 23 augustus 1964 te Vught

1993
drukkerij Benda BV, Nijmegen

Promotor: prof.dr. A. van Oosterom

Co-promotor: dr.ir. J.M. Thijssen

The work described in this thesis was financially supported by the Dutch Cancer Society (Chapter IV-IX), the Netherlands Technology Foundation (Chapter II) and Dornier Medizin Technik GmbH (Chapter III).

The financial support of the Dutch Cancer Society for the printing of this thesis is greatly acknowledged.

Voor ons vader en ons moeder

OVERIGE LEDEN PROMOTIECOMMISSIE

prof.dr. D.J. Ruiter	
prof.dr. B. Oeseburg	
prof.dr. A.F. Deutman	
prof.dr.ir. N. Bom	Erasmus Universiteit Rotterdam
prof.dr.ir. A.P.G. Hoeks	Rijks Universiteit Limburg
prof.dr. H. Ermert	Ruhr Universität Bochum, BRD

Cover illustration: flying foxes near Riung at the northern coast of Flores, Indonesia. Flying foxes are the biggest bats in the world. They can reach a maximum span of 1.65 m. Bats have got a sonar system that beats any commercial medical ultrasound apparatus. They are able to switch any moment from continuous wave doppler to pulse echo ultrasound and combine this information to navigate and to hunt for insects. The bats on the cover are vegetarian. For this reason they do not need such a sophisticated sonar system. Special about their navigation system is that they correlate their acoustical perception with their optical perception to decide where to go.

photography: Ton van der Steen, august 1993

CONTENTS

PREFACE

I must have been eight years old when I was introduced to the public library in Vught, my town of birth. After having read the entire "Wipneus en Pim" and "Pinkeltje" collection, I ran into a small booklet in which some simple domestic physical experiments were described. One of these was the following: Take an empty Dutch milk bottle, or any other bottle that has an inner neck diameter of approximately 4 cm and a contents of approximately 1 litre. Keep the bottle horizontal and put a French wine cork in the aperture of the neck. Keep the bottle in front of your mouth and try to blow the cork into the bottle The thing that will happen now is, that the cork will start moving, but it will not disappear into the bottle but into your face, and the more powerful you blow, the better your chances are for a black eye. It was by then that I discovered the weird character of physics.

I think I ran into my main source of inspiration when I was about fifteen years old. Dr. Pernot was my physics teacher at secondary school. I will never forget how he was lying on the floor in the middle of the class room with a rope in his hand, dirtying his pants and elbows, a blush on his cheeks from enthusiasm, trying to explain the difference between a propagating and a standing wave. I never met anyone who took greater pleasure in performing simple physical experiments than he did. Physics was fun. Inspired by this thought I decided to go and study applied physics at the Technical University in Delft

On the first day in Delft the students were divided into groups of ten, guided by a tutor. One of the first questions my tutor asked was: "Who chose to study physics, because he thinks physics is fun?" Being a freshman from the province, I did not dare raise my hand He warned us that if we came because physics was fun, we had better leave right away, because it was not. I must say it took me a few years over there to recover the charm of physics. It must have been when I studied the oscillation patterns of a carillon bell, using double exposure holography. I remember the moment when I showed the first hologram that had one line of an interference pattern on it to Ad van den Berg, my supervisor. The man stopped breathing and turned red in excitement. After thirty seconds I panicked, because I did not know if I had to kick his bottom or hit him on the back, but luckily he started breathing again, shouting out his excitement.

The man who convinced me to go into medical physics was dr. Rogier van Wijk van Brievingh. He gave a tremendous series of lectures on medical science at the department of Electrical Engineering of the Technical University of Delft. He took me on a study visit to the Experimental Echocardiography Laboratory of the Dijkzigt Hospital in Rotterdam, led by professor Nicolaas Bom. The unconventional way I was shown around there by dr. Charles Lancée made me decide to carry out the final project for my Master's degree, a choice I have never regretted. I think it was there that I learned what science is about

After a lecture I gave in Rotterdam for the Dutch Federation of Ultrasound in Medicine and Biology, dr. Johan Thijssen offered me a job at the Biophysics Laboratory of the department of Ophthalmology of the Academic Hospital Nijmegen. At this laboratory I discovered the extreme importance of communication within a multidisciplinary team. My efforts in Rotterdam and Nijmegen resulted in the thesis that now lies in front of you. I hope you will enjoy reading it, and maybe you are one of the people to even think it contains useful information.

CHAPTER I

INTRODUCTION

EARLY HISTORY

When studying the history of medical diagnostic ultrasound there is one aspect that becomes evident All developments in the field were preceded by technological developments One can say that there has always been a "technology push' The main breakthroughs were preceded by innovations in the war industry The idea of using sound as a carrier of information in medical diagnosis is quite old Auscultation of patients was a diagnostic tool long before anyone thought of medical ultrasound

One of the first inventions leading to diagnostic medical ultrasound was the discovery of the piezoelectric effect by Pierre & Jacques Curie (1880) They discovered that an electric charge is produced in response to the application of mechanical pressure on materials such as quartz and some ceramics Conversely in the same materials mechanical deformation results from an applied voltage The impact of sound waves on the crystal producing a mechanical deformation was transformed into electrical energy and could be recorded with appropriate devices Furthermore the mechanical deformation of a material could be controlled by electrical devices The ultrasound transducer was born By that time a mathematical basis had been given to the theory of sound propagation by Huygens (17th century) and Kirchhoff and Rayleigh (both 19th century) which brings us to the cradle of medical ultrasound

The first attempt to practical application was performed under supervision of Paul Langevin who tried to use high frequency ultrasound to detect submarines during World War I Unfortunately for him, the war was over before the product had been completed His work laid the foundation of SONAR detection, more completely developed during World War II

In between the wars there was a medical interest for ultrasound but this interest was purely therapeutic The "diagnostic" applications were found in industry, where flaws were detected in materials and constructions This flaw detection was based on transmission measurements and later on pulse echo measurements The latter methods were improved significantly by knowledge obtained from SONAR and radar technology during World War II

The first medical picture recorded in history was produced by Dr Karl T Dussik *et al* (1947) who imaged his own skull by means of a hyperphonogram a technique based on transmission The first application of a pulse-echo technique for biological purposes was reported by Ludwig & Struthers (1949) They found that gallstones in biological tissue gave sufficient reflections of ultrasonic energy to allow detection by ultrasonic instruments The first publication about tissue characterization was produced by Wild (1950) He measured the thickness of bowel tissue, in particular the stomach at a frequency of 15 MHz He found that the echo pattern, visualized on an oscilloscope in a normal stomach wall had changed when it was infiltrated by a carcinoma This change in echo pattern appeared before thickening of the tissue occurred

DEVELOPMENTS

Since then many developments have taken place The developments comprise various imaging techniques A-mode, in which the amplitude of the echo is displayed versus time after transmitting the ultrasound pulse (Wild & Reid 1952), which is still used in ophthalmology. M-mode, in which the peaks of a single scan line or a single scan line coded in grey level are displayed and followed in time (Edler & Hertz 1954), useful in echocardiography B-mode, in which the amplitude is coded in grey level and the sound beam is scanned in a plane, so it is possible to display a 2D image of a scanned object (Howry & Bliss 1952). C-mode, in which the amplitude at a fixed distance from the transducer is grey level encoded and the transducer performs a 2D raster scan which results in a 2D cross sectional image (McCready & Hill 1971). Furthermore, there is a recent leaning to 3D imaging.

Parallel to these developments the scanning methods underwent significant evolutions. First, there was only a single element transducer that was static. This could be sufficient for A-mode and M-mode, but for B-mode a more sophisticated technique is necessary. Solutions were found in the use of array transducers or moving single element transducers.

These array transducers can consist of a row of single element transducers that are activated subsequently (stepped linear array, introduced by Bom *et al.* (1971)), resulting in a linear scan, or activated almost simultaneously (phased array, introduced by Somer (1968)). The scanning of the latter is achieved electronically and results in a sector scan. The electronics of the phased arrays gave also possibilities to another array, the annular array. The annular array consists of a set of concentric rings that can be activated independently. By means of this technique it is possible to achieve a variable focus electronically, while using just one transducer. The scanning of this transducer is achieved mechanically and results in a sector scan too Multi focusing at transmission and dynamic focusing at reception are also commonly used in modern linear and phased array equipment.

The shape of the transducers was and is adapted to applications in many medical disciplines. Almost any part of the body can be imaged by an optimized transducer. Trade-offs between lateral resolution and practical use are made according to the size of the contact area. In addition to conventional extracorporeal transducers several types of endoscopic transducers were developed, like transrectal probes (Wild & Reid 1957), transesophageal transducers (Side & Gosling 1972), transvaginal and, more invasive, intravascular and intracoronary transducers (Bom *et al.* 1972)

Together with the development of the types and shapes of the transducers, new piezoelectric materials have been developed. Modern electronics, which are used for transmitter and receiver circuitry, as well as the digital electronics for image processing and documentation have greatly enhanced the image quality and performance of the equipment. These developments, together with improvements of digitization techniques and computer power gave way to a new field: ultrasonic tissue characterization based on spectral parameters.

TISSUE CHARACTERIZATION

During the last two decades several applications of ultrasonic tissue characterization based on spectral parameters were developed. Many parameters were introduced and pilot studies were performed on many organs. Often a multi parameter approach appeared to be necessary.

The parameters were based on attenuation (e.g. Kuc *et al.* 1979, Berger at al. 1987, Garra *et al.* 1987, Parker *et al.* 1988, Oosterveld *et al.* 1991, Romijn *et al.* 1991, Hartman *et al.* 1993) or backscattering (e.g Coleman *et al.* 1985, Lizzi *et al* 1988, Feleppa *et al.* 1986, Romijn *et al.* 1989ab, Thijssen *et al.* 1991, Oosterveld *et al.* 1993, Hartman *et al.* 1993), and sometimes they were based on the texture of conventional B-mode echograms (Nicholas *et al.* 1986, Garra *et al.* 1987, Romijn *et al* 1991, Hartman *et al.* 1993, Thijssen *et al.* 1993). The attenuation parameters can be obtained from the radio frequency (rf)-signals in several ways, all of them having their advantages and disadvantages. For all of these methods, first a correction should be applied for the space and frequency dependent characteristics of the field produced by the transducer (diffraction). The methods described here have been summarized by Oosterveld *et al.* (1991). The first is known as the Spectral Difference method (Kuc & Schwartz 1979): the corrected backscattering spectrum is acquired at various depths and then the Log power spectra are pairwise subtracted, resulting in an attenuation spectrum. A second method is the Multi Narrow Band method. The decay of each frequency component with depth is registered. Another method is known as the Central Frequency Shift method: the decrease of the central frequency of the backscattering spectra versus depth is calculated. A last in vivo applicable frequency domain method is called the Log Power Decay method The Log power spectrum is integrated over the bandwidth and the decay with depth of this power is calculated Apart from these frequency domain estimators also many time domain estimators are applicable. The time domain estimators yield a better resolution, but are much more sensitive to inhomogeneities in the tissue. The method that is mostly used in this thesis is called the substitution method: the spectrum of a rigid surface reflection is acquired with and without a sample of tissue interposed The quotient of these spectra yields the attenuation spectrum. This a very accurate method, but it is not applicable *in vivo*.

The backscattering spectrum is obtained after correcting the spectra for the frequency dependent properties of the equipment, diffraction and the attenuation in the tissue There is information about the size of the scatterers in the slope of the backscattering spectrum and about the reflectivity in the backscattering at the central frequency and the integrated backscatter (i.e. the integrated power of the corrected backscattering spectrum over the bandwidth of the used transducer)

The texture of the B-mode echograms gives information about the number density of scatterers, the distance between structural components, the ratio of structural and diffuse scattering and the reflectivity of the scatterers.

It is beyond the scope of this introduction to give a full survey of the applications of ultrasonic tissue identification around the world. Work that has been an inspiration for the studies in this thesis encompasses the work of the groups of J.G. Miller (cardiology, e.g Miller *et al* 1985, Wickline *et al* 1985), N Bom (cardiology, e.g. Lancée *et al* 1988, Rijsterborgh *et al* 1990), J M. Thijssen (liver, ophthalmology and general modelling, e.g Oosterveld *et al.* 1991, Romijn *et al* 1991), F.L. Lizzi (ophthalmology and liver, e.g. Coleman *et al.* 1985, Lizzi *et al.* 1988), J.C. Bamber (liver, e.g. Bamber & Hill 1981, Bamber *et al.* 1981), M.F. Insana (liver and general modelling, e.g. Insana *et al.* 1990) and F.S. Foster (ophthalmology and acoustic microscopy, e.g. Foster *et al.* 1984, D'Astous & Foster 1986). The scope of the work of the mentioned groups is to find correlations between acoustic parameters and pathology Most of this work suffers from a lack of firm knowledge about the contributions of the various physical interactions between ultrasound and biological tissues.

IN VITRO ULTRASOUND

For the improvement of tissue characterization different strategies are followed First of all the performance of equipment is still improved by enhancing the quality of the electronics, the transducers, digitization, etc

Another approach is to perform *in vivo* measurements and correlate the results to the results of pathological examinations The main merit of this approach is that the conditions are identical to the circumstances in clinical practice The problem with this approach is that these measurements suffer from a lot of distortions The field of the transducer changes with depth Due to this effect, which is called diffraction, the beam width varies with depth, as well as the pulse length and the spectral shape of the ultrasound pulse Another problem is the influence of the intervening tissue The ultrasound beam is attenuated by this tissue and, directly related to this, dispersion occurs The beam propagation is changed by refraction when it passes a transition between objects with different acoustic impedance When using array transducers, there is an additional problem the path from the various array elements to the object of interest is not identical, so the effect of velocity changes in the tissue on the echoes received by separate elements is not identical, causing phase abberation effects Furthermore, there is the problem of temporal changes in the echogeneity caused by phenomena such as heart beat and respiration

In principle it is possible to correct all the effects mentioned According to the number of papers appearing at conferences one can say that the quest for these corrections has become a field of interest as such Since no correction is perfect, it may be clear that for the modelling of phenomena it is better to perform measurements *in vitro* (i e in a laboratory setup) For most phenomena it can be stated if you cannot measure them *in vitro*, you will not find them *in vivo*

When measuring *in vitro* it is possible to locate the specimen exactly in the focus of the transducer so the effect of diffraction is minimal Intervening tissues are not present so they can have no disturbing effect on the measurements Another consequence of the absence of intervening tissue is the absence of attenuation As a consequence it is possible to investigate tissues at much higher frequencies, resulting in better resolutions, and thus more detailed information can be obtained

Furthermore, *in vitro*, many acoustic parameters, especially those related to attenuation and ultrasound velocity can be estimated with a much higher precision as compared to *in vivo*

As a last advantage it is possible to measure effects *in vitro* that are very hard to measure *in vivo*, but which disturb the *in vivo* measurements considerably

Unfortunately, there is a price to be paid for these advantages Conditions present *in vitro* are never the same as those existing *in vivo* After excision the blood circulation stops, the blood starts coagulating and rigor mortis starts Furthermore, the tissue suffers from autolysis, which changes the constituents of the tissue, and it causes gaseous inclusions, which are detrimental to ultrasonic tissue characterization The simplest solution to these problems is measuring immediately after excision Unfortunately, this is not always possible

In order to preserve the tissue over a longer period, fixation is necessary Numerous fixatives are known from pathology The choice of the fixative is often related to the kind of tissue and the intended staining afterwards Many of these fixatives have a disastrous effect on the acoustic properties of biological tissues

A major part of the work described in this thesis is concerned with correlations between local acoustic parameters and local histological composition of biological tissues. In order to be able to perform this study, it first was necessary to find tissue preparation techniques that are suited for both optical and acoustic microscopy. This encompassed not only the fixation of tissue, but also the sectioning techniques. Preparation techniques have been developed for light microcopy for centuries, but most of these techniques cause an essential damage to the tissue in an acoustic sense, and techniques which are optimal for acoustic microscopy produce sections that cannot be used for light microscopic examination.

ACOUSTIC MICROSCOPY

Acoustic microscopy is the general term which applies to high resolution, high frequency ultrasonic inspection techniques that produce images of features beneath the surface of a sample Most of the developments took place in application to non-destructive testing. Acoustic microscopy comprises three different methods ((Kessler 1989), Fig 1).

- Scanning laser acoustic microscope (SLAM, introduced by Korpel *et al.* (1970)).
- C-mode scanning acoustic microscope (C-SAM). This is the improved version of the earlier mentioned C-mode scanner.
- Scanning acoustic microcopy (SAM, introduced by Lemons & Quate (1974))

The scanning laser acoustic microscope (SLAM) is a transmission mode instrument that creates real time images of a sample throughout its entire thickness
A collimated plane wave of continuous wave (CW) ultrasound at frequencies from 10 up to 500 MHz is produced by a piezoelectric transducer located beneath the sample. When the ultrasound travels through the sample, the wave is affected by inhomogeneities in the material. A rapidly scanning laser beam is used as an ultrasound detector. It senses the infinitesimal displacements (rippling) at the surface, created by the ultrasound From the obtained information the ultrasound attenuation and the ultrasound velocity can be deducted.

The C-mode scanning acoustic microcopy (C-SAM) is primarily a reflection mode instrument. A focused spot of ultrasound is generated by an ultrasound transducer. The focusing is achieved by using an acoustic lens or a curved transducer. The transducer is mechanically scanned across a sample in a raster fashion to create an acoustic image. Because the frequencies used for the C-SAM are not too high (10 up to 100 MHz) there is still a penetration of the ultrasound of a few millimetres. The C-SAM is ideally suited for studying phenomena at a specific depth. The acoustic microscope that is used in the studies in the second part of this thesis is a custom-designed C-SAM. Digitizing techniques and software developed for this purpose enable creating images of several spectral acoustic parameters and the ultrasound velocity.

The scanning acoustic microcopy (SAM) has quite some similarities to the C-SAM. The main differences in design are the application of higher frequencies (100 MHz up to 4000 MHz) and the use of a very wide angle acoustic lens. Both contribute to the high lateral resolution and the limited penetration depth. The SAM is best suited for studying surface and direct subsurface effects. The acoustic microscope that is used in chapter VI is a SAM.

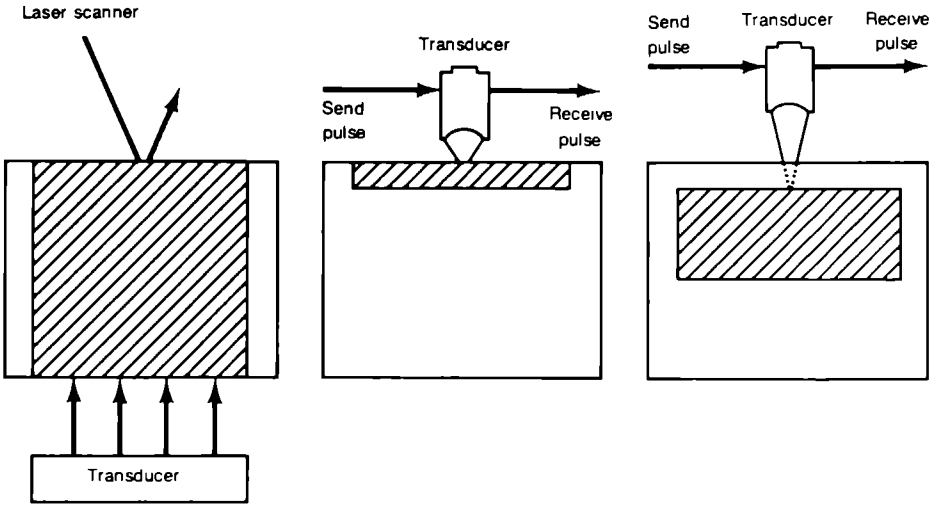

Fig 1 Simplified comparison of three acoustic microscopy techniques, particularly their zones of application (crosshatched area) within a sample
A SLAM
B SAM
C C-SAM

ON THIS THESIS

In this thesis a survey of the potentials of in vitro ultrasonography as an aid for *in vivo* tissue characterization has been studied.

Chapter II is concerned with tissue characterization of the myocardium. Ultrasonic integrated backscatter is measured in normal and early ischemic myocardium. This integrated backscatter varies during cardiac cycle. The variation is different in normal myocardium compared to ischemic myocardium. Other studies revealed that this variation is highly correlated to the variation in myocardial wall thickness. In this study the variation of ultrasonic attenuation and integrated backscatter from the myocardium with wall thickness is investigated.

Chapter III is about the characterization of gallstones. The success of extracorporeal shock wave lithotripsy or chemical dissolution is highly dependent on the chemical composition of the gallstone. The gallstones are divided into various classes based on this composition. These classes are characterized by means of *in vitro* ultrasound.

Chapter IV deals with tissue characterization of the eye lens. In this study the local acoustic parameters of the eye lens were investigated *in vitro*.

Chapter V describes the acoustic properties of the total eye. When a melanoma is diagnosed that is at the back of the eye, the ultrasound passes through various eye tissues before it reaches the melanoma. These tissues will disturb the ultrasound propagation. In order to perform a good quantitative characterization of the tumour, this disturbance should be corrected. For this reason an acoustic model of the eye is necessary In this study the acoustic properties of the various eye tissues are obtained.

Chapter VI and VII are about tissue preparation techniques. The last part of the thesis is concerned with the correlation of local acoustic properties and light microscopic features of biological tissues. Much effort is put in developing tissue processing techniques that are suited for both acoustic and light microscopy. This study is separated into a quantitative and a qualitative part. The influence of various tissue processing techniques on the image quality of acoustic microscopy is investigated by means of a Leitz scanning acoustic microscope, operating at 1.2 GHz (Chapter VI). The influence on the natural acoustic properties of biological tissues is investigated quantitatively at 5 MHz (Chapter VII).

Chapter VIII describes a method to correlate the local spectral acoustic properties of biological tissues to the local histological features. In this chapter the acoustic parameters are described, as well as the signal processing methods used for obtaining them A light microscopic segmentation technique is proposed, as well as a statistical technique to correlate the acoustic parameters to the histological features. This technique also provides a correction for the influence of a histological feature to the correlation of an acoustic parameter to another histological feature.

Chapter IX is concerned with the correlation of local histological features to the acoustic parameters of liver tissue. The method described in chapter VIII is applied to healthy White New Zealander rabbit liver. The correlation is investigated between collagen content, nuclei density, luminal density, and interstitial spaces on the one hand and ultrasound velocity, frequency dependency of attenuation, attenuation at 30 MHz, frequency dependency of backscattering and backscattering at 30 MHz on the other hand

Chapter X gives a summary and an indication of the scientific and clinical value of the work presented in this thesis.

WORKS OF REFERENCE

D'Astous F.T., Foster F S (1986) Frequency dependence of ultrasound attenuation and backscatter in breast tissue. Ultrasound in Med. & Biol. 12: 795-808

Bamber J C., Hill C.R. (1981) Acoustic properties of normal and cancerous human liver. I. Dependence on pathological condition. Ultrasound in Med. & Biol 7: 122-133

Bamber J.C., Hill C.R., King J.A. (1981) Acoustic properties of normal and cancerous human liver. II. Dependence on tissue structure. Ultrasound in Med. & Biol. 7. 135-144

Berger G., Laugier P., Fink M., Perrin J. (1987) Optimal precision in ultrasound attenuation estimation and application to yhe detection of Duchenne's muscular dystrophy carriers. Ultrasonic Imag. 9: 1-17

Bom N , Lancée C.T., Honkoop J., Hugenholtz P.G. (1971) Ultrasonic viewer for cross-sectional analysis of moving cardiac structures. Biomed. Eng. 6: 500-503 and 508

Bom N., Lancée C.T., van Egmond F.C. (1972) An ultrasonic intracardiac scanner. Ultrasonics 10: 72-76

Coleman D.J., Lizzi F.L., Silverman R.H. *et al.* (1985) A model for acoustic characterization of intraocular tumours. Invest. Ophthalmol. Vis. Sci. 26: 545-550

Curie J., Curie P. (1880) Sur l'electricité polaire dans les cristaus hémièdres à facer inclinées. Compt. Rend. Séances Acad. Sci. 91: 383-389

Dussik K.T., Dussik F., Wyt L. (1947) Auf dem wege zum Hyperphonographie des Gehirnes. Wien. Med. Woch. 38/39:425

Edler I., Hertz C.H. (1954) The use of the ultrasonic reflectoscope for the continuous recording of the movements of heart walls. K. Fysiogr. Sallst. Lund Forh 24: 1-19

Feleppa E.J., Lizzi F.L., Coleman D.J., Yaremko M.M. (1986) Diagnostic spectrum analysis in ophthalmology: a physical perspective. Ultrasound in Med. & Biol. 12: 623-631

Foster F.S., Strban M., Austin G. (1984) The ultrasonic macroscope:initial studies of breast tissue. Ultrasonic Imag. 6: 243-261

Garra B.S., Insana M.F., Shawker T.H., Russell M.A. (1987) Quantitative estimation of attenuation and echogenicity: normal state versus diffuse liver disease. Radiology 162: 61-67

Hartman P.C., Oosterveld B.J., Thijssen J.M., Rosenbusch G.J.E., van den Berg, J. (1993) Detection and discrimation of diffuse liver disease by quantitative echography - A retrospective assesment. Invest. Radiol. 28: 1-6

Howry D.H., Bliss W.R. (1952) Ultrasonic visualization of soft tissue structures of the body. J. Lab. Clin. Med. 40: 579

Insana M.F., Wagner R.F., Brown D.G., Hall T.J. (1990) Describing small-scale structure in random media using pulse-echo ultrasound. J. Acoust. Soc. Am. 87: 179-192

Kessler L W (1989) Acoustic Microscopy. Metals handbook Vol. 17 9th edition: Nondestructive evaluation and quality control: 465-482

Korpel A., Kessler L.W., Palermo P.R. (1970) Acoustic Microscope operating at 100 MHz. Nature 232: 110-111

Kuc R., Schwartz M. (1979) Estimating the acoustic attenuation coefficient slope for liver from reflected ultrasound signals. IEEE Trans. Sonics Ultrason. SU-26: 353-362

Lancée C.T., Mastik F., Rijsterborgh H., Bom N. (1988) Myocardial backscatter analysis in animal experiment. Ultrasonics 26: 155-163

Lemons R.A., Quate C.F. (1974) Acoustic microscope, scanning version. Appl. Phys. Lett.: 24: 163- 165

Lizzi F.L., King D.L., Rorke M.C. (1988) Comparison of theoretical scattering results and ultrasonic data from clinical liver examinations. Ultrasound in Med. & Biol. 14: 377-385

Ludwig G.D., Struthers F.W. (1949) Considerations underlying the use of ultrasound to detect gallstones and foreign bodies in tissues. Naval Med. Res. Inst. Reports. Project #004 001 Report No. 4

McCready V.R., Hill C.R. (1971) A constant depth ultrasonic scanner. Brit. J. Radiol. 44: 747

Miller J.G., Pérez J.E., Sobel B.E. (1985) Ultrasonic characterization of myocardium. Prog. Cardiovasc. Dis. 28: 85-110

Nicholas D., Nassiri D.K., Garbutt P., Hill C.R. (1986) Tissue characterization from ultrasound B-scan data. Ultrasound in Med. & Biol. 12: 135-143

Oosterveld B.J., Thijssen J.M., Hartman P.C., Romijn R.L., Rosenbusch G.J.E. (1991) Ultrasound attenuation and B-mode texture analysis of diffuse liver disease: methods and preliminary results. Physics in Med. & Biol. 36: 1039-1064

Oosterveld B.J., Thijssen J.M., Hartman P.C., Rosenbusch G.J E. (1993) Detection of diffuse liver disease by quantitative echography: dependence on a prior choice of parameters. Ultrasound in Med. & Biol. 19: 21-26

Parker K.J., Asztely M.S., Lerner R.M., Schenk E.A., Waag R.C. (1988) In-vivo measurements of ultrasound attenuation in normal or diseased liver Ultrasound in Med. & Biol 14: 127-136

Romijn R L., Thijssen J.M., van Delft J L., De Wolf-Rouendaal D., van Best J , Oosterhuis J.A. (1989a) In vivo ultrasound backscattering estimation for tumor diagnosis: An animal study Ultrasound in Med. & Biol. 15: 471-479

Romijn R.L., Thijssen J.M., van Beuningen G.W.J. (1989b) Estimation of scatter size from backscattered ultrasound. a simulation study. IEEE Trans. Ultrasonics Ferroel. Freq. Control 36: 593-606

Romijn R L, Thijssen J M , Oosterveld, B.J., Verbeek A.M. (1991) Ultrasonic differentiation of intraocular melanomas: parameters and estimation methods Ultrasonic Imag. 13 27-55

Rijsterborgh H , Mastik F., Lancée C T., van der Steen A.F.W, Sassen L.M.A., Verdouw P.D., Roelandt J , Bom N. (1990) Ultrasonic myocardial integrated backscatter and Myocardial wall thickness in animal experiments. Ultrasound in Med. & Biol. 16: 29-36

Side C.G., Gosling R.G. (1971) Non surgical assessment of cardiac function. Nature 232: 335

Somer J.C. (1968) Electronic sector scanning for ultrasonic diagnosis. Ultrasonics 6: 153-150

Thijssen J.M., Oosterveld B.J., Hartman P.C., Rosenbusch G.J.E. (1993) Correlations between acoustic and texture parameters from rf and B-mode liver echograms. Ultrasound in Med. & Biol. 19: 13-20

Wickline S.A., Thomas III L.J., Miller J.G., Sobel B.E , Pérez J.E. (1985) The dependence of myocardial ultrasonic integrated backscatter contractile performance. Circulation 72: 183-192

Wild J J. (1950) The use of ultrasonic pulses for the measurement of biologic tissues and the detection of tissue density changes. Surgery 27: 183

Wild J.J., Reid J.M. (1952) Application of echo ranging techniques to the determination of structures of biological tissues. Science 115: 226

Wild J.J., Reid J.M. (1957) Progress in techniques of soft tissue examination, In: Ultrasound in Biology & Medicine: 30-48 (E. Kelly ed.) AIBS, Washington

CHAPTER II

THE INFLUENCE OF ATTENUATION ON MEASUREMENTS OF ULTRASONIC MYOCARDIAL INTEGRATED BACKSCATTER DURING CARDIAC CYCLE (AN *IN VITRO* STUDY)

A.F.W. van der Steen, H. Rijsterborgh, F. Mastik, C.T. Lancée,
W.M. van Hoorn, N. Bom

ABSTRACT

The purpose of this study was to investigate the dependence of ultrasonic integrated backscatter (IB) and attenuation in myocardium on wall thickness in a state of acute ischemia. Therefore an in vitro experiment was set up in which attenuation, IB and wall thickness of a piece of freshly excised myocardium could be measured almost simultaneously. The myocardium was taken from 11 Yorkshire pigs (25-30 kg) that were sacrificed less then 45 minutes before the experiment. The myocardium was placed in the far field of an ultrasound transducer (3.2-7.2 MHz) and then compressed by a stainless steel sphere. Data were processed off-line.
Backscattering and attenuation were also measured as a function of frequency at 100 % and 75 % wall thickness.
Both attenuation and IB varied during compression. Attenuation had an initial value of 2.19 ± 0.76 dB/cm and a slope of 0.015 ± 0.017 dB/cm% wall thickness. IB had an initial value of -76.9 ± 2.7 dB and a slope of -0.12 ± 0.07 dB/% wall thickness. After subtracting the influence of the attenuation from the IB the initial value of IB was -74.0 ± 2.7 dB and the slope -0.08 ± 0.07 dB/% wall thickness. Attenuation appeared to have a linear dependency on frequency. Backscattering appeared not to increase with increasing frequency without correction of the spectrum for the frequency dependent insonified volume.

INTRODUCTION

Integrated backscatter is a relative measure of the ultrasonic energy backscattered by a small volume of tissue. Integrated backscatter provides a potentially useful index for quantitative ultrasonic characterization of myocardial tissue. It has been shown that integrated backscatter increases as myocardium enters a state of acute ischemia due to an occlusion of a coronary artery (Miller *et al.* 1985, O'Donnell *et al.* 1979, Glueck *et al.* 1985).

It also has been shown that integrated backscatter varies during cardiac cycle (Mottley *et al.* 1984, Wickline *et al.* 1985a, Wickline *et al.* 1985b). This variation in integrated backscatter appeared to differ in ischemic myocardium from normal myocardium. This was a great step

ahead since using the variation in integrated backscatter had the great advantage that the patient can be used as his own reference.

Since the variation in myocardial wall thickness also varies during cardiac cycle, Rijsterborgh investigated the relationship between ultrasonic backscattering and wall thickness (Rijsterborgh *et al* 1990). A significant inverse relationship between myocardial wall thickness and ultrasonic integrated backscatter was found. The relationship was independent of the state of the heart.

In all studies the influence of attenuation has been neglected (Lancée *et al.* 1988, Madaras *et al.* 1988). Variations in measurements of integrated backscatter were assumed to be caused by variations in the backscattering properties of the tissue. In this study the influence of the attenuation on measurements of integrated backscatter is investigated. Therefore an *in vitro* experiment has been set up in which the integrated backscatter and the attenuation could be measured simultaneously at various wall thicknesses. From this it was possible to calculate at what rate attenuation caused variation in measurements of integrated backscatter. Since the measurements were obtained in the far field of the ultrasonic transducer it was also possible to investigate the frequency dependent properties of the myocardium.

METHODS

INSTRUMENTAL SETUP

The instrumental setup which was used in this study is shown in fig. 1 All the experiments were controlled by an IBM computer system (AT-3) which was described extensively elsewhere (Lancée *et al.* 1988).

A transducer block was mounted in a watertank filled with a physiological saline solution (fig 2) The transducerblock contains a broadband "non focused" ultrasonic transducer (Krautkramer-Branson, Lewiston, PA, USA, centre frequency 5.2 MHz, -20 dB-bandwidth 4 MHz, effective diameter 5 mm) In front of the transducer is an interface to ensure that the measurements are all obtained in the far field of the transducer. It consists of a perspex block with a conic cavity in it The cavity is filled with physiological saline solution. The cavity is bounded by a stiff stretched fasson membrane (thickness 25 μm) at a distance of 3 cm of the transducer, which is nearly transparent for ultrasound at the used frequencies The interface is constructed in such a way that no reflections that are caused by the interface are present in the region of interest during the measurements. A stainless steel sphere with a diameter of 30 mm is placed at the centerline of the ultrasonic field. The sphere had a dual function. It is able to compress ischemic myocardium and it behaves like a perfect reflector.

The sphere was moved along the transducer axis by a stepmotor which was interfaced with the computer. The computer controlled the size of the steps (an integer times a unit step of 10 μm) and recorded the position of the sphere.

The ultrasound transducer was connected to an inhouse developed transmitter/wide band amplifier (input impedance 100 ohm, switchable gains 29 dB and -11 dB, -6 dB cut-off frequencies 1.2 and 10 MHz) which was externally triggered with a repetition frequency of 1 kHz. The amplified ultrasound signal was filtered by a 5th order 10 MHz low-pass Chebyshev filter and connected to a digital oscilloscope (Lecroy 9400A), which was interfaced to the computer

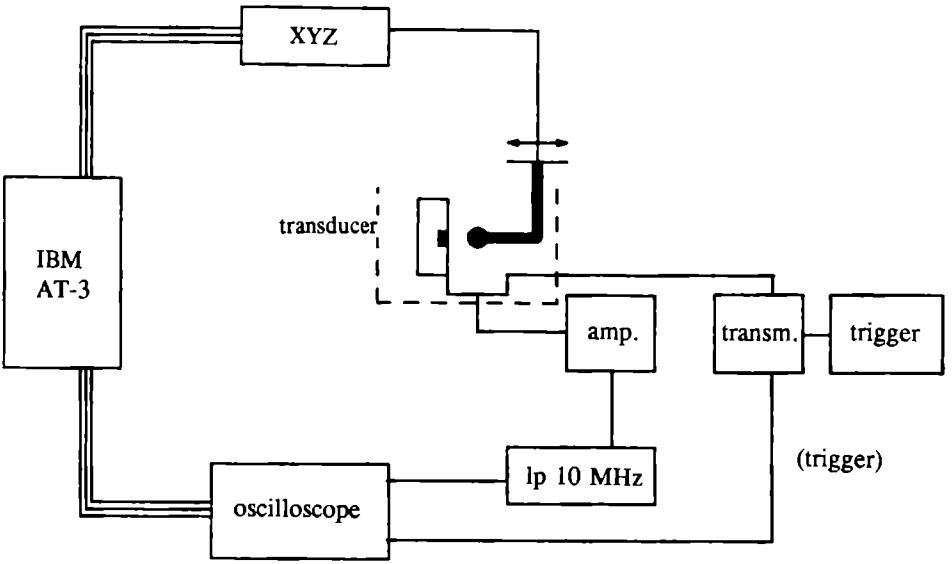

Fig 1 The instrumental set up that is used to measure ultrasonic backscatter and attenuation from myocardium at various wall thicknesses in vitro

EXPERIMENTAL PROTOCOL

First the watertank setup was aligned in such a way that the sphere was at the centre of the ultrasound beam and that movements were made along the axis of the beam. Then the transducer block was moved from the watertank.

Subsequently a piece of fresh left ventricular myocardium was attached to the transducer block. The myocardium was obtained from 25-30 kg Yorkshire pigs, sacrificed less than 45 minutes before the experiment. The heart is excised and put in a physiological saline solution. Then a myocardial area of approximately 7 x 7 cm. was prepared for examination. The myocardium was prepared in such a way that no papillary muscle was insonified by the transducer during the experiment. The myocardium was attached to the transducer block with the epicardium against the membrane. The transducer block was then put back in the watertank without loss of the alignment. Then the sphere was positioned against the endocardium as is shown in fig. 2. This is the initial position of the experiment. All experiments were performed at room temperature (20 $\pm$ 2 °C).

From the initial position the sphere was moved in 50 steps towards the transducer block thus compressing the myocardium. Since the block was rigid the distance between the block and the sphere was equal to the instantaneous wall thickness. The number of steps was fixed, the size of the steps was freely adjustable. The size of the steps was chosen so that a natural

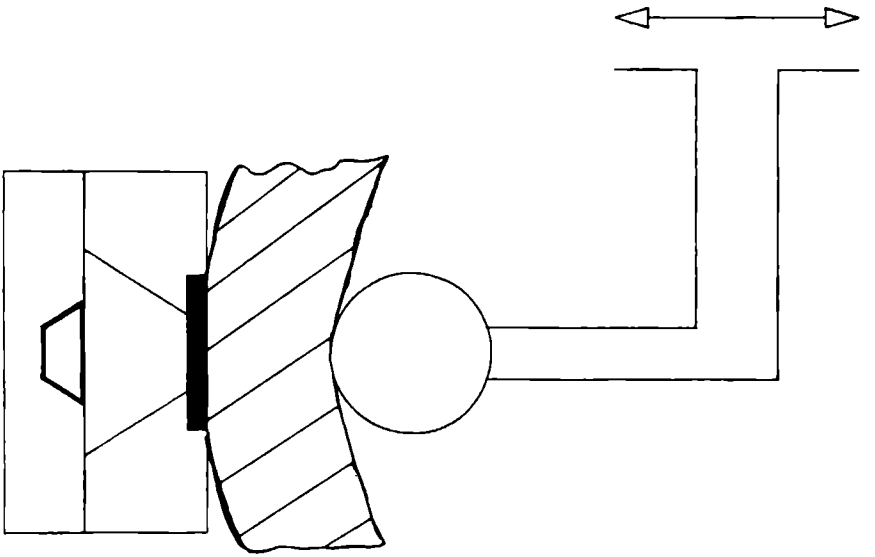

Fig 2 The watertank set up The set up is mounted in a physiological saline solution A piece of freshly excised myocardium is attached to a transducerblock The transducerblock contains a broadband transducer In front of the transducer there is a perspex interface with a conic shaped cavity in it filled with a physiological saline solution The conic cavity is bounded by a stiff stretched fasson membrane at a distance of 3 cm from the transducer At the center of the ultrasound beam there is a stainless steel sphere which is positioned against the myocardium It can move along the axis of the ultrasound beam thus compressing the myocardium

thickness range of the heartwall in ischemic state was achieved during the experiment (i e 100 % to approximately 60 % wall thickness) The experiments consisted of three stages
I The sphere moves towards the myocardium but the myocardium is not squeezed yet Both the attenuation and the backscattering are constant in this stage
II The sphere squeezes the myocardium The attenuation decreases and the backscattering increases
III The pressure on the membrane get that high that it starts to move The measured effects are a combination of compression and translation of the myocardium
Since in stage I and III no objective measure for the wall thickness is defined, only the data from stage II are used for data processing During stage II the translation of the membrane was less than 0 1 mm The boundary between stage I and II is taken as 100 % wall thickness

At each position of the sphere a backscattering measurement or a measurement of the sphere reflection was performed

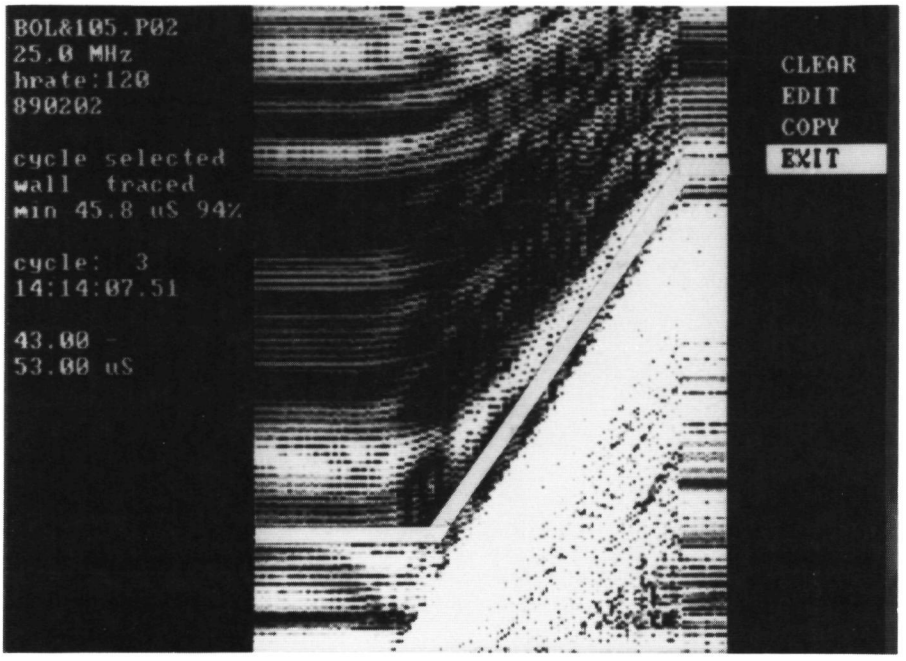

Fig. 3. An M-Mode that is constructed from the obtained data. In vertical direction the delay time after the ultrasound pulse is displayed, in horizontal direction the position of the sphere is displayed. As can be seen there is no compression of the myocardium at the first sphere positions. Then the myocardium gets only compressed during some positions and then the myocardium gets compressed and translated because the membrane starts to bend. The transition between the second and the third phase can not clearly be seen. The white line indicates the upper boundary of the window which is used to calculate the integrated backscatter. The saturation of the amplifier in the right lower corner of the image is caused by the reflection of the stainless steel sphere. The horizontal stripes at the right side of the M-Mode are artificial. This region is not used for further data processing.

DATA ACQUISITION

First a measurement cycle was recorded with -11 dB gain. Ultrasound signals from a time interval containing the sphere echo (app. 54 μs - 64 μs following the transmitter pulse) were digitized with 8-bit resolution at a sample frequency of 25 MHz. The digitized rf-data was temporarily stored in the extended RAM of the computer. This was done for the 50 positions of the sphere yielding the sphere echo strength as a function of wall thickness. The amplifier was switched to +29 dB gain for a second measurement cycle. The ultrasound signals from the myocardial tissue at a time interval app. 43 μs - 53 μs following the transmitter pulse were digitized. This data was also stored. This process was repeated for the same 50 positions of

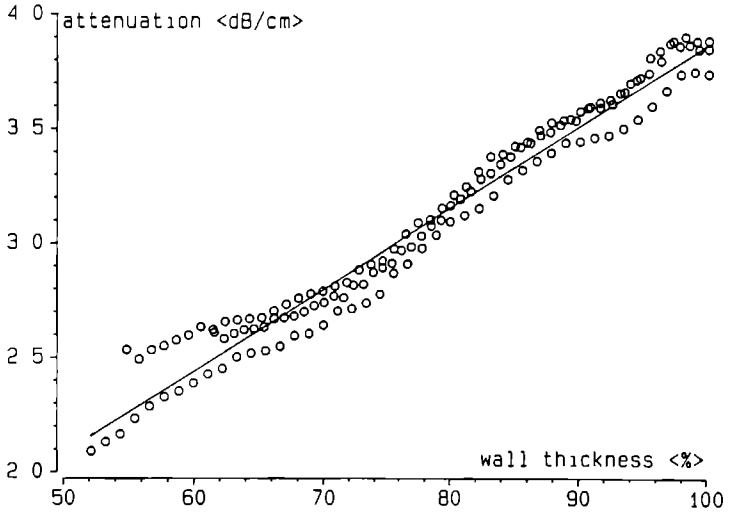

Fig 4 Attenuation as a function of percentage myocardial wall thickness Three experiments that are performed within 30 minutes on the same piece of myocardium are displayed

the sphere as in the previous cycle. The result is the backscattering from the region of interest as a function of wall thickness.

For both the sphere echo and the backscattering 5 measurement cycles were recorded with the myocardium at the same position and then stored on the computer harddisk. The whole procedure took about 10 minutes. The complete procedure was repeated another 2 times with increasing range of compression (up till 100 % to approximately 50 % wall thickness), but again with the myocardium at the same position.

Afterwards the myocardium was removed and sphere echo measurements are repeated as reference These measurements were necessary to calculate the attenuation of the myocardium.

Data processing

General

The data were processed off-line The 50 rf-lines required at the 50 positions of the sphere were put side by side in a greyscale image, thus obtaining an M-Mode (fig. 3). From these M-Modes ultrasound spectra were calculated by a Fourier transformation using the array processor (Data Translation 7020) of the computer system. A split cosine bell window (p=0.1; (Bloomfield 1976)) was chosen to diminish leakage of energy across frequency components. The length of the window in case of the sphere echo M-Mode was chosen 3 μs with the sphere echo right in the centre of the window The length of the window was chosen relative in such a way that during the experiment the window moved along with the sphere. The gatelenght at different compressions is equal to the gatelenght at 100 % wall thickness times the percentage compression

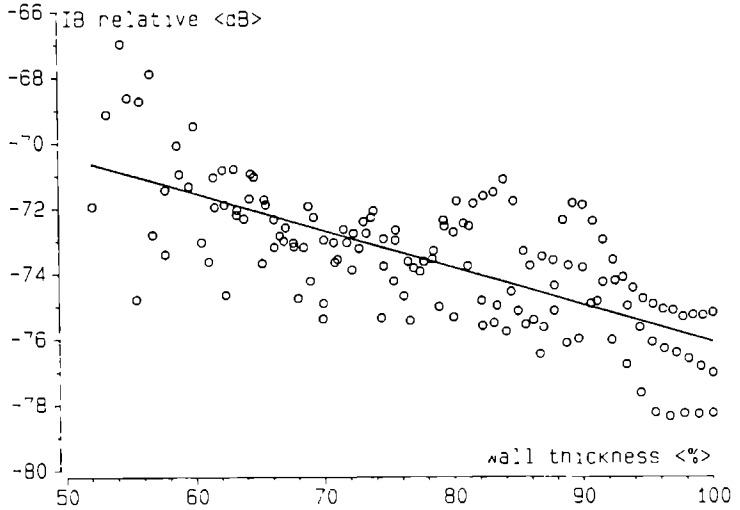

Fig 5 Integrated backscatter as a function of percentage myocardial wall thickness. Three experiments that are performed within 30 minutes on the same piece of myocardium are displayed

In this way IB was calculated from the same region of the myocardium all over the measurement cycle. For each sphere position the following spectra were achieved:
1 averaged backscattering power spectrum K(f) [dB]
2 averaged sphere echo power spectrum through myocardium L'(f) [dB]
3 averaged sphere echo power spectrum through physiological saline solution L"(f) [dB]

From these spectra the following parameters were calculated.
(the exact derivations of these parameters are given in Appendix A)

ATTENUATION

The attenuation α was calculated from the sphere echoes with and without the tissue interposed and the instantaneous wall thickness. Fig 4. gives an example of the attenuation versus percent wall thickness during stage II for 3 experiments performed on the same piece of myocardium within 30 minutes. As can be seen there is a linear dependency on wall thickness and there is no noticeable decay of the myocardium during the experiments. The dependence of the attenuation on percent wall thickness was determined by simple linear regression. The attenuation was characterized by its value at 100 % wall thickness and the slope of the dependency on percent wall thickness.
The power of the sphere reflection with and without the tissue interposed P^+ and P have been calculated for precisely the same sphere positions. The propagation velocity of ultrasound of about 5 MHz in myocardium is 3.5 % higher than the propagation velocity in the saline solution.

As a result of this P^+ and P were not calculated exactly at the same place in the field of the transducer. Because P varies very little with the sphere position the influence of this artefact has been neglected.

ATTENUATION TRANSFER FUNCTION

The attenuation transfer function $A_{trans}(f)$ describes the frequency dependency of the attenuation and was calculated from the spectra of the reflection with and without the tissue interposed and the instantaneous wall thickness. The attenuation transfer function was calculated for 100 % and 75 % wall thickness.

BACKSCATTERING TRANSFER FUNCTION

The backscattering transfer function $B_{trans}(f)$ describes the frequency dependency of the backscattering and was calculated from the averaged backscattering power spectrum K(f) and the transfer function of the measurement system M(f). M(f) was obtained by measuring the echo of a stainless steel plate at a distance corresponding to 44 μs. $B_{trans}(f)$ was normalized to the window size. The backscattering transfer function was calculated at 100 % and 75 % wall thickness.

INTEGRATED BACKSCATTER

The integrated backscatter (IB) was calculated as the bandwidth average of the backscattering transfer function. Fig. 5. displays an example of IB versus percent wall thickness during stage II for 3 experiments performed on the same piece of myocardium within 30 minutes. The dependence of IB on percent wall thickness was determined by simple linear regression. IB was characterized by its value at 100 % wall thickness and the slope of the dependency on percent wall thickness.

ATTENUATION CORRECTED BACKSCATTERING TRANSFER FUNCTION

The backscattering transfer function was corrected for the attenuation The attenuation corrected backscattering transfer function was calculated at 100 % and 75 % wall thickness.

ATTENUATION CORRECTED INTEGRATED BACKSCATTER

Integrated backscatter has been corrected for attenuation. The dependence of IB_{cor} on percent wall thickness was determined by simple linear regression. IB_{cor} was characterized by its value at 100 % wall thickness and the slope of the dependency on percent wall thickness.

Experiments were selected which could be used for further processing. The selection criteria were:

- The tissue should be less than 45 minutes old at the start of the experiment.
- The tissue should have an initial wall thickness of at least 11 mm.
- It should be possible to define a time window of at least 2.7 μs.

15 pigs hearts were subject of the experiments and 11 pig experiments met these criteria. Each of the pig hearts was the subject of 3 procedures, resulting in 33 experiments. From these experiments the average, standard deviation, interpig variation and intrapig variation of values at 100 % wall thickness and the slope of the plot as a function of wall thickness of integrated backscatter, attenuation and corrected integrated backscatter have been calculated.

RESULTS

The mean values and standard deviations of the attenuation measurements are presented in table I. The frequency dependent attenuation at 100 % and 75 % wall thickness are depicted in figs. 6 a and b. The backscattering transfer function and the corrected backscattering transfer function are presented in figs. 6 c,d,e and f respectively. The mean values and standard deviations of the integrated backscatter measurements, corrected for attenuation are also given in table I.

DISCUSSION

In this study the wall thickness dependency of integrated backscatter and attenuation is investigated. Further the frequency dependency of backscattering and attenuation in myocardium is investigated. It was found that integrated backscatter increases when the excised myocardial wall is compressed This was also found by other investigators (Rijsterborgh *et al.* 1990, Mottley *et al.* 1984, Wickline *et al.* 1985a, Wickline *et al.* 1985b). These investigators did *in vivo* studies on the variation of integrated backscatter during cardiac cycle. Since their measurements were acquired in the near field of the transducer it was not possible for them to obtain ultrasonic integrated backscatter with a moving window like in this study. Nevertheless they found the same tendency with a fixed window

In the present study it was found that the attenuation decreases when the myocardium is compressed *in vitro*. Attenuation is caused by absorption and omnidirectional scattering (Morse and Ingard 1968). Since backscattering varies during cardiac cycle it is not surprising that attenuation varies too. But, since backscattering increases when the myocardium is compressed, attenuation should increase too, from this point of view. Another possible explanation is found in the fact that the attenuation in liquids varies as a function of pressure. For water at 30 °C an increase in pressure of 100 mmHg, which is a reasonable estimate of the pressure variation during cardiac cycle *in vivo*, causes a decrease in attenuation of about 3.5 % (Matheson 1971) This is not enough to cover for the measured variation in attenuation in this study (about 30%) So the attenuation in the solid components of the myocardial fibers must decrease when the fibers are put under pressure.

In previous studies that investigated the integrated backscatter as a function of cardiac cycle, the influence of the variation of attenuation on measurements of integrated backscatter is neglected (Madaras *et al.* 1988, Lancée *et al* 1988).

From this study it can be concluded that measuring variation in integrated backscatter is measuring a summation of two effects:

1 change in backscattering from the region of interest.

2 change in attenuation caused by the myocardium between the scatterers and the transducer.

The change in attenuation intensifies the variation in integrated backscatter. The absolute change in attenuation is such that it theoretically could be used as a tissue identification parameter itself. If we use the figures from table I and we take the variation in wall thickness during cardiac cycle from 0.7 cm to 1.4 cm, we find a variation in attenuation of the total myocardial wall (visa versa) during cardiac cycle of 4.2 dB. If we should measure the backscattering from intra ventricular blood during the cardiac cycle, this variation should occur

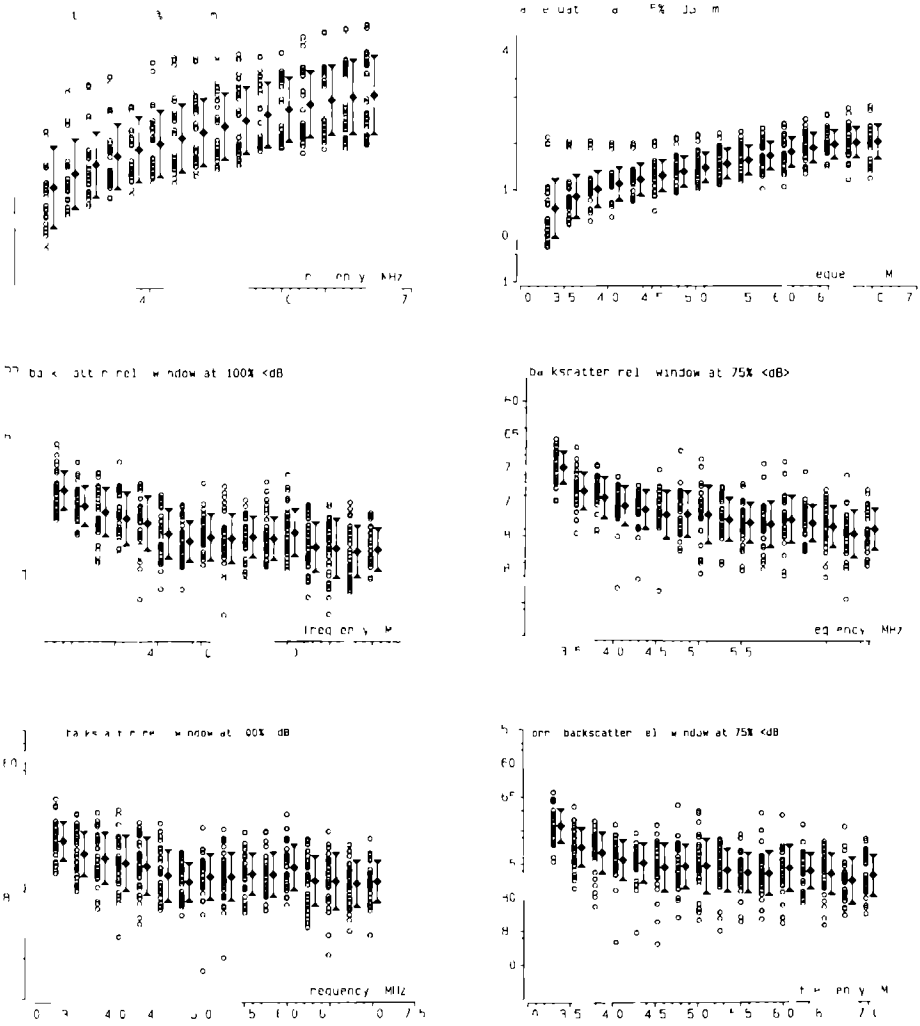

Fig 6 The ultrasound parameters of excised myocardial tissue as a function of frequency at 100 % wall thickness and 75 % wall thickness The mean values and standard deviations are shown as diamonds and bars respectively The open circles represent the individual measurements

A attenuation at 100 % wall thickness
B attenuation at 75 % wall thickness
C backscatter at 100 % wall thickness
D backscatter at 75 % wall thickness
E attenuation corrected backscatter at 100 % wall thickness
F attenuation corrected backscatter at 75 % wall thickness

Table I *The average values, standard deviations, interpig variations and intrapig variations of attenuation, integrated backscatter and corrected integrated backscatter. Depicted values are values at 100 % wall thickness and the slope of the dependency on wall thickness*

	μ	SD	SD_{inter}	SD_{intra}
α slope <dB/cm%>	0 015	0.017	0.017	0.004
α 100 % <dB/cm>	2 19	0.76	0 78	0.12
IB slope <dB/%>	-0 12	0.07	0.06	0 05
IB 100 % <dB>	-76 9	2.7	2 3	1 9
IB_{cor} slope <dB/%>	-0 08	0 07	0.06	0.05
IB_{cor} 100 % <dB>	-74 0	2.7	2.3	1 8

myocard
(n=33, N=11)

It should be mentioned here that all the measurements were performed *in vitro* at room temperature and the compression of ischemic myocardium during systole is modelled by the compression of a piece of myocardium with a stainless steel sphere. It is not clear how these experiments correspond to *in vivo* measurements. It is however clear that there is a contribution of change in attenuation to the change of integrated backscatter with wall thickness.

The myocardial attenuation is linearly dependent on frequency. From this it can be concluded that the major cause for the attenuation *in vitro* is absorption and not omnidirectional scattering (Morse & Ingard 1968) This is also found by other investigators (Lyons *et al.* 1986).

The myocardial backscattering that is measured is even after correction for attenuation independent of frequency. This could be caused by the fact that the spectrum was not corrected for the frequency dependent insonified volume of scatterers. After correction of the spectrum for the frequency dependent insonified volume there would appear a positive frequency dependency of the measured backscattering.

CONCLUSIONS

When left ventricular myocardium is compressed *in vitro* the ultrasonic integrated backscatter increases and the ultrasonic attenuation decreases. The measurements of integrated backscatter are measurements of two phenomena i.e. backscattering and attenuation. The magnitude of the attenuation changes are such that it may prove to have potential as a parameter for tissue identification Attenuation appeared to have a linear dependency on frequency. However

backscattering appeared not to increase with frequency without correction of the spectrum for the frequency dependent insonified volume.

WORKS OF REFERENCE

Bloomfield P. (1976) Fourier analysis of time series: an introduction. New York: John Wiley: 80-85

Glueck R.M., Mottley J.G., Miller J.G., Sobel B.E., Pérez J E. (1985) Effects of coronary artery occlusion and reperfusion on cardiaccycle dependent variation of myocardial ultrasonic backscatter. Circ.Res. 56: 683-689

Lancée C.T., Mastik F., Rijsterborgh H., Bom N. (1988) Myocardial backscatter analysis in animal experiment. Ultrasonics 26: 155-163

Lyons M.E., Chivers R.C., Parker K.J. (1986) Absorption dominates attenuation in soft tissue. Proc IEEE Ultrasonics Symposium, Williamsburg

Madaras E I., Perez J., Sobel B.E., Mottley J.G., Miller J.G. (1988) Anisotropy of the ultrasonic backscatter of myocardial tissue: II. Measurements *in vivo*. J. Acoust. Soc. Am. 83: 762-769

Matheson A.J. (1971) Molecular acoustics. John Wiley & Sons Ltd. London

Miller J.G , Pérez J.E., Sobel B.E. (1985) Ultrasonic characterization of myocardium. Prog. Cardiovasc. Dis 28: 85-110

Morse P M., Ingard K U. (1986) Theoretical Acoustics chap. 8 McGraw-Hill Inc. New York

Mottley J.G., Glueck R.M., Pérez J.E., Sobel B.E., Miller J.G. (1984) Regional differences in the cyclic variation of myocardial backscatter that parallel regional differences in contractile performance J. Acoust. Soc. Am. 76: 1617-1623

O'Donnell M., Bouwens M., Mimbs J.W., Miller J.G. (1979) Broadband integrated backscatter: An approach to spatially localized tissue characterization *in vivo*. Proc. IEEE Ultrasonics Symp. 79: 175-178

Rijsterborgh H , Mastik F., Lancée C.T., van der Steen A F W, Sassen L.M.A., Verdouw P.D., Roelandt J., Bom N. (1990) Ultrasonic myocardial integrated backscatter and Myocardial wall thickness in animal experiments. Ultrasound in Med. & Biol. 16: 29-36

Wickline S.A., Thomas III L.J., Miller J.G., Sobel B.E., Pérez J.E. (1985) The dependence of myocardial ultrasonic integrated backscatter contractile performance. Circulation 72: 183-192

Wickline S A., Thomas III L.J., Miller J.G., Sobel B.E., Pérez J.E (1985) A relationship between ultrasonic integrated backscatter and myocardial contractile function. J. Clin. Invest. 76: 2151-2160

APPENDIX A

The attenuation α was calculated from:

$$\alpha = \frac{-(10\,log\frac{P^+}{P^-})}{2d} \quad [dB/cm] \tag{A1}$$

with α = Attenuation [dB/cm]
P^+ = power calculated from:

$$P^+ = \int_{3.2}^{7.2} L^+(f)\,df \quad [W] \tag{A2}$$

f = frequency [MHz]
P = power calculated from:

$$P^- = \int_{3.2}^{7.2} L^-(f)\,df \quad [W] \tag{A3}$$

d= wall thickness of the myocardium [cm]

The attenuation transfer function A_{trans} was calculated from:

$$A_{trans}(f) = \frac{10\,log\,\frac{L^-(f)}{L^+(f)}}{2d} \quad [dB/cm] \tag{A4}$$

The backscattering transfer function B_{trans} was calculated from:

$$B_{trans}(f) = 10\,log\,\frac{K(f)/t_w}{M(f)} \quad [dB] \tag{A5}$$

with t_w = the lenght of the time window [μs]

the integrated backscatter IB was calculated from.

$$IB = 10\log\left(\int_{f_2}^{f_1} \frac{K(f)/(f_b \cdot t_w)}{M(f)}\, df\right) \quad [dB] \tag{A6}$$

with f_b = the bandwidth of the transducer [MHz]

The backscattering transfer function was corrected for attenuation with:

$$B_{cor}(f) = B_{trans}(f) + A_{trans}(f) \cdot 2r \quad [dB] \tag{A7}$$

with $B_{cor}(f)$ = the corrected backscattering transfer function [dB]
r = the distance to the middle of the region which is being processed [cm]

The integrated backscatter was corrected for attenuation with:

$$IB_{cor} = IB + \alpha \; 2r \quad [dB] \tag{A8}$$

with IB_{cor} = the corrected integrated backscatter [dB]

CHAPTER III

IN VITRO CLASSIFICATION OF GALLSTONES BY QUANTITATIVE ECHOGRAPHY.

A Goedegebure, A F W van der Steen, J M Thijssen

ABSTRACT

Gallstones (n=20) were classified by dual energy CT into three main classes pure cholesterol stones (I), combination stones (II) and calcium stones (III) Further sub-classification was possible by using morphological criteria The acoustic measurements that were performed were measurements of the velocity of sound, the attenuation coefficient slope with frequency and intercept at 4 5 MHz, the attenuation coefficient slope per unit of time, the backscattering characteristics and the appearance of B-mode echograms The velocity of sound in calcium stones ($c = 1695 \pm 107$ m/s) was distinctly lower than in those containing some cholesterol ($c > 2000$ m/s) The attenuation coefficient slope ranged from 4 3 to 16 2 dB/(cm·MHz), the 4 5 MHz intercept from 21 to 66 2 dB/cm The lowest values were found for the pure cholesterol stones (class IA), the highest values for subclass IIB (combination stones with shell) The attenuation coefficient slope per unit of time was distinctly lower ($< 0\ 50$ dB/(μs·MHz)) for the cholesterol stones than for the combination and calcium stones ($> 0\ 64$ dB/(μs·MHz)) The backscattering spectrum was approximated by a straight line fit and the slope for the cholesterol stones was lower than for the combination and calcium stones ($< 0\ 75$ dB/MHz vs $> 1\ 0$ dB/MHz, respectively) The latter two parameters were assessed by in vivo applicable methods The front echo level was found to be more than 5 dB higher for class IIB as compared to the other classes while the spectral backscattering level at 4 5 MHz was considerably higher for both classes IIB and III The B-mode echograms showed that a strong front echo in combination with a strong attenuation of the remaining echo signals was mainly found for stones of classes IIB and III A significant difference between the group of stones that are suitable for lithotripsy and dissolution treatment (classes IA,IB and IIA) and the non-treatable calcium containing stones (classes IIB and III) was found for the velocity of sound ($p < 0\ 01$), the attenuation coefficient slope per time unit ($p < 0\ 10$), the slope of the backscattering spectrum ($p < 0\ 05$) and the 4 5 MHz intercept ($p < 0\ 01$) B mode classification yielded no complete distinction of these two groups of stones

It can be concluded that in vivo assessment of quantitative characteristics (front reflection, backscattering characteristics, attenuation coefficient slope per unit of time) in combination with the B-mode characteristics might be useful for in vivo gallstone classification

INTRODUCTION

The interest in the assessment of the chemical composition of gallstones was raised by the introduction of oral bile-acid dissolution (Dantzinger *et al.* 1972, Bell *et al.* 1972). Further enhancement of the interest was due to the introduction of extra-corporal shock-wave lithotripsy (Sauerbruch *et al.* 1986) Criteria were developed for the selection of patients, which were based on conventional X-ray imaging and X-ray computerized tomography (CT).

The success rate of lithotripsy is critically dependent on the calcium contents of gallstones (Sackmann *et al.* 1988, Tsuchiya 1990): the higher the calcium contents, the lower the succes rate As was shown by Brakel *et al* (1990) the density of stones in CT-images (Hounsfield Units) is highly positively correlated to the calcium contents ($r=0.90$) and inversely proportional to the cholesterol contents ($r=-0.80$). These authors proposed an upper limit of 140 HU for stones to be selected for lithotripsy. Further criteria are the number and size of the stones.

One of the earliest applications of ultrasound echography in medicine was concerned with the detection of gallstones (Ludwig & Struthers 1949). In recent years many papers were devoted to this subject and to the possible differentiation of stones, related to their chemical composition, size and morphology. Two reasons may be mentioned for this increased interest of echography: the non-ionising nature of the ultrasound and the simple diagnostic procedure. Moreover, the piezoelectric shockwave sources, which have been introduced in recent years, are readily combined with a diagnostic transducer system for detection, differentiation and treatment monitoring of stones

Conventional B-mode echography allows for a qualitative assessment. One of the most obvious signs of the presence of stones is the occurrence of a "shadow", i.e. lowered, or absent, echoes distal to a stone. This sign is even more obvious than the mere presence of a stone in the B-mode image Several authors (Carroll 1978, Filly *et al.* 1979, McIntosh & Penney 1980) came to the conclusion that a shadow is detectable only when stones are larger than 3 mm Moreover, for small stones a narrow sound beam at the depth of the stone, is required Therefore, the gallbladder should preferably be localized in the focal zone of the transducer. The shadow effect is related to the ultrasound attenuation by the stone (Purdom *et al* 1980). Since the attenuation was shown to be negatively correlated to the cholesterol contents of the stones (Lau *et al.* 1989), it might also be concluded that the shadow is correlated to the cholesterol contents This latter conclusion is, however, not easily related to the observation by Greiner *et al.* (1988) who did not find any echographic difference between cholesterol and calcified stones as was evidenced by CT images.

Quantitative ultrasound methods were employed by a few authors. Swobodnik (1985) performed an extensive *in vitro* study, in which he registered radio frequency (rf-) echo lines with transducers of 5 and 10 MHz. The most important result he obtained was that a reasonable differentiation was possible between pure cholesterol stones and pigmented stones by a bi-variate analysis of "granularity" vs. "peak amplitude". Granularity is the backscattered ultrasound level from inner parts of the stone, relative to the peak amplitude and multiplied by the duration of the scattering signal. Lau *et al.* (1989) found an inverse relationship between ultrasound attenuation coefficient slope with frequency and the cholesterol percentage. Purdom *et al.* (1980) found a surprisingly large range for both the attenuation coefficient (5 to 23 dB/(cm · MHz)) and the velocity (1750-2400 m/s).

Table I *Classification criteria from CT scans and optical appearance (size, morphology)*

classes	IA	IB	IIA	IIB	IIC	IIIA	IIIB
chemical							
cholesterol	++	++	+	+	+	-	-
bilirubin	--	-	±	±	±	--	+
calcium carbonate	--	-	±	±	±	++	--
calcium phosphate	--	-	±	±	±	--	+
morphology							
layered (l)	+	±	-	--	--	--	--
radial (r)	-	±	±	--	--	--	--
homogeneous (h)	+	±	-	-	--	+	++
inhomogeneities (i)	--	±	±	±	++	-	-
nucleus (n)	--	±	++	-	-	-	-
shell (s)	-	±	-	++	-	-	-
fissures (f)	-	±	±	±	±	--	--
inner texture							
granular(g)	--	-	±	±	±	++	+
crystalline(c)	++	+	±	±	±	--	-
outer texture							
irregular (ir)	--	-	-	--	±	++	+
smooth (sm)	++	+	+	+	+	--	-
size							
diameter [mm]	3-15	>5	>5	>5	>5	3-10	3-10
colour							
black	--	--	--	-	-	++	+
grey/green	-	-	-	+	-	-	-
brown	±	±	±	±	±	-	+
ochre/orange	±	±	±	--	±	--	--
white	±	-	-	--	-	--	--

meaning of symbols: ++ highly present, + present, ± possibly present
- low or not present, -- not present

In the present study the gallstones were examined *in vitro*, both by CT and ultrasound The aim of the study was to measure the ultrasonic characteristics of stones with the highest precision possible, and to relate these to the quantitative CT characteristics and to the morphology and structure of the stones as was assessed by visual inspection.

Furthermore, an attempt is made to find a unique relationship between these quantitative acoustic characteristics and parameters derived from the B-mode images, in order to obtain a method for *in vivo* echographic differentiation of gallstones.

Based on some reports that can be found in the literature the following characteristics can be used in distinguishing gallstones (cf Meyers & O'Donohue 1973, Bills & Lewis 1975, Been *et al.* 1979, Malet *et al* 1984, 1986).

1. Chemical composition: the three dominating components are cholesterol, calcium compounds and bilirubin. Calcium compound can be carbonate, phosphate, or bilirubinate
2. Internal structure. can be homogeneous throughout the stone, or consisting of various kinds of structures: outer shell, layered, or radially structured, small local inhomogeneities, nucleus, fissures
3. Texture of the stone material (visual): fine, granular, crystalline, non-crystalline
4. Outer appearance: smooth, or rough surface, size 2-30 mm, colour· white, ochre, orange, brown, grey, green, black

A classification survey is shown in Table I. A gross classification is made on the basis of chemical composition into pure cholesterol stones (class I), pure "calcium" stones (class III) and combination stones (class II). These three main classes are further sub-classified, based on morphological and textural features as will be obvious from Table I.

As can be seen in the Table, sub-classes IIB, IIIA and IIIB have an outside surface with a high calcium concentration. For this reason these stones are not well suited for lithotripsy treatment. A reformulation of the goal of this study might be then to develop and assess methods to differentiate stones of these classes from those belonging to one of the other classes.

METHODS

MATERIAL

Gallstones were received after surgical removal in two hospitals in Munich. The stones were kept in buffered physiological saline solution and transported to the Biophysics Laboratory by surface mail. After reception the stones were stored in the saline solution, whereas the acoustic measurements were made with the stones in a degassed saline solution

A sub-group of stones, which was assessed to be cholesterol stones or combination stones by CT scanning, was cut and polished subsequently in such a way that slices with flat and parallel surfaces of 2.5 mm thickness were obtained. After slicing the slices were kept at 6 °C in a degassed physiological saline solution for at least 24 hours to resolve small gas bubbles that could have been absorbed by the slices during the polishing (Cloostermans *et al.* 1986). After slicing these stones could be further differentiated by visual inspection and precise acoustic measurements were possible.

A total of 47 stones was received, 6 of which appeared to contain fissures with gaseous inclusion on CT-scans, and 21 were too small for measurement The number of stones containing gas was higher than could be expected from the literature.

X-RAY COMPUTER TOMOGRAPHY (CT)

In order to obtain a qualitative classification, the stones were first examined using X-ray Computer Tomography. The stones were kept in plastic tubes, filled with physiological saline and placed in a CT-scanner (Somatom DR III, Siemens). The tubes were taped together in rows of 5 to 7. The position was controlled by using the scanner in the conventional (Single Energy) mode. As in Single Element mode the X-ray absorbtion can be either caused by a high density or a high atomic number of the material, a series of adjacent slices was acquired in dual energy mode (Cann 1988, Goodsit *et al.* 1987, Kalender *et al.* 1987). Double Energy mode enabled differentiation and yielded two series of images: water equivalent and calcium equivalent images. In this way, the distributions of cholesterol, and calcium compounds could

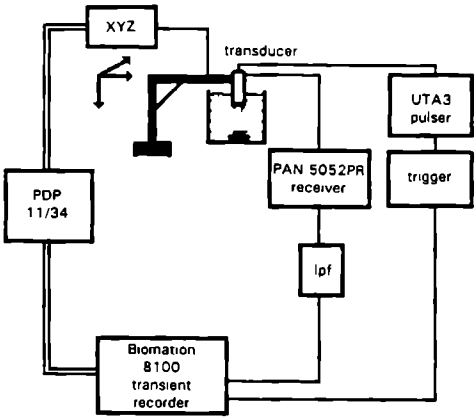

Fig 1 Scheme of the measurement equipment

be adequately assessed. The images were documented on X-ray film.

ULTRASOUND MEASUREMENTS

EQUIPMENT

The scheme of the measurement equipment is shown in Fig. 1. (cf van der Steen *et al* 1991, Chapter VII). The ultrasound transducer (Panametrics, Inc., V308), focused at 6 cm, diameter 23 mm, central frequency 5 MHz, -10 dB bandwidth 5 MHz, was fixed in an XYZ-translation system (Marzhauser, GmbH) and positioned in a tank filled with degassed physiological saline solution. The transducer was excited by a short electrical pulse from a pulser (Aerotech Laboratories, Inc., UTA-3), which was externally triggered. The transducer was also connected to a receiver (Panametrics, Inc., 5052 PR), which was employed at a fixed gain of +40 dB amplification. The amplified echo signal was then low-pass filtered by a four section Bessel filter (K & L, Inc.) with a -3 dB at 15 MHz cut-off, to yield anti aliasing and a reduction of high frequency noise components. The filtered signal was digitized by a transient recorder (Biomation Inc. 8100) at a sampling rate of 20 MHz, and in 8 bits The accuracy of digitization was enhanced by using a averaging procedure as described by van der Steen *et al.* (1991, Chapter VII). The recorder was synchronized to the ultrasound transmission pulses and a fixed delay was incorporated to compensate for the water path. The transient recorder was interfaced to and software controlled by a digital computer (Digital Equipment Corp. PDP 11/34).

MEASUREMENT PROCEDURE

This procedure (cf. Foster *et al.* (1984), van der Steen *et al.* 1991, Chapter VII) is explained schematically in Fig 2., whereas Fig 1 gives an overview of the geometry. The transducer is mounted in the XYZ-translation system and directed perpendicularly towards a thick glass plate at the bottom of the water tank. On top of this plate a plastic ring of 2 mm thickness was laid, which was covered on the top side by a thin ($\leq$ 3 μm) polyethylene membrane.

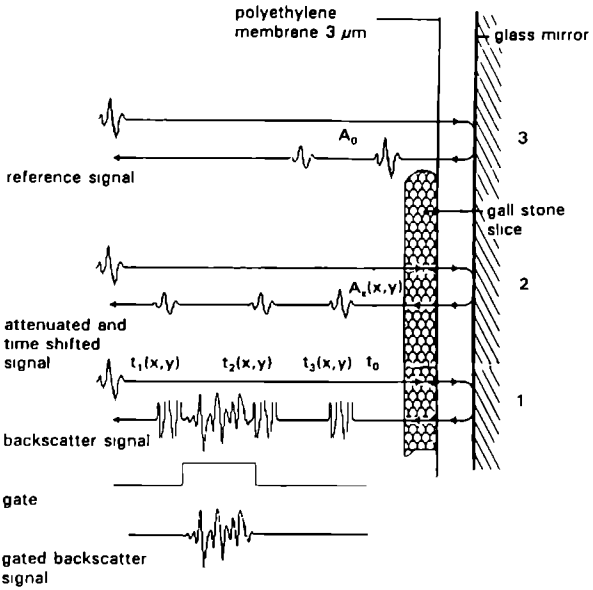

Fig 2 Scheme of the in vitro measurements (rotated anti clock wise over 90° 1 radio frequency trace of echoes at high gain setting, gating of scattering signal, 2 trace of rf-echoes at lower gain setting, t1 = time of front echo of stone, t_2 = time of bottom echo of stone (membrane) t_x = time of echo from glass plate (amplitude A.(x,y)), 3 reference rf-echo from glass plate (amplitude A_o) after removal of stone

This membrane attenuated the ultrasound by less than 0 1 dB in the frequency range involved During a measurement the gallstones were placed on top of the membrane, resulting acoustically in a coincidence of the bottom surface of the stone with the membrane. Moreover, this bottom surface was acoustically clearly distinct from the top surface of the glass plate With the stone in position the first acquisition was made with the receiver attenuator at 0 dB (trace 1 in Fig 2) yielding the backscattering signal. Then a second acquisition was made at attenuation -10 dB or -20 dB (trace 2), yielding a trace containing three peaks, caused by echoes from the top and bottom surfaces of the stone and from the glass plate, respectively. The third acquisition was made at an attenuation of -30 dB and after the stone had been removed, yielding the trace (3) which was used as a reference plate reflection.

When measurements were made of slices of the stones, this acquisition procedure was repeated while scanning the transducer over a 2.5x2.5 mm^2 square area, in a 5x5 grid (i.e. at 0 5 mm distances), which resulted in a C-scan. Then the transducer was shifted two times and for each new position the whole scanning procedure was repeated.

When measuring the intact stones the transducer was moved until a high front echo was obtained. A C-scan (5x5 positions) was performed around this point. Then the stone was reorientated two times and the procedure was repeated after each rotation In this way three orthogonal scans were acquired. For each of the three orientations of the stone a B-scan was performed, i e. the transducer was scanned linearly in either the X-, or the Y-plane, with a step size of 0 25 mm. Care was taken to extend the scan in both directions far enough to pass beyond the sides of the stone

The measurement procedures described so far, with the end of the focal zone of the transducer at the depth of the glass plate (67 mm from the transducer), yield acoustic parameters which are not significantly biased by the beam characteristics (Verhoef *et al.* 1985) or by the plate reflection (van der Aarssen *et al.* 1989) The -6 dB beam diameter of the transducer was 0.8 mm in the focal zone. For the larger intact stones the front echo was recorded somewhat in front of the focal zone, but the beam diameter never exceeded 1 5 mm.

Processing of echographic signals

Velocity estimation

The velocity of sound, c, in the stones was estimated with the substitution method (cf Verhoef *et al.* 1985, Cloostermans *et al.* 1986, van der Steen *et al.* 1991, Chapter VII) The echo times t_0 through t_3 (see Fig. 2.), obtained for every position in the scanned grid, were used to calculate the velocity of sound c and the local thickness of the slice d:

$$c = c_0 \left(1 + \frac{(t_0 - t_3)}{(t_2 - t_1)} \right) \quad [m/s] \tag{1}$$

where c = unknown velocity in stone
c_0 = measured velocity in saline at room temperature:(1500 $\pm$ 3) m/s

$$d = c \frac{(t_2 - t_1)}{2} \quad [cm] \tag{2}$$

The time difference (t_2-t_1) was assessed by measuring the time of the peak amplitudes, after demodulation For slices the time difference (t_0-t_3) was estimated by using the spectral phase difference method (Verhoef *et al.* 1985) For intact stones a peak detection was performed on the envelope of the echo traces. First the sample with the maximum amplitude was selected, after which a centroid estimation over nine samples was performed, resulting in an accurate estimation of the peak position (van der Steen *et al.* 1991, Chapter VII). Both methods achieve a subsampling-interval time resolution. The precision of the velocity measurements following from Eq. (1) is better than one percent.

Attenuation coefficient

Again the substitution method was used (i.e. traces 2 and 3 in Fig. 2.) for the slice measurements. The echoes from the glass plate a_r and a_0 were Fourier transformed, and the amplitude spectra (A_r and A_0, respectively) were calculated. The logarithms of these spectra

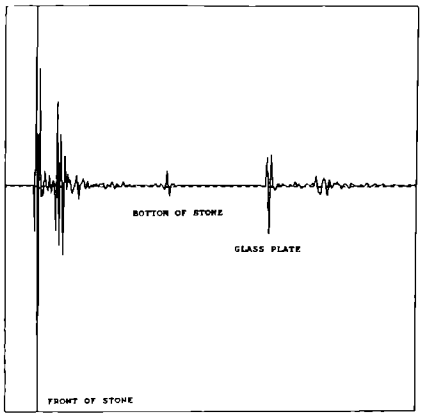

Fig 3 rf-echogram of stone (cf trace 2 in Fig 2)

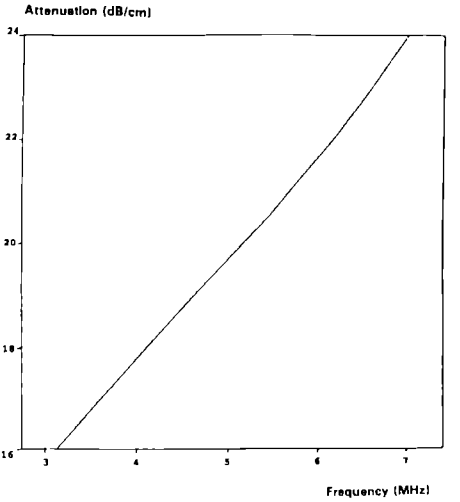

Fig 4 Representative example of the attenuation coefficient versus frequency (dB/cm), calculated from the rf-signals of one glass plate reflection with a stone interposed and one reference reflection

(i e. in dB) were subtracted, and the result was divided by the local thickness of the stone, that was estimated by Eq. (2). This procedure resulted in the attenuation coefficient as a function of frequency:

$$\alpha(f) = -\frac{20\,log\,(A_s(f)/A_0(f))}{2d} \quad [dB/cm] \tag{3}$$

where $\alpha(f)$ = attenuation coefficient

The factor of 2 in front of the thickness d is due to the two way travel of the echoes from the plate. An example of the radio frequency (rf-) echogram of a stone, which is equivalent to trace 2 in Fig. 2., is shown in Fig. 3. The first echo on the left is the front echo of the stone, the glass plate echo is separated by a water path of approximately 2 mm from the bottom of the stone. The corresponding picture of the attenuation coefficient vs. frequency, as was derived with Eq. (3), is shown in Fig. 4. A linear least squares fit was performed over the frequency range from 3 to 6 MHz, yielding the slope α of the attenuation coefficient and the intercept at 4.5 MHz, i.e.

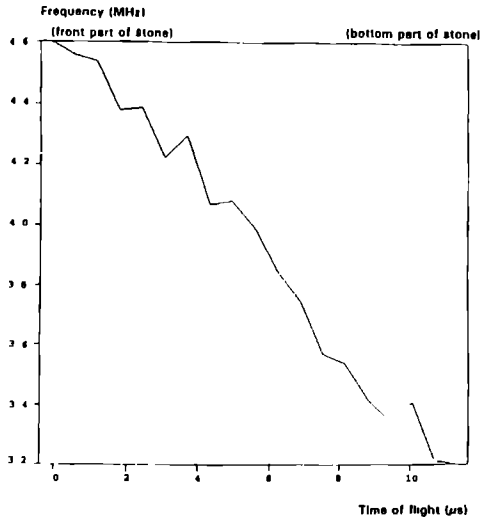

Fig 5 Average over one orientation of a stone of the centroid frequency vs time (i e depth), from which attenuation coefficient per unit of time is estimated

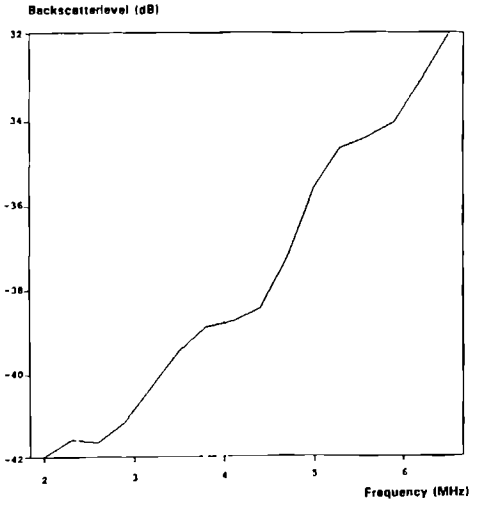

Fig 6 Backscattering spectrum (dB), after attenuation correction and averaging over one orientation of a stone

$$\alpha(f) = \alpha_{4.5} + \alpha(f - 4.5) \quad [dB/cm] \tag{4}$$

with f in units of MHz

The attenuation in the intact stones could not be measured with the substitution method, since the high attenuation of most stones caused relatively weak plate reflections of which the spectra were not reliable over a considerable frequency band.

Anticipating and investigating the possibility of obtaining a quantitative assessment of the attenuation *in vivo*, a different procedure was developed additionally. This second method is based on the property of a Gaussian spectrum to remain invariant (in shape) under an attenuation coefficient, which is linear with frequency. Therefore, the attenuation can be described as a downshift of the peak frequency (Dines & Kak 1979, Kuc *et al.* 1979), or of the centre of gravity frequency of the amplitude spectrum (centroid frequency, f_c) (Fink *et al.* 1983). This can be described by:

$$\alpha = -\frac{1}{2}\frac{(8.7\Delta f_c)}{(\sigma_f^2 \Delta z)} \quad [dB/(cm \cdot MHz)] \tag{5}$$

where Δf_c = centroid frequency shift due to attenuation
σ_f = standard deviation of amplitude spectrum

Table II *Classification criteria from B-mode echograms*

class	characteristics		
	front	centre	posterior
A	medium no interfaces	homogeneous, weakly attenuating	comet tails
B	strong interfaces	homogeneous, weakly attenuating	comet tails
C	strong shell	homogeneous, weakly attenuating	comet tails
D	strong, shell	nucleus, weakly attenuating	comet tails
E	strong, shell	highly attenuating	comet tails
F	strong, shell	highly attenuating	-

σ_f = standard deviation of amplitude spectrum
Δz = thickness of attenuating medium (cm)

or, when replacing Δz by ½ $c\Delta t$, and inserting σ_f = 1.8 MHz (this is the value for our transducer (measured)):

$$\alpha c = -2.69 \frac{\Delta f_c}{\Delta t} \quad [dB/(\mu s \cdot MHz)] \qquad (6)$$

As can be noticed, Eq. (6) describes the attenuation per unit of time, rather than per unit of distance (see also Fig. 5.). Therefore, it is not necessary to know the sound velocity any more, and it can be concluded that this parameter is ideally suited to be used *in vivo*, when applied to the backscattered echoes from the inner parts of the stones.

From the echo traces obtained at the lowest attenuator position (trace 1 in Fig. 2.) a windowed part, containing the scattering from the stone, was Fourier transformed. This Fourier transformation was carried out on small subwindows (25 samples long). Fifty percent overlapping Hanning windows were used to prevent distortion of the obtained spectra. The centroid frequencies of these spectra were calculated and the centroid frequency obtained at the same depth were averaged i.e. they were laterally averaged. This procedure was repeated at all depths for the 8 windows employed. Next a straight line was fitted through the scatter plot of centroid shift Δf_c vs time Δt (cf. Eq. 6). The slope of this fit was inserted in Eq. 6 to yield the attenuation coefficient per unit of time. A goodness of fit criterion was calculated to assess the precision of the slope value and thereby of the attenuation coefficient.

Table III *Results of classification according to criteria in Table II*

	number of stones	
class	CT	optical
IA	4	3
IB	6	5
IIA	1	2
IIB	5	5
IIC	-	1
IIIA\B	4	4

BACKSCATTERING ANALYSIS

For the backscattering analysis the backscattering spectra of the first eight windows (as defined in the foregoing sections) were calculated for all acquired sweeps. Then the spectra obtained at the same depth were averaged (i.e. laterally averaging), and the ensemble averaged spectra as a function of depth were corrected for the estimated attenuation (cf. van der Steen *et al.* 1991, Chapter VII) After this correction a second averaging is possible, because the depth trend is removed now. So for each measurement one spectrum resulted, which was normalized by a division by the spectrum obtained from the echo obtained from a plane reflector (Romijn *et al.* 1991, van der Steen *et al.* 1991, Chapter VII) Finally a straight line was fitted through the logarithm of the resulting spectrum (cf. Lizzi *et al.* 1986, Romijn *et al.* 1989, 1991) between 2 and 6.5 MHz. An example of a backscattering spectrum is shown in Fig 6 The backscattering spectrum could thus be characterized by two parameters: the intercept at 4.5 MHz ,$b_{4.5}$, and the slope value, b, i e.

$$b(f) = b_{4.5} + b(f - 4.5) \quad [dB] \tag{7}$$

B-MODE ECHOGRAMS

The rf-lines of the linear B-scan were demodulated by calculating the modulus of the analytic signal. This method is often called a "software" demodulation by a Hilbert transform (Whalen 1971, Thijssen *et al.* 1990). The procedure results in a pure envelope signal, without further need for low-pass filtering as in hardware demodulation. The so-called "video" scan lines obtained by this procedure were coded into grey levels after a logarithmic compression. Further assessment of the B-mode images obtained by this procedure was made by visual inspection according to the criteria listed in Table II.

One quantitative parameter was, however, taken from the unprocessed data: the maximum peak level reached at one of the scan lines of a stone. This maximum corresponds to the maximum reflectivity of the outer surface of the stones, which is a direct measure of the impedance of this surface, when the impedance of the surrounding medium is known. This of course is the case for the *in vitro* measurements, but more difficult *in vivo*. Nevertheless it seemed interesting

Table IV *Mean, and standard error of the mean, of acoustic parameters of stone slices Separate data for centre of stones and for periphery*

CT-class	velocity (m/s) c ± s.e.	attenuation coefficient slope [dB/(cm · MHz)] α ± s.e.	attenuation coefficient at 4.5 MHz [dB/cm] $\alpha_{4.5}$ ± s.e.
centre:			
IA (4)	2251 ± 67	4.3 ± 0.9	21.0 ± 5.1
IB (5)	2178 ± 37	11.6 ± 1.2	54.1 ± 5.8
IIA (1)	1553	-	-
IIB (1)	2198	16.2	66.2
periphery:			
IA (3)	2187 ± 77	6.9 ± 1.2	33.1 ± 8.7
IB (6)	2258 ± 66	7.8 ± 1.2	32.5 ± 4.9
IIA (1)	2368	7.5	36.7
IIB (1)	2210	14.8	63.1

to establish the possible differences between different kinds of stones. The reflectivity was expressed in dB relative to the reflection level of the glass block, at the same distance to the transducer as was the top of the stone.

RESULTS

Classification

A total of 20 stones was involved in the complete study. The CT and optical classification criteria of the individual stones are listed in table A1. Most of the acoustic measurements and methods were not performed with each of these stones. Not all stones were measured as sliced parts and not all intact stones measurements could be used due to equipment problems. Therefore, the numbers of stones used for every measurement are listed in the tables together with the results. The classification, while using Table I, was made by considering the images obtained with single- and dual energy CT scanning (see Fig. 7., cf. Methods: X-ray CT) and in addition morphological and optical texture characteristics (see Fig. 8., cf. Introduction) were used to further sub-classify the pure and mixed cholesterol stones (main classes I and II). The latter assessment was performed after these stones were cut and polished into slices with parallel surfaces. The final results are shown in Table III. The CT classification was maintained throughout this study, because of the quantitative character of this modality regarding the calcium contents of the stones. The details of the classification are given in Appendix A, Table A1. As can

Table V Mean, and standard error of the mean, of acoustic parameters of intact stones

CT class	velocity [m/s] c ± s e
IA(4)	2188 ± 47
IB(6)	2149 ± 49
IIA(1)	2027
IIB(5)	2060 ± 70
III(4)	1695 ± 107

CT class	attenuation coeff slope [dB/(μs MHz)] αc ± s e	backscattering slope [dB/MHz] b ± s e
IA(2)	0 47 ± 0 07	0 75 ± 0 37
IB(4)	0 46 ± 0 12	0 60 ± 0 38
IIA(1)	0 65	0 99
IIB(4)	0 66 ± 0 07	1 99 ± 0 35
IIIB(4)	0 78 ± 0 22	1 09 ± 0 4

be noticed in Table III nine stones (subclasses IIB, IIIB) were of the types not suitable for shockwave stone destruction

Sliced stones

Velocity of sound

As is explained in the Methods, after slicing the stones a very accurate, local, measurement of the velocity of sound is possible A distinction was made between measurements performed in the centre of a slice and in peripheral locations. The results are listed separately in Table IV The standard deviation of the group mean values was considerably larger than both the measurement precision and the standard deviation per stone, i e the between stones spread exceeds the within stones spread The standard error of the mean value is mentioned in Table IV if more than one stone was measured. The velocities of the four classes appear to be not significantly different, nor is a systematic trend throughout the classes obvious

Attenuation

The distinction between centre and periphery was maintained for the attenuation parameters. the attenuation coefficient slope, α, and the attenuation coefficient at 4.5 MHz, $\alpha_{4.5}$ The results are presented also in Table IV. As can be observed the attenuation coefficient parameters are considerably higher in the centre of stones in classes IB and IIB, and in the periphery of class IIB, as compared to other classes A significant difference between the attenuation of the central and of the peripheral parts is found for the stones of class IB (paired t-test, $p < 0.01$).

Table VI *B-mode classification, maximum front echo level (rf) in dB and backscattering level at 4 5 MHz, both relative to glass plate reflection*

CT class	B-mode class	max. front echo [dB]
IA(4)	A(1),B(2),C(1)	-20.7 ± 3.5 *
IB(6)	A(2),C(1),D(2),E(1)	-18.8 ± 3.0 **
IIA(1)	D(1)	-27.3
IIB(5)	C(2),E(3),F(1)	-13.3 ± 2.0
III(3)	E(1),F(2)	-21.0 ± 3.4

* 2 stones
** 3 stones

CT class	backscattering $b_{4\,5}$ ± s.e. [dB]
IA(2)	-40 ± 1
IB(4)	-41 ± 3
IIA(1)	-43
IIB(4)	-27 ± 2
IIIB(4)	-30 ± 1

INTACT STONES

VELOCITY OF SOUND

Fifteen rf-signals with distinguishable front, bottom and glass plate reflections were selected out of the totally 75 recorded echo traces for every stone, in order to obtain an accurate estimate for the velocity of sound The precision was assessed for each stone from the velocity values at the 15 positions, the spread within stones was of the order of 45 m/s. The mean values for the classes are presented in Table Va, together with the standard error of the mean. The stones containing a considerable amount of calcium (classes II, III) yielded a relatively large spread between stones, but low mean values. The difference of class III from all the other classes is remarkable.

Fig 7 *Three examples of CT-scans of stones (opposite page)*
A Conventional CT-scan (SE-mode) On this scan it is clearly visualized that all three stones have a shell There is a fissure in the shape of a Mercedes Benz sign in the middle stone
B Water equivalent scan (DE-mode)
C Calcium equivalent scan (DE-mode) In this scan it is clearly seen that only the left stone has a calcium shell

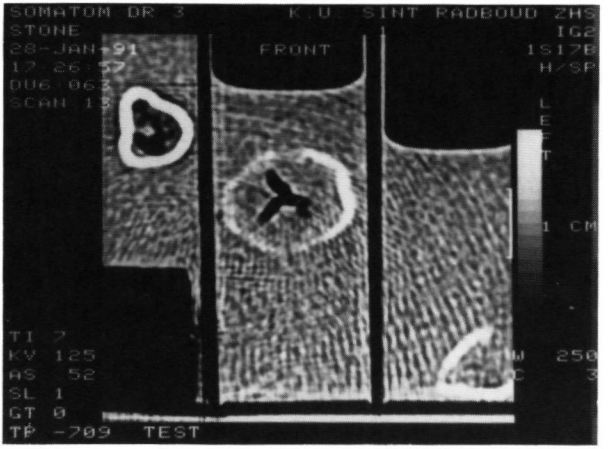
SOMATOM DR 3
K.U. SINT RADBOUD ZHS
STONE
IG2
28-JAN-91
FRONT
1S17B
H/SP
L
E
F
T
1 CM
TI 7
KV 125
AS 52
SL 1
GT 0
W 250
C 3
TP -709 TEST

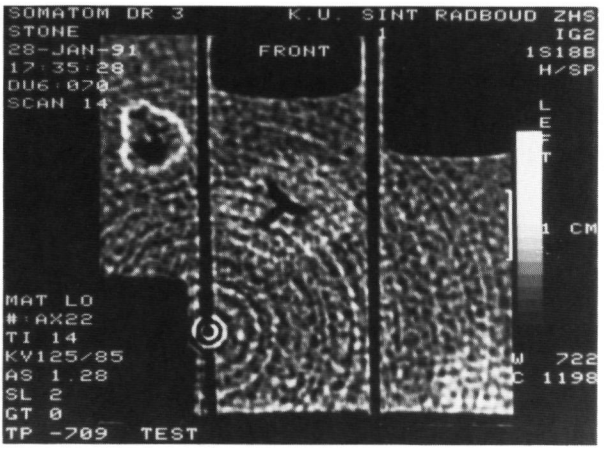
SOMATOM DR 3
K.U. SINT RADBOUD ZHS
STONE
IG2
28-JAN-91
FRONT
1S18B
H/SP
L
E
F
T
1 CM
MAT LO
#:AX22
TI 14
KV125/85
AS 1.28
SL 2
GT 0
W 722
C 1198
TP -709 TEST

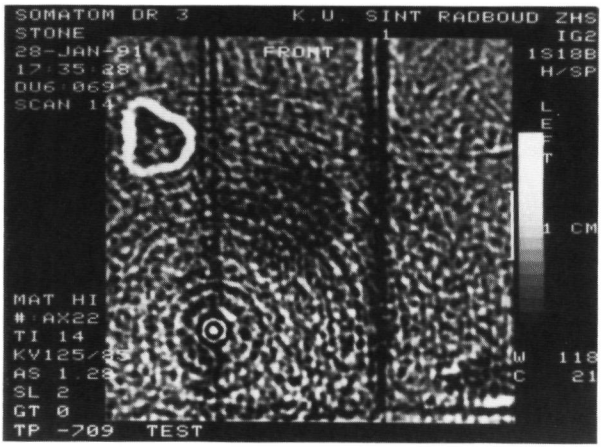
SOMATOM DR 3
K.U. SINT RADBOUD ZHS
STONE
IG2
28-JAN-91
FRONT
1S18B
H/SP
L
E
F
T
1 CM
MAT HI
#:AX22
TI 14
KV125/85
AS 1.28
SL 2
GT 0
W 118
C 21
TP -709 TEST

ATTENUATION

The substitution method could not be used for accurate attenuation coefficient estimation for the intact stones, for reasons previously mentioned in the Methods. The slope of the attenuation coefficient per unit of time could be estimated from the internal backscattering, using Eq (6) The results are shown in Table Vb, middle column. The mean values for the cholesterol stones are significantly lower ($p < 0.10$) than for the calcium containing stones. This difference is of the order of 0.20 dB/(μs · MHz).

BACKSCATTERING

The slope and intercept at 4.5 MHz of the straight line fit of the averaged backscattering spectra (eq. 7) were used as backscattering parameters. The spread within stones was of the order of 0.1 dB/MHz. The mean and standard error of the mean of the backscattering spectral slope for the five classes of stones is listed in Table Vb, right column. The slope found for the cholesterol stones (I) is lower than for the calcium containing stones (II, III) The backscattering intercept at 4.5 MHz is listed in Table VIb, which is discussed in the next section

B-MODE IMAGES

The results of the visual B-mode classification, by using the criteria of Table II are shown in Table VIa, left column, and three examples are shown in Fig. 9. The membrane echo apparently is interrupted below the stone, due to the large mismatch of the velocity within the stones, as compared to that in the surrounding saline solution This shortened imaging of gallstones occurs of course also *in vivo*! Most B-mode images showed at both sides of the stones a tail-like narrow echo pattern, which is known in literature as 'the comet tail artefact' It has been used as criterion for *in vivo* B-mode classification of gallstones (Tsuchiya *et al* 1986) The shadowing effect reported in the literature, which is due to the high attenuation of the stones, cannot be seen in the present echograms.

The calcium stones of class III and IIB (calcium shell) are listed mainly in echographic classes E and F, which are characterized by a strong front reflection and a strong attenuation of the backscattered echoes from the inner part of the stone. The comet tail was absent for three of these stones (class F) The other stones are mainly classified in the classes A, B, C and D which seem to be more characteristic for cholesterol like stones. Both classes C and E contain cholesterol stones as well as calcium containing stones

The front echo level which is displayed in table VIa shows a significantly lower value for the calcified stones of class IIB (t-test, $p<0.05$). The values of the other classes are more than 5 dB higher. The spectral backscattering level at 4.5 MHz (table VI) is significantly higher for the stones of both classes IIB and III (t-test, $p < 0.01$). The difference with the other classes is about 10 dB.

DISCUSSION

The acoustic measurements with the sliced stones yielded accurate values for the velocity of sound and the attenuation coefficient. Sound velocities between 2178 and 2368 m/s were found for all scanned parts, with the exception of the centre part of the class IIA stone The velocities found for the centre part of most of the stones seem lower than those for the periphery However, a paired t-test showed no significant difference ($p > 0.10$).

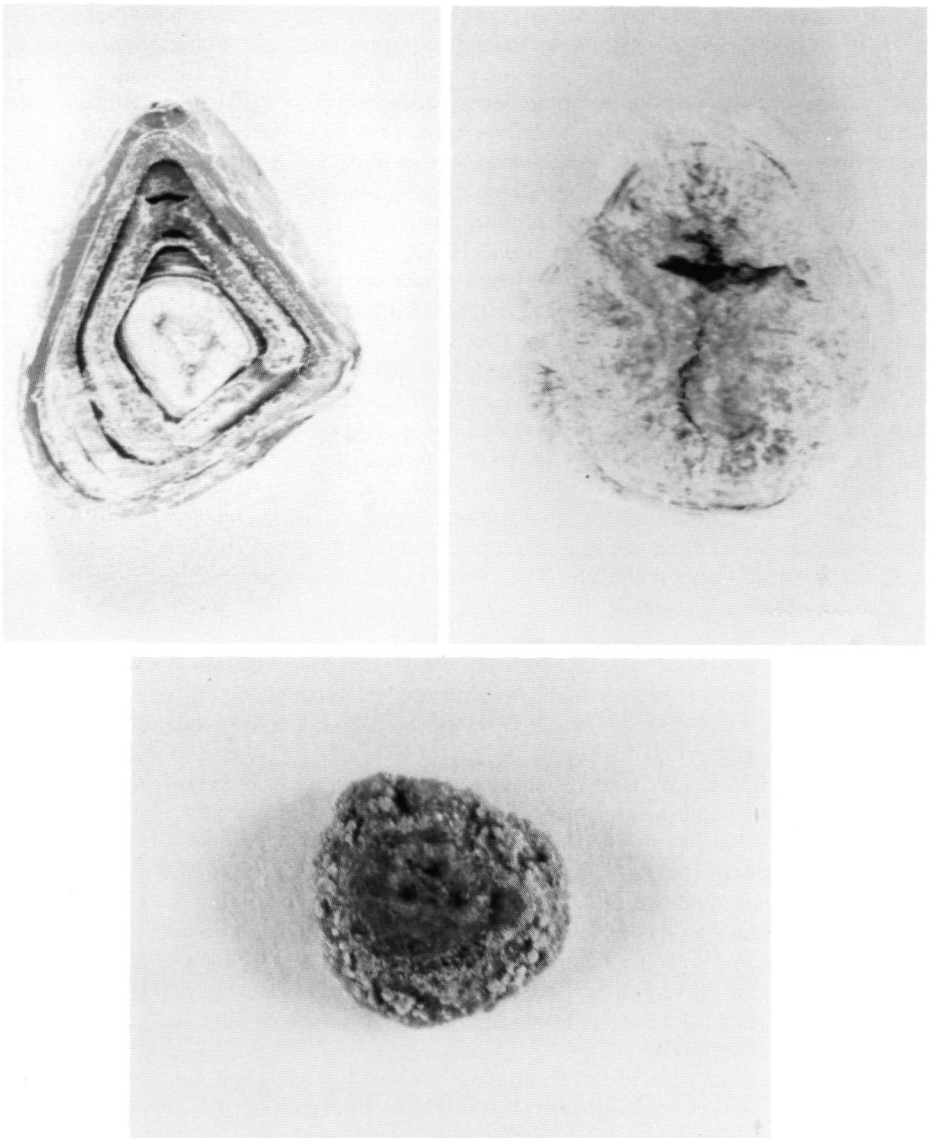

Fig. 8. Appearance of three examples of stones after slicing.
A. CT class 1A
B. CT class 1B
C. CT class IIB

A remarkably large range of values was found for the slope of the attenuation coefficient (4 3 - 16 2 dB/(cm MHz)) The lowest values were found for the pure cholesterol stones (IA) the highest value for the calcium containing stone of class IIB The attenuation coefficient slope values for the centres of the combination cholesterol stones (IB) are significantly higher than for the peripheral parts of these stones (paired t test, $p < 0\ 01$) The CT-images showed a clearly visible higher density in the centres of most of the IB stones which indicates that presence of other materials than cholesterol causes an increase of the attenuation coefficient These results confirm the inverse relationship between cholesterol contents and attenuation coefficient which was found by Lau *et al* (1989)

The velocity of sound data for the intact stones in table V display a systematic decrease with increasing class number (from I to III) which indicates an inverse relationship between velocity and the calcium contents of the stones In addition to the substitution method, some methods were developed to obtain attenuation and backscattering parameters from the internal backscattering of the intact stones The data for the attenuation coefficient slope per unit of time are consistent with the attenuation data for the sliced stones a correlation coefficient of 0 67 was present ($p < 0\ 01$) This result implies that a method has been found that is applicable *in vivo*!

The inverse relationship between cholesterol contents and attenuation parameters which was found for the slices, is confirmed by the values for the attenuation coefficient slope per unit time for intact stones (table Vb) The differences of these values between different classes in table Vb are smaller than in table IV

The backscattering spectral slope data in table V also display low values for cholesterol stones (class I) and higher values for calcium containing stones (classes II and III) It can be concluded then that cholesterol stones as compared to combination stones (II) and calcium like stones (III) are characterized by a higher velocity of sound a lower attenuation coefficient and a lower backscattering slope

Stones which have an outside surface with a high calcium concentration are not well suited for lithotripsy and dissolution treatment The differentiation potential of the acoustic parameters of table V with regard to this clinical relevant classification criterion has been investigated by applying t tests for each of these parameters The velocity of sound of the group of stones suited for lithotripsy and dissolution treatment ('L group' = classes I and IIA) is found to be significantly higher than that of the other group of stones belonging to classes IIB and III ($p < 0\ 01$) The attenuation coefficient slope per unit time of the L group is significantly lower ($p < 0\ 10$), and the backscattering slope is also significantly lower ($p < 0\ 05$) These latter two parameters seem to be suitable for clinical application since they can be obtained with *in vivo* applicable methods

The B mode echograms reveal no visible characteristics that enable a complete distinction of stones of the L-group from stones of classes IIB and III The classification in table VI shows that a high front echo level in combination with highly attenuating scatter signals from the inner part of the stone is observed for most of the stones belonging to classes IIB and III The comet tail artefact was observed in most of the B mode echograms It seemed to be caused by the shortened imaging of the stone which is maximal at the middle and minimal at the sides of the stone due to the difference in acoustic path length of the sound beam within the stone This effect mainly depends on the velocity of sound in the stone, but it is also influenced by the shape of the stone The comet tails were found to be absent for only three of the nine stones, belonging to classes IIB and III Therefore, detection of comet tails in B-mode echograms

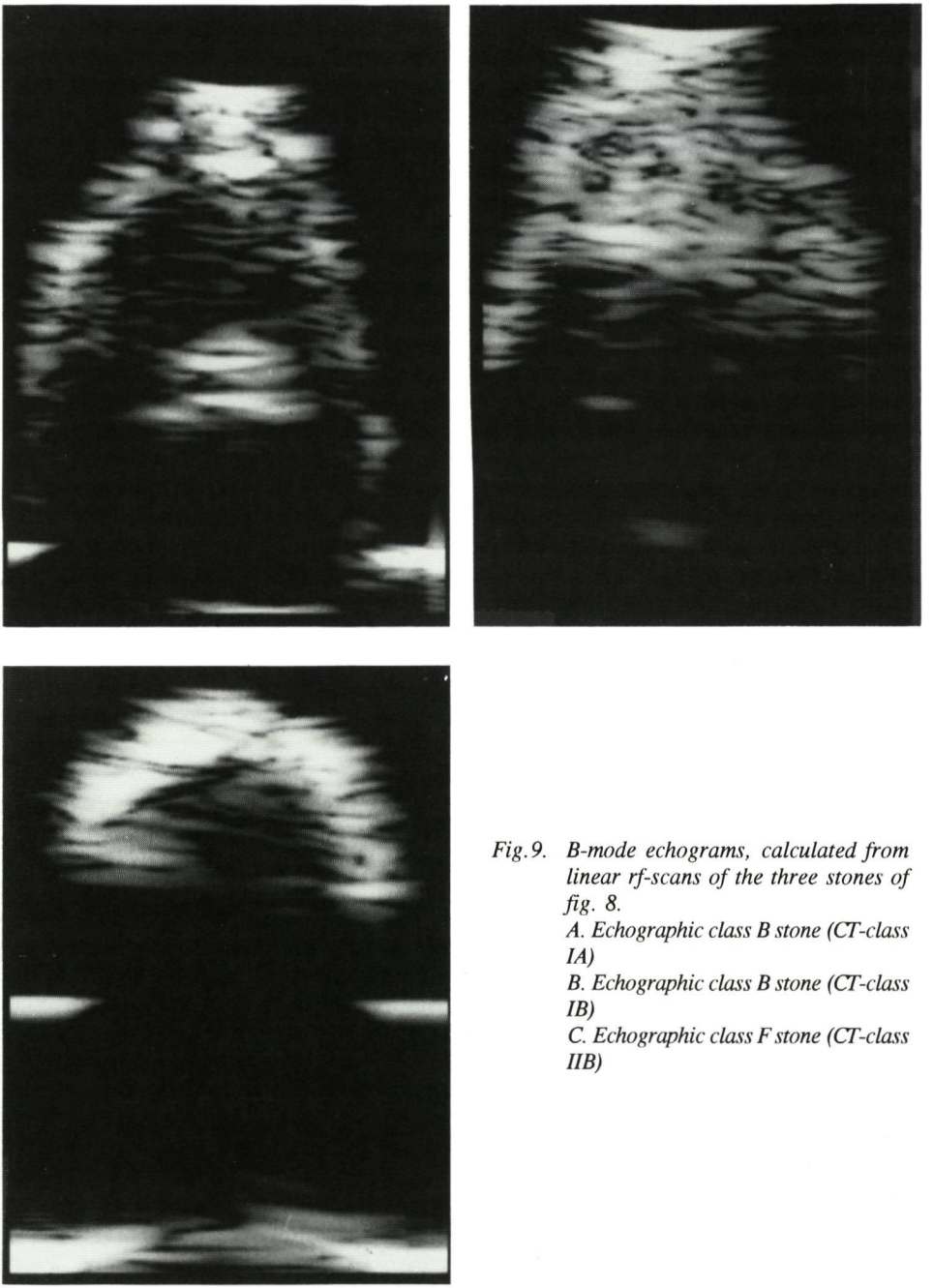

Fig. 9. B-mode echograms, calculated from linear rf-scans of the three stones of fig. 8.
A. Echographic class B stone (CT-class IA)
B. Echographic class B stone (CT-class IB)
C. Echographic class F stone (CT-class IIB)

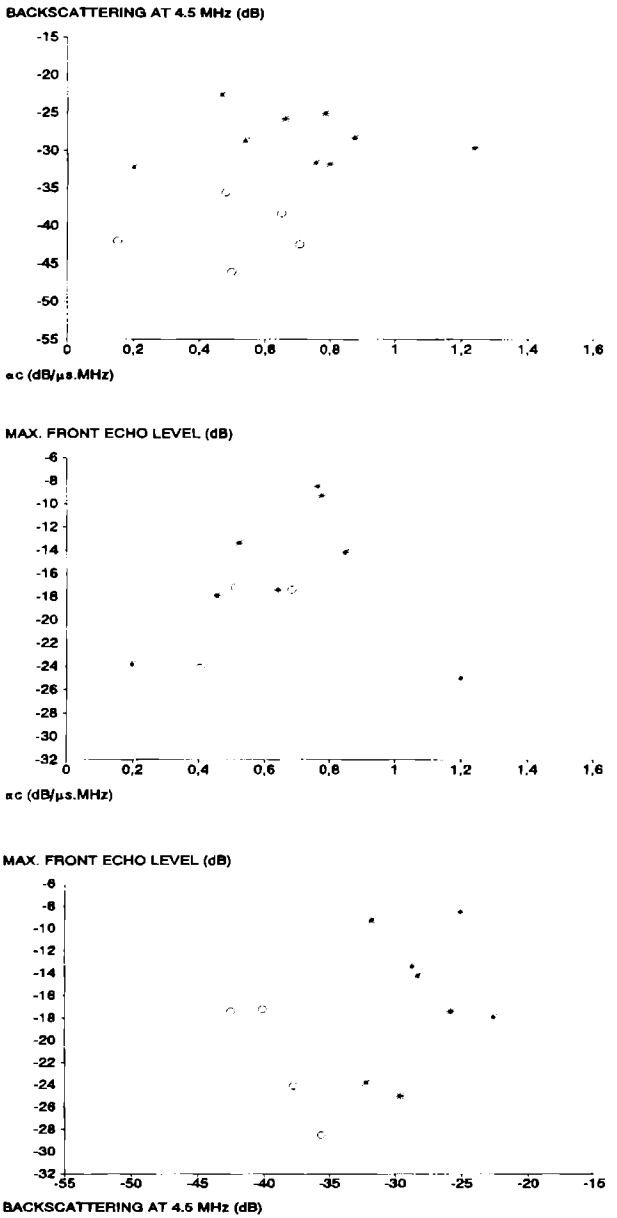

Fig. 10 2D Scatter plots of the maximal front echo level, the backscattering at 4.5 MHz and the attenuation per unit of time. All three parameters can be obtained in vivo. The stones that are suited for lithotripsy are represented by circles, the stones that are not suited for lithotripsy by asterisks.

does not seem to be a reliable criterion for classifying stones in the L-group.

The backscattering level at 4.5 MHz, which is a quantification of the appearance of the inner part of the stones at the B-mode echogram, is found to be 10 dB higher for classes IIB and III as compared to the other classes. The distinctly higher absolute front echo levels found for the stones of class IIB (table VI) are in agreement with the B-mode characteristics of these stones. Fig. 10. shows 2D scatterplots of three parameters that can be obtained *in vivo*. From these plots it can be seen that it is possible to distinguish *in vivo* between the group suited for lithotripsy and the other group.

A practical problem in the assessment of echo levels from B-mode images is the influence of transducer characteristics (centre frequency, focusing) and of the control settings of the equipment (Time Gain Compensation (TGC), overall gain) on the grey levels. Therefore, any consistent results may be obtained only while working with a specified transducer and while operating at fixed control settings. A further complicating factor is the attenuation of ultrasound in intervening tissue layers. This influence might be removed to a great extent by a near TGC slope setting equivalent to 0.5 dB/(cm MHz) for the body wall and a flat TGC in the following depth zone encompassing the gallbladder.

WORKS OF REFERENCE

van den Aarssen M., Verhoef W.A., Thijssen J.M. (1989) Influence of absorbing and scattering media on the propagation of ultrasound. J. Acoust Soc. Am. 85: 567-575

Been J.M., Bills P.M., Lewis D. (1979) Microstructure of gallstones. Gastroent. 76: 548-555

Bell G.D., Whitney B., Dowling R.H. (1972) Gallstone dissolution in man using chenodeoxycholic acid. N. Lancet 2: 1213-1216

Bills P.M., Lewis D. (1975) A structural study of gallstones. Gut 16: 630-637

Brakel K., Lameris J.S., Nijs H.G.T., Terpstra O.T., Steen G., Blijenberg B.C. (1990) Predicting gallstone composition with CT: *in vivo* and *in vitro* analysis. Radiology 174: 337-341

Can C.E. (1988) Quantitative CT for determination of bone mineral density: A Review. Radiology 166: 509-522

Carroll B.A. (1978) Gallstones: *in vitro* comparison of physical, radiographic and ultrasonic characteristics. Am. J. Roentgenol. 131: 223-226

Cloostermans M.J.T.M., Mol H., Verhoef W.A., Thijssen J.M., Kubat K. (1986) In vitro estimation of acoustic parameters of the liver and correlations with histology. Ultrasound in Med. & Biol. 12: 39-51

Danzinger R.G., Hofmann A.F., Schoenfield L.J., Thistle J.L. (1972) Dissolution of cholesterol gallstones by chenodeoxycholic acid. N. Engl. J. Med. 286: 1-8

Dines K.A., Kak A. (1979) Ultrasonic attenuation tomography of soft tissues. Ultrasonic Imag. 1: 16-33

Filly R.A., Moss A.A., Way L.W. (1979) *In vitro* investigation of gallstone shadowing with ultrasound tomography. J. Clin. Ultrasound 7: 255-262

Fink M., Hottier F., Cardoso J.F. (1983) Ultrasonic signal processing for in-vitro attenuation measurement: short time Fourier analysis. Ultrasonic Imag. 5: 117-135

Foster F.S., Strban M., Austin G. (1984) The ultrasonic macroscope: initial studies of breast tissue Ultrasonic Imag. 6:243-261

Goodsit M.M., Rosental D.I. (1987) Quantitative computed tomography scanning for measurements of bone and bone marrow fat content. A comparison of Single- and Dual-Energy techniques using a solid synthetic phantom. Investigative Radiology 22: 799-810

Greiner L., Rebensburg S., Jakobeit Ch., Wenzel H. (1988) Sonografische Gallenstein-Binnenreflexmuster-Artefakt oder reale Information. Z. Gastroent. 26: 61

Kalender W.A., Klotz E., Suess C. (1987) Vertebral Bone mineral analysis: An integrated approach with CT. Radiology 164: 419-423

Kuc R., Schwartz M. (1979) Estimating the acoustic attenuation coefficient slope for liver from reflected ultrasound signals. IEEE Trans. Sonics Ultrason. SU-26: 353-362

Lau T.H , Forster F.K, Baron R.C. (1989) Ultrasonic classification of gallstones. In: McAvoy, B.R. ed. 1989 IEEE Ultrasonics Symp. Proc., New York: IEEE: 1011-1014.

Lizzi F.L., Ostromogilsky M., Feleppa F.J., Rorke M.C, Yaremko, M M. (1986) Relationship of ultrasonic spectral parameters to features of tissue microstructure. IEEE Trans. Ultrasonics Ferroel. Freq. Control. UFFC-33: 319-329

Ludwig G.D , Struthers F W. (1949) Considerations underlying the use of ultrasound to detect gallstones and foreigh bodies in tissues. Naval Med. Res. Reports, no. 4

Malet P.F., Takabayashi A., Trotman B.W., Soloway R.D., Weston N.E.(1984) Black and brown pigment gallstones differ in microstructure and microcomposition. Hepatology 4: 227-234

Malet P F., Williamson C.E., Trotman B.W., Soloway R.D. (1986) Composition of pigmented centres of cholesterol gallstones. Hepatology 6: 477-481

McIntosh D.M.F., Penney H.F. (1988) Gray-scale ultrasonography as a screening procedure in the detection of gallbladder disease. Radiology 136: 725-727

Purdom R C., Thomas S.R., Kereiakes J.G., Spitz H.B. (1980) Ultrasonic properties of biliary calculi. Radiology 136: 729-732

Romijn R L., Thijssen J.M., van Beuningen G.W.J. (1989) Estimation of scatterer size from backscattered ultrasound: a simulation study. IEEE Trans. Ultrasonics Ferroel. Freq. Control. 36: 593-606

Romijn R.L., Thijssen J.M., Oosterveld B.J , Verbeek A.M. (1991) Ultrasonic differentiation of intraocular melanomas: parameters and estimation methods. Ultrasonic Imag. 13: 27-55

Sackmann M., Delius M., Sauerbruch T., Holl J., Weber W. (1988) Shock-wave lithotripsy of gall-bladder stones; the first 175 patients. N. Engl. J. Med. 38: 393-397

Sauerbruch T., Delius M., Paumgartner G., Holl J., Wess O. (1986) Fragmentation of gall-stones by extracorporal shockwaves. N. Engl. J. Med. 314: 818-822

van der Steen A.F.W., Cuypers M.H.M., Thijssen J.M., de Wilde P.C.M. (1991) Influence of histochemical preparation on acoustic parameters of liver tissue, a 5 MHz study. Ultrasound in Med. & Biol. 17: 879-891

Swobodnik, W.(1985) Habilitationsschrift, University of Ulm

Thijssen J.M., Mol H., Timmer M.R. (1985) Acoustic parameters of ocular tissues. Ultrasound Med. Biol. 11: 157-161

Thijssen J.M., Oosterveld B.J., Romijm R.L. (1990) Phase derivative imaging III: theoretical derivation of first and second order statistics. Ultrasonic Imag. 12: 17-34

Tsuchiya Y., Ohto M., Yazawa T. (1986) Ultrasonic properties of gallstones: differentiation between cholesterol stones and pigment stones. Bil. Tract. Pancr. 7: 1483-1491

Verhoef W.A., Cloostermans M.J.T M., Thijssen J.M. (1985) Diffraction and dispersion effects on the estimation of ultrasound attenuation and velocity in biological tissues. IEEE Trans. Biomed. Eng 32. 521-529

Whalen, A.D. (1971) Detection of Signals in Noise. New York, Academic Press

APPENDIX

In this Appendix the properties of the individual stones are summarized (Table A1). CT-class, CT-morphology, classification by optical inspection and other optical properties are included, as well as the size of the stones.

Table A1 *Full listing of CT and optical classification criteria of stones (n=20) in this study. The meaning of the symbols used in the third and fifth colomn can be found in table II*

stone	CT class	CT morphology	optical class	optical morphology/ texture/ colour	size (mm)
1	IA	h	IA	n,c	10
2	IB	n	IIA	n,c	13
3	IA	h	IA	l,c,sm	11
4	IA	h	IA	l,c,sm	10
5	IB	n	IB	s,r,(n),c	13
6	II	s	IIB	s,n,c,ir	5
7	II	n	IIA	n,g,l,c	13
8	IA	h	IB	s,l,c	16
9	IB	s	IB	s,r,c	18
10	IB	n	IIC	l,c/g	10
11	IB	s	IB	s,r,n,c	16
12	IB	s,n	IB	s,r,(n),c	12
13	IIB	s	IIB	sm	6
14	IIB	s	IIB	sm	10
15	IIB	s	IIB	sm	5
16	IIB	s	IIB	sm	6
17	IIIA/B	h	IIIB	ir	5
18	IIIA/B	h	IIIA/B	ir	6
19	IIIA/B	h	IIIB	ir	3
20	IIIA/B	h	IIIB	ir	3

CHAPTER IV

ULTRASONIC SPECTROSCOPY OF THE PORCINE EYE LENS

A F.W. van der Steen, C.L. de Korte, J.M. Thijssen

ABSTRACT

The purpose of the work is to measure and study the acoustic characteristics of the porcine eye lens and find correlations with chemical and optical parameters, obtained from literature. Ultrasonic spectroscopy was performed by using a scanning acoustic microscope (frequency 20 MHz, resolution 150 μm). The transducer performed a two-dimensional scan over a central slice (1 mm thickness) of porcine lens (n=10). A double transmission pulse-echo method was used to acquire the ultrasonic data from the lens. Two dimensional images were reconstructed of the local ultrasound velocity and the frequency dependent ultrasound attenuation. Axial and equatorial profiles of these parameters were calculated from the images. The acoustic parameters are not constant, but show a systematic dependence on the location within the lens. The profiles of the acoustic parameters are similar in shape to profiles of the protein and water contents of eye lens and to the profiles of the optical refractive index. A thorough quantitative correlation study is indicated, which should be based on detailed protein content data in porcine lenses.

INTRODUCTION

Measurements of the acoustic characteristics of various ocular tissues have been made since the early days of diagnosis by ultrasound (i.e. echography). The techniques employed for measuring the velocity of ultrasound were rather sophisticated. Greenspan & Tschiegg (1957) applied a "sing around" technique in which the received signal was used to drive the transmitter circuit. Both a through-transmission technique, where the transmitted pulse was measured by a separate receiving transducer, and a double transmission technique, in which the echo from a ground plate supporting the specimen was received by the transmitting transducer, were used.

Another technique made use of a so-called interferometer. The ultrasonic equipment was connected simultaneously to two transducers and operated in pulse-echo mode. One transducer was directed onto the tissue specimen and the other was mounted in a water bath in which a plate could be positioned at an accurate adjustable distance. By moving this latter plate until its echo coincided exactly with the echo from the ground plate covered by the specimen, a rather accurate assessment of the velocity of sound could be made (Jansson & Sundmark 1961). Surveys of the velocity data have been published in the literature (Coleman *et al.* 1977, Thijssen *et al.* 1983, Thijssen *et al.* 1985, Haigis 1989, Goss *et al.* 1978).

There is limited data concerning the attenuation of ultrasound in ocular tissues in the literature At the transmitting frequencies of the transducers employed in diagnostic ultrasound equipment the attenuation by the relatively thin ocular tissues is low For this reason estimating the attenuation from the oscilloscope image of the echo traces could not be highly accurate (Oksala & Lehtinen 1958, Coleman *et al* 1977, Thijssen *et al.* 1983, Thijssen *et al.* 1985, Haigis 1989, Goss *et al.* 1978).

In the present paper the calculations of the ultrasound velocity and attenuation parameters were made after analog-to-digital conversion (ADC) by a digital oscilloscope. The computer programs enabled a calculation of the time of flight of echoes in a double-transmission technique by using a spectral method with a high precision (Thijssen *et al.* 1983, Thijssen *et al.* 1985, Verhoef *et al.* 1985) The attenuation parameters were estimated using another spectral method. Moreover, a two-dimensional scan was made by an acoustic microscope, yielding two-dimensional images of the local values of three acoustic parameters: the velocity of ultrasound, the attenuation at 20 MHz and the frequency dependence of the attenuation coefficient.

Thijssen *et al.* (1983,1985) made single measurements of the ultrasound velocity and the attenuation coefficient of some ocular tissues, while using basically the same spectroscopic methods as discussed in the present paper. However, they did not succeed in measuring the characteristics of the eye lens with great precision because it appeared difficult to align the transducer exactly perpendicular to both the anterior and posterior lens surfaces simultaneously

The measurements discussed in the present paper were performed on a flat slice of the porcine lens, taken from the centre and containing the eye axis. In these slides the acoustic parameters were calculated at a high resolution. In this way the local acoustic parameters could be measured as a function of location in the lens. Because the acoustic parameters showed a systematic gradient from the centre to the periphery of the lens, and because some correlations of the parameters with tissue components were known from the literature, further attempts were made to relate the acoustic measurements to protein, water and optical refractive index data.

METHODS

Materials

Porcine eyes (4 months) were obtained from the municipal slaughtery and measured within four hours post mortem. The anterior segment of the eyes was removed circularly at the limbus by a pair of scissors. The zonula fibres were then cut and the lens capsula was carefully removed by the scissors. The lens was sliced by a comb-like cutting knife. A slice of 1 mm. that contained the eye axis was cut and taken for measurements (Fig. 1.). Damage to the cortex could not be prevented in all cases due to the sectioning method. For this reason in some of the ten lenses that were measured the attenuation could not be estimated in the area of the cortex.

Instrumentation

The basis for the techniques used here was introduced by Foster *et al.* (1984). It is a scanning microscope technique operating at supra-microscopic resolution level. This resolution is directly related to the characteristics of the employed ultrasound transducer The transducer that is used in this study (V317, Panametrics Inc , central frequency 20 MHz, -6 dB bandwidth 11 MHz, diameter 6 mm., focal length 12.5 mm.) yields a resolution of 0.15 mm.

The measurement equipment has been extensively described in earlier publications (van der Steen *et al.* 1991, van der Steen *et al.* 1993a, Chapter VII-VIII). The ultrasound transducer is mounted in a 3D microscope positioning system ($\Delta x = \Delta y = 1\ \mu m$, Δz continuously adjustable) (Marzhauser, GmbH). The transducer is excited by a short electrical pulse from a transmitting device (AVG-3-C, Avtech, Inc.). The echoes received at the transducer are preamplified by a custom-made receiver (20 dB, bandwidth at -6 dB: 0.5-150 MHz) and then, after passing an anti-aliasing low pass filter (7th order Bessel, cut off frequency 70 MHz), digitized in 8 bit by a digital oscilloscope (DSA 601, Textronix, Inc.) at a sampling rate of 100 MHz. The oscilloscope was interfaced to an IBM compatible PC that also controlled the XY-translation of the cross-table. After completion of a scan the data were transferred for off-line processing to a minicomputer (Microvax 3200, Digital Equipment, Inc.).

Measurements

The lens slice was put on a horizontal plexiglass plate in a physiological saline solution and then covered by a polyethylene membrane ($3\mu m$ thickness, ultrasound attenuation less than 0.2 dB). The transducer was lowered into the liquid until the focus of the sound beam reached the top surface of the plate. The computer then controlled a 2D raster scan, (100x80 points), while pulse-echo measurements were performed on-the-fly after every 150 μm translation. Then the lens was removed and a reference scan was performed at exactly the same positions as the first one. Measurements were performed at room temperature (20 °C). A full scan took 17 minutes.

Data processing

At each of the measurement points the ultrasound velocity and two spectral attenuation parameters were calculated. The local velocity was calculated from the known velocity in physiological saline solution and the times of flight of the reference plexiglass plate reflection, the plexiglass plate reflection with the lens interposed and the membrane reflection (Thijssen *et al.* 1983, Thijssen *et al.* 1985, Verhoef *et al.* 1985). The local attenuation spectrum was calculated from the spectra of the two plexiglass reflections and the local thickness of the lens that was calculated from the same data as the local velocity (Appendix A). It was characterized by the slope of the spectrum between 17 and 23 MHz, (which corresponds to the - 6dB bandwidth of the measurement system after attenuation in the lens specimen) and the value at 20 MHz.

2D images of the three acoustic parameters were constructed and displayed without any filtering. Profiles of the parameters along the axial and equatorial axes were obtained from these images. First a 3x3 points mean filter was applied to the image and then the profiles were estimated horizontally and vertically through the centre of the image. These profiles were obtained in 10 lenses and then averaged.

A least square second order polynomial fit to these profiles was calculated along the axis of the lens from the centre of the lens to the anterior and the posterior side and along the equator form the centre to the edge. The model that is used for this fit corresponds to:

$$A(r) = \beta_0 + \beta_1 r + \beta_2 r^2 \qquad (1)$$

where: A = local value of parameter
β_0 = value of parameter in centre

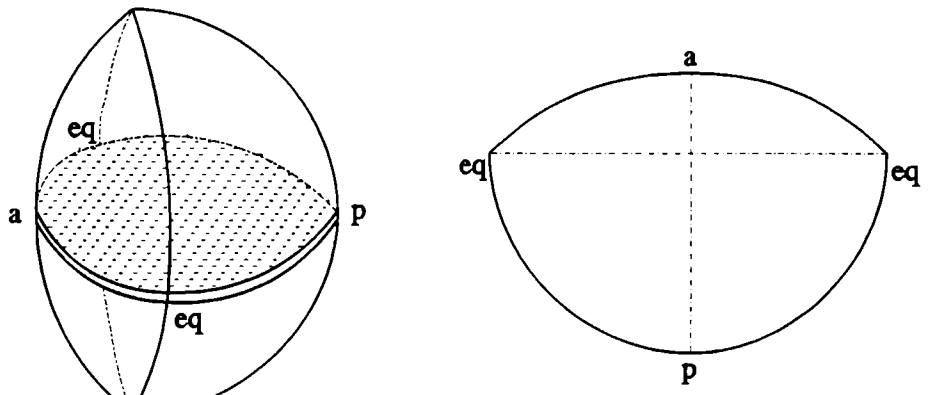

Fig. 1. The section that is cut from the eye lens.
A. Position of axial section
B. Section with profiles directions indicated.

β_1, β_2 = constants of increase with increasing eccentricity
r = distance to centre (i.e. eccentricity) [mm]

The fit was performed on those data that were not affected by cutting artifacts, as assessed from the averaged profiles of the attenuation at 20 MHz. The artifacts were considered to be present from the eccentricity where there was an obvious increase in the 95% confidential limits of the data towards larger eccentricities (Figs. 3,4.). The same boundaries were taken in all parameter profiles.

The Pearson correlation coefficient of the acoustic parameters was calculated in this region in the axial profiles of the separate lenses and then averaged. Before the averaging a Fisher-Z transform was applied to correct for the asymmetric distribution of the Pearson correlation coefficient (Snedecor & Cochran 1979, van der Steen *et al.* 1993b, Chapter IX). After averaging the inverse Fisher-Z transform was applied to the average correlation coefficient and the boundaries of the 95% confidence interval.

Furthermore the average values of the acoustic parameters along the anterior-posterior profiles (i.e. along the eye axis) were calculated. These values correspond to the bulk values that were measured in history and can be found in literature.

RESULTS

Velocity of ultrasound

An example of a 2D image of the ultrasonic velocity of the eye lens is shown in Fig. 2B. The grey levels have been encoded such that increasing whiteness indicates higher velocity (1500-1700 m/s) A gradual decrease of the ultrasound velocity from the centre to the periphery of the lens becomes evident in Fig 2B. The mean data of the velocity (n = 10) along the axial- (i e centre-anterior and centre-posterior) and the equatorial axes are shown in Fig. 3A. and 4A. The 5 and 95 percentiles are displayed by dashed lines in these plots. The best fitting second order polynomial regression lines were calculated and are shown as drawn lines. The parameters of this fit are listed in Table I. The choice of the polynomial approach has been inspired by a paper on refractive index profiles, as is discussed further-on (Discussion) and by the obvious parabolic shape of the profiles. It can be seen in Fig. 3A. that the anterior range from the centre of the nucleus to the cortex border is smaller than that for the posterior part.

Ultrasound attenuation

The 2D image of the attenuation coefficient at 20 MHz is shown in Fig. 2C. As with the velocity (Fig. 2B), the attenuation coefficient is highest in the centre of the nucleus and gradually decreases towards the periphery, both in axial and in equatorial directions. The already mentioned damage to the equatorial cortex by the slicing knife shows clearly in the measured profiles (Figs. 3B. and 4B) For this reason the second order regression analysis was limited to the central part of the profiles The parameters of the fitted lines are listed in Table I

The slope of the linear regression fit to the attenuation coefficient vs frequency data was also used for calculating 2D images of the lens sections, an example is shown in Fig 2D. Although the latter image displays more irregularities than the other two shown in Figs 2B. and 2C., the trend of the grey levels from centre to periphery is quite similar. The profiles calculated along the axial and equatorial axes of the lens section are displayed in Figs. 3C. an 4C A second order curve fit was performed also for the slope data, the parameters of which are listed in Table I.

Correlations

The average Pearson correlation coefficients of the acoustic parameters along the eye axis, as well as the values for the 95 % confidence limits are listed in table II. The correlation between the velocity and the attenuation at 20 MHz is very high. The correlation with the attenuation coefficient slope is somewhat lower This is probably caused by the fact that this parameter is harder to estimate (See Fig 2D.).

Average values

The average values of the acoustic parameters over the eye axis are listed in table III. These data are suited for a comparison with data on measurements of intact lenses from literature.

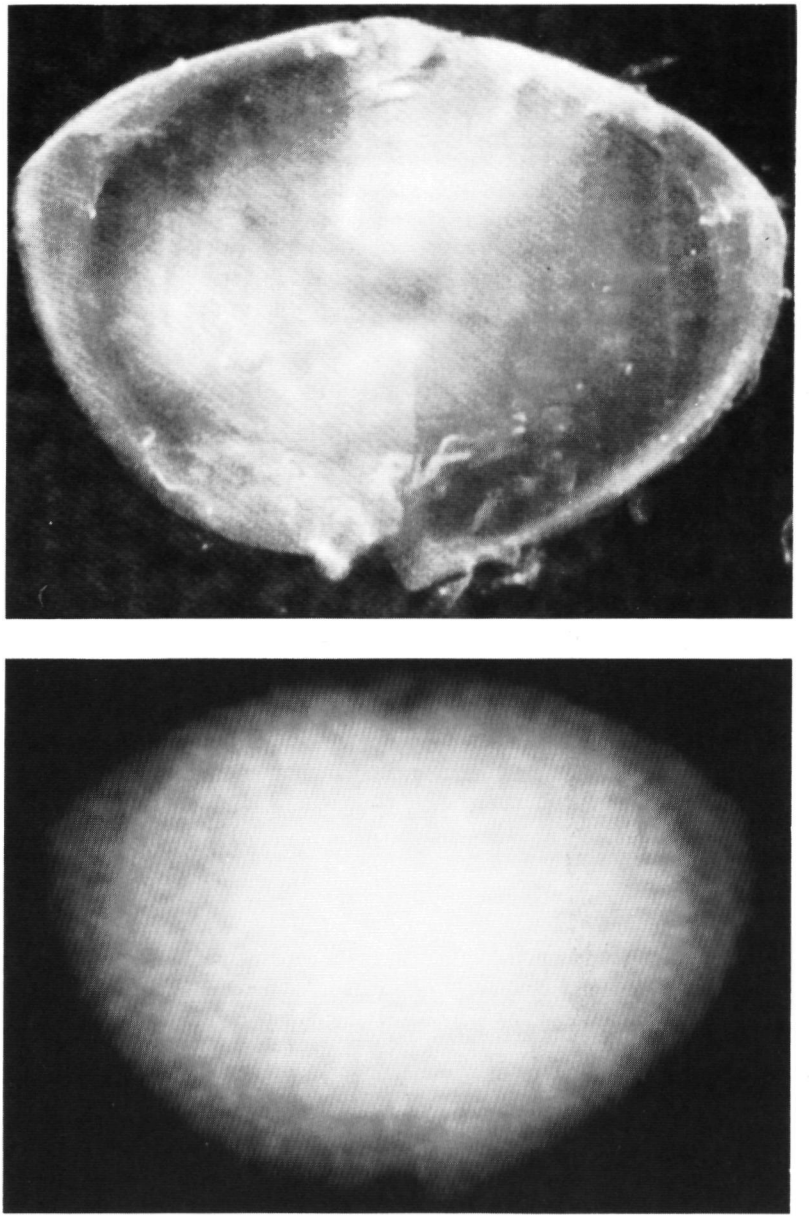

Fig. 2. Optical and acoustical parametric images of a representative slice of eye lens. Minor cutting artifacts are visible in all four images at the anterior and posterior cortex.
A. Optical image
B. 2-D velocity of ultrasound (range 1500 to 1700 m/s)

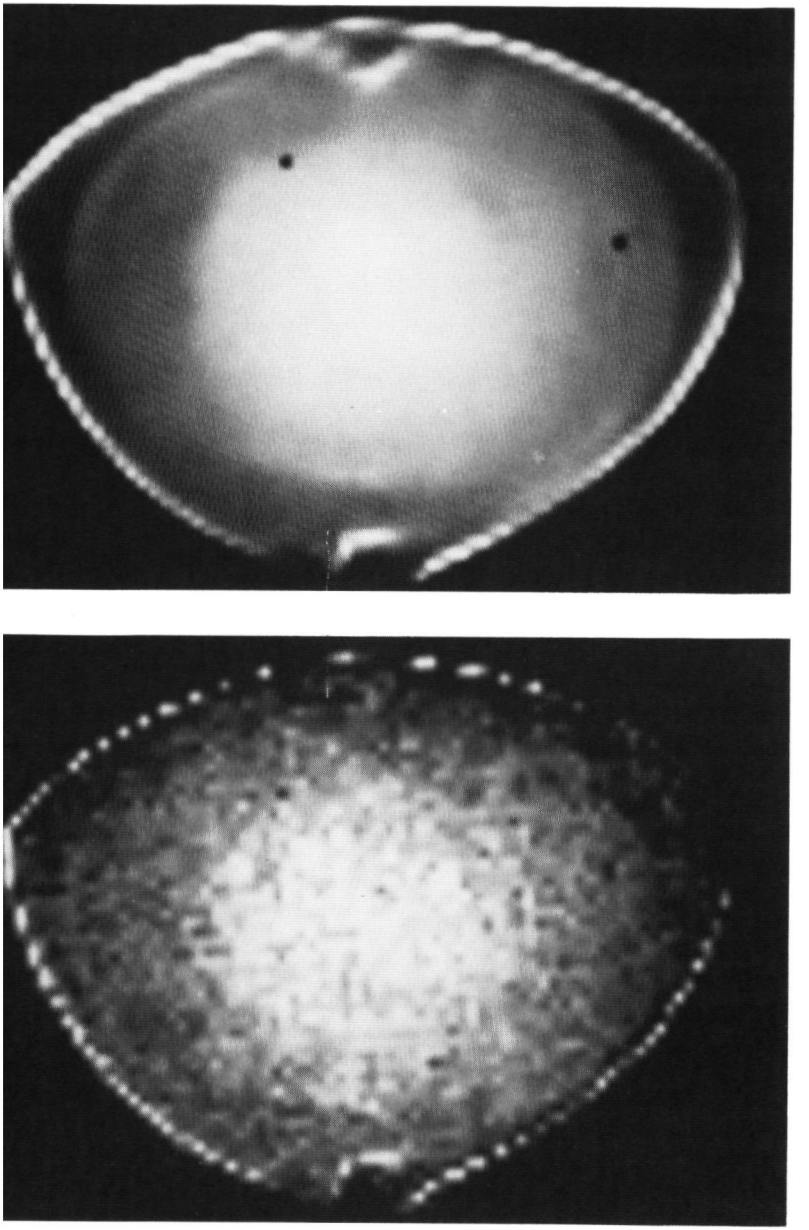

C. 2-D attenuation coefficient at 20 MHz (range 0 to 50 dB/cm)
D. 2-D attenuation coefficient slope (range 0.5 to 2.35 (dB/cm · MHz))

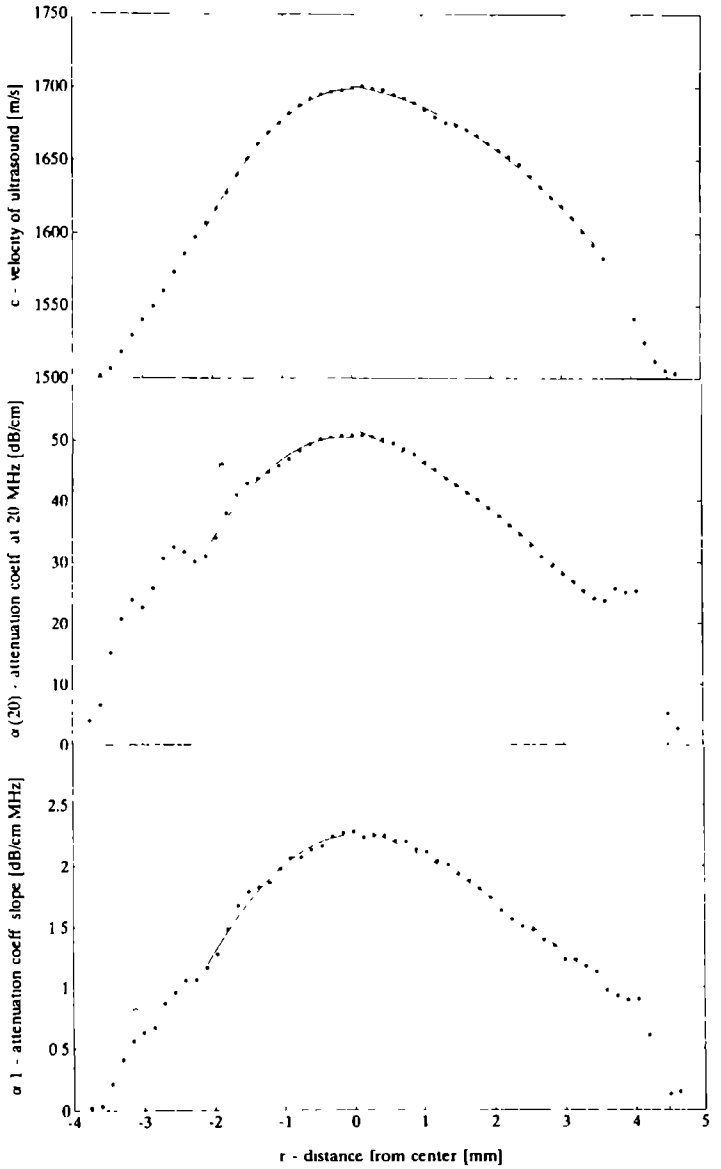

Fig. 3. Profiles of the ultrasound parameters in the eye lens along the eye axis, from anterior to posterior. Mean data are indicated by asterisks and 5% and 95% percentiles by dashed lines. In the profiles least square second order polynomial fits are displayed by a drawn line (See also Table I).
Upper panel: ultrasound velocity
Middle panel: attenuation coefficient at 20 MHz
Lower panel: attenuation coefficient slope

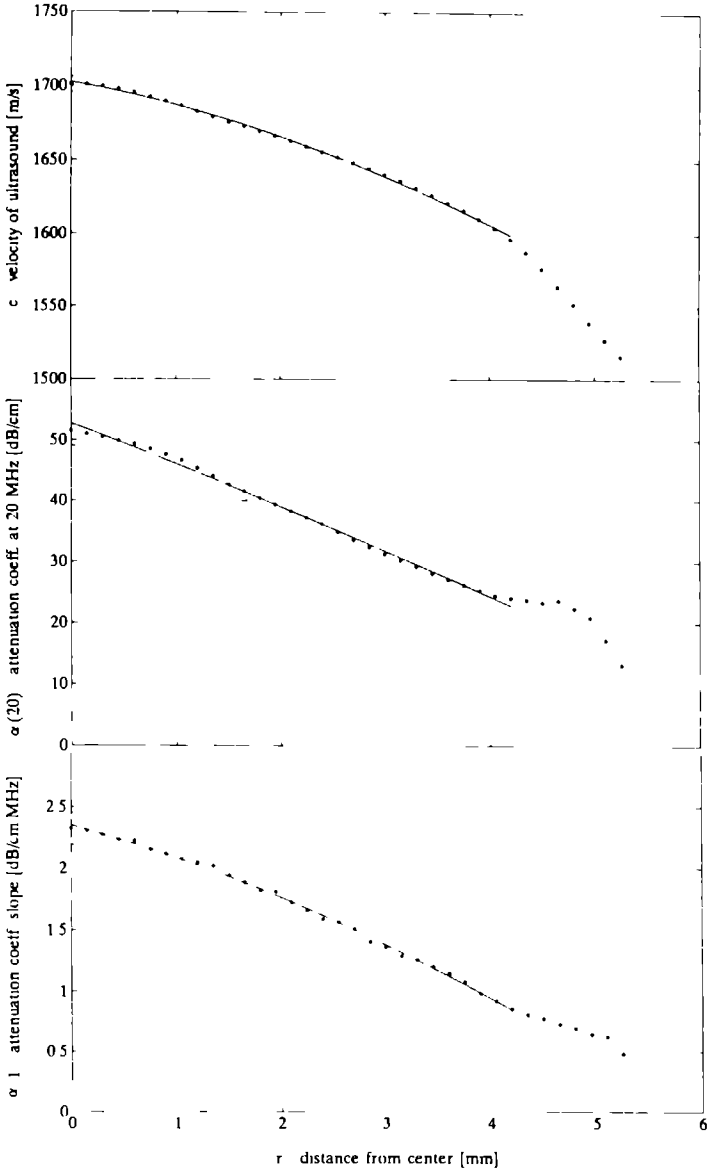

Fig 4 Profiles of the ultrasound parameters in the eye lens perpendicular to the eye axis. Mean data are indicated by asterisks and 5% and 95% percentiles by dashed lines. In the profiles least square second order polynomial fits are displayed by a drawn line (See also Table I)

Upper panel ultrasound velocity
Middle panel attenuation coefficient at 20 MHz
Lower panel attenuation coefficient slope

Table I *Parameters of second order regression fit through data of Figs 3 and 4*

	profile	β_0	β_1	β_2	RMSE
velocity	EQ	1703	-12.6	-2.9	1.084
[m/s]	AA	1699	0.0	-21.6	0.971
	AP	1701	-6.9	-7.0	1.551
$\alpha(20)$	EQ	52.84	-6.72	-0.10	0.558
[dB/cm]	AA	50.34	1.26	-4.77	0.725
	AP	51.82	-4.57	-1.09	0.479
α_1	EQ	2.35	-0.239	-0.028	0,018
[dB/cm.MHz]	AA	2.25	-0.011	-0.236	0,041
	AP	2.33	-0.206	-0.048	0,040

Table II *Averaged Pearson correlation coefficients and 95 % confidence limits of the acoustic data*

	velocity	$\alpha(20)$	α_1
velocity	1.000	0.963 (0.915-0.984)	0.915 (0.877-0.942)
$\alpha(20)$		1.000	0.892 (0.824-0.935)
α_1			1.000

Table III *Averaged values of the acoustic parameters along the eye axis*

velocity	1629 m/s
$\alpha(20)$	36.6 dB/cm
α_1	1.52 dB/cm · MHz

DISCUSSION

Three acoustic parameters were measured in the porcine eye lens and imaged at a high resolution (0.15 mm). The obtained results show that these parameters are not constant in the eye lens. The velocity varies within the lens from 1500 to 1700 m/s. Former papers only mentioned one value for the ultrasonic velocity in the porcine lens, probably presuming that it was constant over the lens. The values from literature (Goss *et al.* 1978) range from 1627 to 1672, with an exception of the value measured by Yamamoto *et al.* (Quoted by Goss *et al.* (1978)) who measured a value of 1530 m/s. The average value along the eye axis found in this study is 1630 m/s (Table III) which is well within the range of the values from literature. No values were found for the attenuation of porcine lenses.

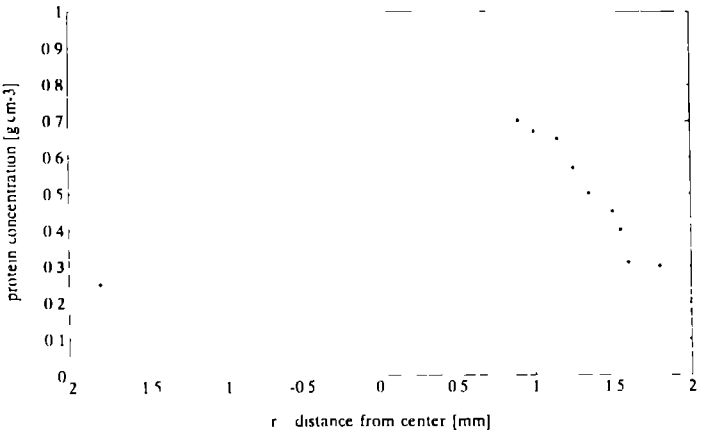

Fig 5 Axial protein profile in a rat lens as measured by Philipson (1969)

The profiles found in this study showed great similarity with profiles of protein content in the lens of mammals, other than pig, that were found in literature (Philipson 1969, Huizinga *et al.* 1989) (Fig. 5.) The results of the detailed measurements of the acoustic parameters of the porcine lens cannot directly be related to the chemical constituents, nor to the structural properties, because of the limited data from literature; only one paper was found: Deussen *et al.* (1989) estimated the water contents of the nucleus (60 percent), the anterior cortex (84 percent) and the posterior cortex (75 percent). It is known from the ultrasound literature that the velocity of ultrasound is modified with respect to the ultrasound velocity in water primarily by the globular proteins (denoted by P in the following) and the structural proteins, i.e. the collagen (C). These effects would be reversed by the lipid contents, which is of the order of two percent in the lens and is neglected in this discussion. Goss *et al* (1980) extrapolated the following relation for the velocity (obtained from other data from literature, acquired at varying temperatures, average 27°C):

$$c = c_0 + 3.2 \cdot P + 6.5 \cdot C \quad [m/s] \tag{2}$$

where c_0 = ultrasound velocity in a physiological saline solution [m/s].
Due to the absence of collagen in the lens this formula reduces to:

$$c = 1500 + 3.2 \cdot P \quad [m/s] \tag{3}$$

where the velocity in physiological saline solution has been taken 1500 m/s.

When the data of Deussen *et al.* (1989) are inserted in Eq.(3) the velocities in Table IV are obtained. These values are at least in the correct range as can be seen by comparing with Fig. 3. A more detailed quantitative correlation of protein content and ultrasound velocity is not possible from our data, because a profile like Fig. 5. is not available for the protein in porcine lenses.

Table IV *Mean velocity values predicted from porcine protein concentrations (Deussen and Pau 1989)*

	percentage proteins	velocity of ultrasound c [m/s]
ant cortex	16	1564
nucleus	40	1641
post cortex	25	1593

A formula equivalent to Eq (1) was found by regression analysis of the profile of the refractive index of bovine lenses Piercionek 1989) The refractive index n is related to the protein concentration P in a similar fashion (Cambell 1984) as the ultrasound velocity, (Eq. (3)) the modified so-called Gladstone-Dale formula (Barer & Joseph 1954)

$$n = n_0 + \Delta_p \; P \qquad (4)$$

where n_0 = refractive index of saline solution ("solvent") = 1 335 (Philipson 1969)
Δ_p = protein specific increase factor ($=2\ 5\ 10^{-3}\ [\%]^{-1}$, as can be deduced from Philipson (1969), for rat lenses)

Therefore, the profiles obtained by ultrasonic velocity measurements should be closely related to those valid for the optical index of refraction if Eq. (3) is valid in the eye lens, since both are linearly related to the protein concentration profiles.

No simple relationship is found in literature between protein content and attenuation. Goss *et al.* (1980) measured attenuation in globular protein solutions and collagen suspensions at various concentrations, but were inconclusive about biological tissues The profiles measured in this study show great similarity to the profiles of velocity measurements The Pearson correlation coefficient of attenuation coefficient at 20 MHz and velocity is higher than 0 96, see table II This means that once the relationship between protein content and ultrasound velocity is exactly known, a relationship between protein and attenuation in the eye lens easily can be deducted

It can be stated then, that the velocity and attenuation profiles, as well as the optical refractive index profiles have to display a comparable shape when plotted vs. distance from the centre In principle by using Eqs. (3 and 4) all the profiles can be predicted once the parameters of the protein concentration profile in Eq (1) are estimated These data will hopefully be produced in near future

WORKS OF REFERENCE

Barer K., Joseph S. (1954) Refractometry of living cells. I. Basic principles. Q J Microscop Sci 95: 399-423

Campbell M.C.W. (1984) Measurement of refractive index in an intact crystalline lens. Vision Res. 24: 409-415

Coleman D.J., Lizzi F.L., Jack R.L. (1977) Ultrasonography of the Eye and Orbit Philadelphia, Lea and Feibiger

Deussen A., Pau H. (1989) Regional water content of clear and cataractous human lenses. Ophthal Res. 21: 374-380

Foster F.S., Strban M., Austin G (1984) The ultrasonic macroscope. initial studies of breast tissue. Ultrasonic Imag. 6: 243-261

Goss S.A., Johnston R.L., Dunn F. (1978) Comprehensive compilation of empirical ultrasonic properties of mammalian tissues J Acoust. Soc. Am. 64: 423-457

Goss S.A , Frizell L.A., Dunn F. (1980) Dependence of the ultrasonic properties of biological tissue on constituent proteins. J. Acoust Soc. Am. 67: 1041-1044

Greenspan M., Tschiegg C.E (1957) Speed of sound in water by a direct method. Rev Sci Instr. 28: 257-265

Haigis W (1989) Akustische Daten der Gewebe und Flussigkeiten des menschlichen Korpers (insbesondere von Augen und Orbita) In: Buschmann W, Trier HG. Ophthalmologische Ultraschaldiagnostik. Berlin/Heidelberg/New York, Springer-Verlag: 394-398

Huizinga A., Bot A.C.C., de Mul F.F.M., Vrensen G.F.J.M., Greve J. (1989) Local variation in absolute water content of human and rabbit eye lenses measured by Raman microspectroscopy. Exp Eye Res.48: 487-496

Jansson F , Sundmark E (1961) Determination of the velocity of ultrasound in ocular tissues at different temperatures Acta Ophthal. 39: 899-910

Kontonassios T., Ophir J. (1987) Variance reduction of speed of sound estimation in tissues using the beam tracking method. IEEE Trans UFFC 34: 524-536

Nicholas D. (1982) Evaluation of backscattering coefficients for excised human tissues: results, interpretation and associated measurements Ultrasound in Med. & Biol. 8: 17-28

Oksala A., Lehtinen A. (1958) Absorption of ultrasound in the aqueous humour, lens and vitreous body. Acta Ophthal. 36: 761-768

Philipson B. (1969) Distribution of protein within the normal rat lens. Invest. Ophthal 8: 258-270

Piercionek B.K. (1989) Growth and aging effects on the refractive index in the equatorial plane of the bovine lens. Vision Res 12: 1759-1766

Snedecor G.W , Cochran W.G. (1979) Statistical methods 6th edition, 10th printing, Iowa state University Press, Iowa

van der Steen A.F.W., Cuypers, M.H.M., Thijssen J.M., de Wilde P.C.M. (1991) Influence of histochemical preparation on acoustic parameters of liver tissue: a 5 MHz study Ultrasound in Med. & Biol. 17: 897-891

van der Steen A.F.W., Thijssen J.M., van der Laak J.A.W.M., Ebben G.P.J., de Wilde P C.M. (1993a) A new method for correlation of acoustic spectroscopic microscopy (30 MHz) and light microscopy. J. Microscopy (in press)

van der Steen A.F.W., Thijssen J.M., van der Laak J.A.W.M., Ebben G.P.J., de Wilde P.C.M. (1993b) Correlation of histology and acoustic parameters of liver tissue on a microscopic scale. Ultrasound in Med. & Biol. (in press)

Thijssen J.M., Mol H.J.M., Cloostermans M.J.T.M., Verhoef W.A., *et al.* (1983) Acoustic parameters of ocular tissues. In: Hillman JS, LeMay MM, eds. Ophthalmic Ultrasonography. The Hague/Boston/Lancaster, Dr. W. Junk Publ.: 455-450

Thijssen J.M., Mol H.J.M., Timmer M.R. (1985) Acoustic parameters of ocular tissues. Ultrasound in Med. & Biol. 11: 157-161

Verhoef W.A., Cloostermans M.J.T.M., Thijssen J.M. (1985) Diffraction and dispersion effects on the estimation of ultrasound attenuation and velocity in biological tissues. IEEE Trans Biomed Eng: 521-529

CHAPTER V

SPECTRAL ACOUSTIC PROPERTIES OF EYE TISSUES

C.L. de Korte, A.F.W. van der Steen, J.M. Thijssen

ABSTRACT

The ultrasound velocity and frequency dependent attenuation of human and porcine eye tissues (cornea, lens, retina, choroid, sclera, vitreous body) were measured in the frequency range from 17 to 23 MHz. The results for the ultrasound velocity were compared to values taken from literature and appeared to be in the same range. Next, a comparison made between the acoustic parameters of human and porcine eyes showed that the porcine eye can serve as an animal model for the human eye. A mathematical operation is used to extrapolate the attenuation to the lower frequencies that are commonly used in clinical equipment. Finally, a first attempt was made to investigate the age dependence of the acoustic parameters of human tissues: some tissues showed a significant age effect.

INTRODUCTION

In ophthalmology, the interest in quantitative echography has a long tradition. During the late fifties and early sixties, several authors reported on measurements of the sound velocity in various ocular tissues. Interferometric and electronic techniques were used for the measurements. Compilations and summaries of these data can be found in several publications (Coleman *et al.* 1977, Chivers & Parry 1978, Duck 1980, Goss *et al.* 1980, Thijssen *et al.* 1985, Haigis *et al.* 1989). Data can be found in this literature on human eyes and e.g. porcine eyes, at room temperature and at body temperature. Most probably because of the small thickness of the retina and choroid, data on these structures are scarce reported. Only one paper was found that gave some values (Thijssen *et al.* 1985).

Attenuation by ocular structures has been reported in the literature mentioned before, but the data are rather sparse. Moreover, the data were based on the visual equalization of the echo amplitudes, by using a calibrated gain control for the adjustment. The precision and accuracy of this technique of attenuation measurement remains unclear.

In addition to these fundamental approaches of quantitative measurement, in clinical echo-ophthalmology one is using visual, but still quantitative, assessments of the reflectivity level and echo decay in tissues (Buschmann 1966, Ossoinig 1974, Poujol 1981). These clinical approaches have been expanded by a quantitative analysis of the echographic signals and images by computer methods. This latter work started with the analysis of demodulated (video) A-mode lines (Decker 1973, Trier *et al.* 1973, Thijssen *et al.* 1981) and has evolved to *in vivo* clinical pilot studies based on spectral analysis of radio frequency echosignals and texture analysis

of B-mode images (Lizzi *et al.* 1976, Trier *et al.* 1983, Coleman *et al.* 1985, Feleppa *et al.* 1986, Romijn *et al.* 1991, Thijssen *et al.* 1991)

These latter studies were based on the concept of homogeneous backscattering media, while neglecting the disturbance of the propagation of ultrasound by ocular structures. In particular, the reflectivity level and backscattering spectrum are more susceptible to be influenced by such disturbances. The aim of the present study was to estimate the sound velocity and attenuation characteristics of the relevant ocular structures: cornea, lens, vitreous, retina, choroid and sclera. These data will enable the investigation of the influence of ocular structures on the ultrasonic beam propagation. Because most melanomas are assessed by transocular scanning, the beam has to travel forth and back through the eye, and it passes several structures. The aforementioned problem of measuring the attenuation coefficient of thin layers necessitated the authors to employ a relatively high ultrasound frequency: 20 MHz. The estimated attenuation parameters, therefore, have to be extrapolated to other frequencies (clinical frequencies 5 to 10 MHz) To this end a model is proposed, describing the frequency dependence of the attenuation coefficient

Because of the relative abundance of acoustic data of porcine eyes in the early literature and the relatively poor availability of human donor material, this study comprises both types of eyes. The human eyes comprised a range of the age of donors and a first attempt was made to assess any age dependence of the acoustic parameters of the various ocular structures.

METHODS

Materials

Porcine eyes (4 months old) were obtained from the municipal slaughtery and measured within four hours post mortem The separate eye tissues were taken from different pigs. At least 10 samples were measured for all tissues. The cornea was removed by cutting it together with the limbus to prevent swelling, which will start at the edge. The lens was taken by removing the total anterior segment of the eye. The lens fibres were cut and the lens was taken out. Next it was placed in a comblike knife and a slice of 1 mm was cut, containing the eye axis, as shown in Fig. 1. (van der Steen *et al.* 1993a). Due to the slicing method the cortex could not always be prevented from damaging. Retina, choroid and sclera tissue samples were taken by cutting a piece of tissue at the equator of the eyeball. The retina was prepared by separating it from the choroid. The choroid was taken by selecting a piece of tissue at the equator of the eyeball among two of the major blood vessels, present at the equator. Here the choroid was not strongly fixed to the sclera. The sclera was prepared in the same way as the choroid. The vitreous body was taken after removing the anterior segment and the lens.

Human eyes ($n=13$) were obtained from donor eyes in an age range from 19 to 86 years. All tissues, except for the cornea, were measured 24 to 36 hours post mortem. Because the corneas had been used for transplantation, no corneas were obtained from these donor eyes. The measured corneas were keratocone and taken from patients who received a cornea transplantation. The parts of these corneas that were selected for measurement were taken from areas having a normal curvature. The lens, retina, choroid and sclera tissues of human eyes were prepared in the same way as the porcine tissues.

EQUIPMENT

An extensive description of the scanning acoustic microscope (SAM) has been given by van der Steen *et al* (1993b), (Chapter IV). With this microscope it is possible to measure local acoustic parameters of samples of biological tissues. The transducer used in this study had a central frequency of 20 MHz and yielded a lateral resolution of 0.15 mm.

ACQUISITION

The tissues were placed in a watertank, filled with a degassed physiological saline solution of 20 °C. To determine the acoustic parameters three protocols have been used

The first protocol has been used for lens slices and is described in Chapter IV The slice was placed on a horizontal plexiglass plate and covered by a polyethylene membrane. A scan of measurements was performed with and without the tissue interposed.

The second protocol has been used for curved tissues, which had reflections that were in the order of 10% of the plexiglass reflection (cornea and porcine sclera) It has been described by Goedegebure *et al.* (1992, Chapter III). The tissue was positioned on a ring (thickness 2 mm, $\varnothing_{inside}$ 6 mm, $\varnothing_{outside}$ 16 mm), and the back surface of the tissue was 0.5 mm in front of the plexiglass plate (Fig. 3B). Again a scan was performed with and without the tissue interposed.

The third protocol is called the variable path length method (Verbeek *et al* , 1981). It has been used to determine the ultrasound velocity in the vitreous body. The space between the transducer (with the focus at the top of the plexiglass plate) and the plexiglass plate was totally filled with two vitreous bodies (this because the volume of one vitreous could not fill the entire space between transducer and the focal zone of the transducer). Five scans (10x10 points $\Delta x=\Delta y=75$ μm.) at different distances to the focus (-0 50, -0.25, 0.00, 0 25, 0.50 mm) were performed.

DATA PROCESSING

The local ultrasound velocity, the attenuation at 20 MHz ($\alpha(20)$) the attenuation spectral slope at 20 MHz (α_1) were obtained using the data processing described in Chapters III and IV

The velocity in the vitreous body was calculated by performing a linear regression analysis of the mean time-of-flight of the echo versus the vertical position of the transducer (Thijssen *et al* 1985).

The precision of the estimation of the velocity is dependent on the thickness of the tissue (3 0% (i e 24 m/s) for a tissue with a thickness of 100 μm up to 0 3% (i.e. 2.4 m/s) for a thickness of 1.0 mm)

The precision of the attenuation parameters was dependent on the accuracy of the thickness estimation, the actual attenuation (which is thickness dependent) and the accuracy of the DSA, which is 7 bits effectively. After calculation of the attenuation spectrum from the rf-data and the interpolation of the attenuation spectrum, an exact estimation for the intrinsic accuracy of the attenuation parameters could not be calculated anymore.

The frequency dependence of the attenuation is determined by fitting the following function to the data (Wells 1977, Bamber 1985):

$$\alpha(f) = A_{f_0} \cdot \left(\frac{f}{f_0}\right)^b \quad [dB/cm] \tag{1}$$

Like in the aforementioned literature, f_0 was taken 1 MHz.
In this formula it is implicitly assumed that the attenuation is zero at 0 MHz. The parameters of the model were obtained from the data as follows:

$$b = 20 f_0 \frac{\alpha_1}{\alpha(20)} \tag{2}$$

$$A_{f_0} = \frac{\alpha(20)}{20^{20 f_0 \left(\frac{\alpha_1}{\alpha(20)}\right)}} \quad [dB/cm] \tag{3}$$

The attenuation at clinical frequencies can be determined from Eq. 1.

The age dependence of the acoustic parameters of the human eyes has been investigated. Since the number of observations was low, it was not possible deduce a good model from the data by fitting. Linear regression has been proven to be a good model to describe the age effects of acoustic parameters in liver tissue (Hartman *et al.* 1991). For this reason this model was applied. The significance of an age effect is investigated by dividing the observations in two groups (younger than 50 years and older than 50 years) and then applying a Wilcoxon test to the groups. This is a non parametric rank test.

STATISTICS

From the acoustic parameters the following variables were calculated (Armitage, 1973):

1. mean — mean of the parameter
2. sd — standard deviation
3. sd_{inter} — inter tissue standard deviation
4. sd_{intra} — intra tissue standard deviation

These statistical parameters were calculated for the cornea, retina, choroid and sclera. The parameters of the lens were determined along the axial profile. A 3x3 points mean filter was applied over the full scan to smooth local variations. Next, the average along the profile was calculated. The mean and inter-lens standard deviation (sd_{inter}) of the average value of all profiles were calculated. For the vitreous body the mean and standard deviation (sd_{inter}) of the values of the velocity were calculated

RESULTS

The acoustic parameters of human and porcine eye tissues are listed, respectively in Table I and Table II. The values of statistical variables were given for all tissues except the lens and the vitreous. The value for the intra individual spread of these tissues, as well as the thickness was not obtained from the measurements as was described above.

The estimated attenuation parameters of Eq. 1 are summarized in Table III. It is shown that the order b is higher than 1 except for the lens. The parameter A_f shows a large standard deviation.

The results of the linear regression analysis and Wilcoxon tests to investigate the influence of the age on the acoustic parameters for the human eye tissue are summarized in Table IV and an example is given in Fig. 1. Some caution should be taken to the interpretation of the values for the coefficients and p values because of the limited number of observations from which they were deduced. The attenuation parameters show a significant age effect in the lens ($p < 0.05$). The sclera expresses a significant age effect for all three parameters ($p < 0.05$).

DISCUSSION

The results of the sound velocity measurements (Tables I and II) display an intra individual standard deviation which is comparable to the value that can be expected from the error analysis (see Methods, Data Processing). The inter individual standard deviation may be explained from several phenomena: biological variability of the acoustic characteristics, influence by the temperature at which the measurements were performed, and for the human tissues, the effect of age.

The temperature of the physiological saline solution in which the measurements were performed was not controlled actively. The temperature was measured and a range of 20 ± 1 °C was observed. Since the value of the reference velocity is always taken as the velocity in saline solution at 20 °C and the temperature effect will be practically identical for both the ocular tissues and saline in this short range (2 °C), this effect is negligible.

The inter individual standard deviation of the velocity data for the human cornea and retina are much larger than for the porcine eye. However, the velocity data for the retina did not display a significant age dependence (Table IV). Therefore, it has to be concluded that the most obvious explanation of the inter individual standard deviation of the velocity data of the retina is the biological variability of this acoustic parameter. The inter individual spread in the acoustic parameters of the human cornea is larger than that of the porcine data. This can be ascribed mainly to the quality of the tissues available for this study (see Materials section) and the limited number of samples.

The data for the lens were calculated from the axial profiles. Despite the damage to the cortex of some lenses, the standard deviations are relatively low. This means that if there was a significant effect caused by these damages, it was a consistent effect.

The attenuation data of the retina and choroid in Tables I and II display a relatively large spread with a significant contribution of the intra individual standard deviation. Two explanations can be given for this low precision: the contribution of an appreciable variability of the sound velocity due to the involvement of the thickness estimate in the calculation of the attenuation coefficient, and the accuracy of the estimation of the actual attenuation, which is essentially

Table I The acoustic parameters of human eye tissues

tissue	thickness [μm]	parameter	mean	sd	sd_{inter}	sd_{intra}	unit
cornea	500	c	1572.3	14.8	15.5	6.1	[m/s]
(n=4)		α(20)	10.03	4.47	5.03	1.77	[dB/cm]
		α_1	0.78	0.42	0.39	0.27	[dB/(cm · MHz)]
lens	-	c	1590.1	-	6.37	-	[m/s]
(n=13)		α(20)	27.6	-	4.85	-	[dB/cm]
		α_1	1.19	-	0.29	-	[dB/(cm · MHz)]
retina	100	c	1576.5	45.0	38.0	26.7	[m/s]
(n=11)		α(20)	11.4	4.9	3.0	3.9	[dB/cm]
		α_1	1.15	0.87	0.42	0.77	[dB/(cm · MHz)]
choroid	175	c	1530.8	23.6	16.0	21.6	[m/s]
(n=10)		α(20)	10.0	5.65	5.94	3.26	[dB/cm]
		α_1	0.95	0.76	0.40	0.80	[dB/(cm · MHz)]
sclera	500	c	1597.0	20.3	14.7	14.6	[m/s]
(n=11)		α(20)	12.88	3.22	3.04	1.84	[dB/cm]
		α_1	0.97	0.47	0.22	0.42	[dB/(cm · MHz)]
vitreous b. (4 prep.)	-	c	1513.5	-	3.2	-	[m/s]

Table II The acoustic parameters of porcine eye tissues

tissue	thickness [μm]	parameter	mean	sd	sd_{inter}	sd_{intra}	unit
cornea	800	c	1587.8	5.9	2.6	5.4	[m/s]
(n=18)		α(20)	13.7	1.9	1.7	0.9	[dB/cm]
		α_1	1.15	0.22	0.14	0.17	[dB/(cm · MHz)]
lens	-	c	1633.3	-	10.7	-	[m/s]
(n=6)		α(20)	37.2	-	4.97	-	[dB/cm]
		α_1	1.33	-	0.15	-	[dB/(cm · MHz)]
retina	200	c	1548.5	21.3	15.1	15.7	[m/s]
(n=10)		α(20)	9.19	2.75	2.20	1.76	[dB/cm]
		α_1	0.83	0.56	0.31	0.50	[dB/(cm · MHz)]
choroid	300	c	1546.8	21.3	19.5	11.7	[m/s]
(n=8)		α(20)	19.27	7.55	3.39	6.92	[dB/cm]
		α_1	1.56	0.89	0.29	0.85	[dB/(cm · MHz)]
sclera	500	c	1653.8	17.8	11.1	14.3	[m/s]
(n=12)		α(20)	22.92	7.48	4.56	6.48	[dB/cm]
		α_1	1.68	0.50	0.31	0.41	[dB/(cm · MHz)]
vitreous b. (5 prep.)	-	c	1500.7	-	5.2	-	[m/s]

Table III Coefficients of the fit to the attenuation spectra

	human				porcine			
	b		A_{f0} [dB/cm]		b		A_{f0} [dB/cm]	
tissue	mean	sd	mean	sd	mean	sd	mean	sd
cornea	1.56	0.06	0.10	0.05	1.69	0.09	0.09	0.04
lens	0 86	0 18	0.98	0.61	0.74	0.10	0.75	0 37
retina	1.87	0.32	0.06	0.05	1.80	0.57	0.17	0.33
choroid	2.13	0 86	0.09	0.09	1.65	0.37	0.21	0.17
sclera	1.49	0 14	0.73	0.31	1.50	0.30	0 20	0 17

low due to the limited thickness of these tissues. The wavelength of the employed transducer is of the order of 75 μm, whereas, the retinal and choroidal thickness of the human eye was found to be 100 and 175 μm, respectively The porcine retina and choroid were two times thicker and a comparison of the data in Table I vs. Table II shows indeed an intra individual standard deviation which is much lower for the porcine retina and choroid than for the human tissues.

Since the human data are relevant for future quantitative echographic work, a comparison has been made with data found in the literature. A summary of the results is shown in Table V, where for the velocity the mean and the range of literature data at room temperature are listed. A clear difference is found only for the human lens The question then arises whether the low value of the present study has to be ascribed to the estimation procedure In the past, the measurements were performed on intact lenses, whereas in this study the average was taken of the axial profile of the velocity. Due to minor damages on the cortex a straightforward comparison might not be possible. However, the values for the porcine data are well within the range of the literature data, and these were obtained using the same procedure as used for the human measurements, so it is unlikely that the procedure is the reason for the discrepancy with literature values.

A further argument may be an age related effect. In the present study lenses were measured without any visible sign of cataract and spanned a wide age range Since other authors did not mention the presence or absence of cataract, the reported values might have been obtained from lenses that were cataractous to some extent. The velocity of the eye lens was shown to depend on the severity and the type of cataract, and it can be assumed to depend on the stage of cataract development (Coleman *et al.* 1975, Pallikaris & Gruber 1981)

The question whether the porcine eye may serve as an animal model for the human eye in quantitative ultrasound studies can be addressed by comparing the results of Tables I and II Significant differences appear for the lens and the sclera, both for the velocity and the attenuation parameters An explanation should presumably be found in (chemical) composition of these tissues. This question is considered to be outside the scope of the present paper. It may be concluded, however, that the porcine eye can serve as an animal model for quantitative studies, when taking the before mentioned differences into consideration.

The frequency of the employed transducer (20 MHz) induces the necessity to extrapolate the obtained attenuation data to lower diagnostic frequencies (for example 7.5 MHz, Romijn

Table IV Age dependence of acoustic parameters of human eye tissues

tissue	parameter	value at age=0	increase per yr.	p-value (obtained from Wilcoxon test)
lens	c	1586.7	$7.7 \cdot 10^{2}$	0.31
(n=10)	$\alpha(20)$	21.3	$1.1 \cdot 10^{1}$	0.04
	α_1	0.64	$9.3 \cdot 10^{3}$	<0.01
retina	c	1622.8	$-7.7 \cdot 10^{1}$	0.26
(n=11)	$\alpha(20)$	11.9	$-8.4 \cdot 10^{-4}$	0.85
	α_1	1.07	$1.3 \cdot 10^{-3}$	0.99
choroid	c	1518.7	$2.6 \cdot 10^{1}$	0.17
(n=10)	$\alpha(20)$	2.4	$1.4 \cdot 10^{-1}$	0.05
	α_1	0.62	$7.2 \cdot 10^{3}$	0.42
sclera	c	1665.0	$4.9 \cdot 10^{1}$	0.02
(n=11)	$\alpha(20)$	6.9	$9.9 \cdot 10^{-2}$	0.04
	α_1	0.39	$9.2 \cdot 10^{3}$	0.02

et al. 1991). Since, the linear fit through the attenuation coefficient vs. frequency generally could not be reasonably extrapolated to zero attenuation at zero frequency, the model of the power function (Eq. 1.) was proposed. This model has been used in other applications of quantitative echography (Wells 1977, Bamber 1986).

As can be seen in Table III the values for the power b have a reasonable precision, but the factor $A_{(0)}$ appears to be rather variable. This can be explained from Eqs. 2 and 3. It is shown from Eq. 2 that b is determined from a quotient of α_1 and $\alpha(20)$. These parameters are highly correlated in eyes. This is observed during this study (R ranged from 0.70 up to 0.92) and reported in literature (van der Steen *et al.* 1993a). For this reason the variance in b is smaller than the variance in α_1 and $\alpha(20)$ (Tables I and II). Since b has a low standard deviation, the denominator of Eq. 3 will have a low standard deviation. The precision of $\alpha(20)$ however is fully present in the numerator, so it will show up in the precision of the factor A. The power b can be estimated very accurately even for thin layers like choroid and retina. It should be mentioned that since the power b is larger than one for most tissues, even minor variations in b cause significant effects on the extrapolation to higher frequencies.

It should be born in mind that the attenuation is measured as a bulk parameter. However, when the values are extrapolated to 7.5 MHz the layer thickness of the retina and choroid is in the order of the wavelength. This means that the geometry of the tissue should be taken into account (Brekhovskikh, 1980). When the thickness is small as compared to the wavelength, the tissue will become transparent for ultrasound.

The effect of aging on the acoustic characteristics of ocular tissues was investigated and was found to be significant for the attenuation in the lens and for all parameters of the sclera ($p<0.05$). Due to the limited number of eyes involved in the study these conclusions are

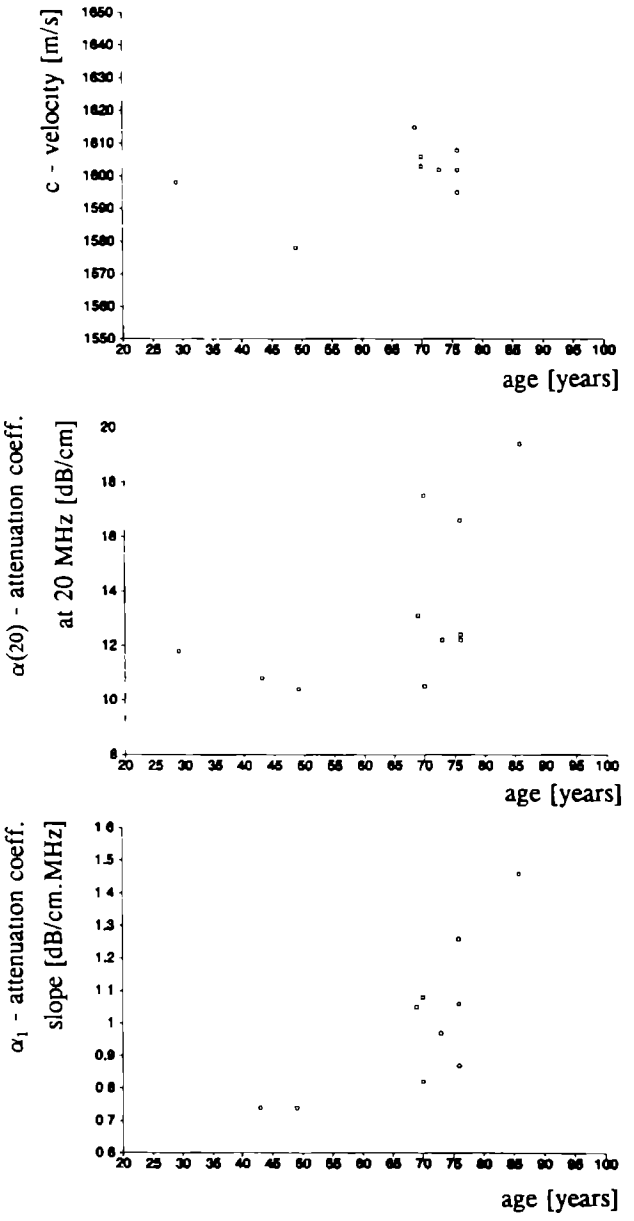

Fig 1 The acoustic parameters of the human sclera versus the age
A velocity
B attenuation coefficient at 20 MHz
C attenuation coefficient slope between 17 and 23 MHz

Table V Velocity in ocular tissues taken from literature

Tissue	Human	Reference	Porcine	References
	mean (range) [m/s]		mean (range) [m/s]	
Cornea	1559 (1553-1565)	1,5	1565 (1555-1580)	1,3,5
Lens	1631 (1620-1638)	1,2,5	1644 (1627-1657)	1,2,4,5
Retina	1538	5	1532	5
Choroid	1527	5	-	-
Sclera	1608 (1583-1613)	1,2,5	1635 (1609-1661)	1,2,5
Vitreous	1503 (1490-1514)	1,2,5	1499 (1497-1505)	1,2,5,6

1) Rivara & Sanna, 1962 2) Araki 1961 3) Yamamoto, 1961 4) Jansson & Sundmark, 1961 5) Thijssen *et al* 1985 6) Jansson & Kock 1962

preliminary and further investigation is indicated. This conclusion is supported by independent observations (Afschrift *et al.* 1985, Hartman *et al.* 1991) that most of the acoustic parameters estimated for liver tissue display an age dependent effect. Once this effect has been established with sufficient precision, it can be corrected for, thus enhancing the accuracy of quantitative echography.

WORKS OF REFERENCE

Afschrift M., Cuvelier C., Ringoir S., Barbier F (1987) Influence of pathological state on the acoustic attenuation coefficient slope of liver. Ultrasound Med. Biol. 13: 135-139

Araki M. (1961) Studies on refractive elements of human eye by ultrasonic wave. Jap. J. Clin. Ophthal. 15: 111-119

Armitage P. (1973) Statistical Methods in Medical Research. Oxford: Blackwell Scientific Publications

Bamber J C. (1986) Attenuation and absorption. In: Hill, C.R. ed. Physical Principles of Medical Ultrasonics. New York: John Wiley & Sons

Brekhovskikh L.M. (1980) Waves in Layered Media. New York: Academic Press, Chapter 1

Buschmann W. (1966) Einfuhrung in die Ophthalmologische Ultraschalldiagnostik. Leipzig: Thieme Verlag

Chivers R.C., Parry R.J. (1978) Ultrasonic velocity and attenuation in mammalian tissues. J. Acoust. Soc. Am. 63: 940-953

Coleman D.J., Lizzi F.L., Franzen L.A., Abramson D.H. (1975) A determination of the velocity of ultrasound in cataractous lenses. In: François, J , Goes, F , eds. Bibliotheca Ophthalmologica. 83. Basel, Karger: 246-251

Coleman D.J., Lizzi F.L., Jack R L. (1977) Ultrasonography of the Eye and Orbit. Philidelphia: Lea & Febinger

Coleman D.J., Lizzi F.L., Silverman R.H., Helson L., Tarpey J.H., Rondeau M.J. (1985) A model for the acoustic characterization of intraocular tumors. Inv. Ophthalmol. Vis. Sci. 26: 545-550

Decker D., Epple E., Leiss W., Nagel M. (1973) Digital computer analysis of time amplitude ultrasonograms from the human eye. II. Data processing. J. Clin. Ultrasound 1. 156-159

Duck F.A. (1992) Physical Properties of Tissue: a Comprehensive Reference Book. London: Academic Press

Feleppa E J., Lizzi F.L., Coleman D.J., Yaremko M.M. (1986) Diagnostic spectrum analysis in ophthalmology: a physical perspective. Ultrasound Med. Biol. 12: 623-631

Goedegebure A., van der Steen A.F.W., Thijssen J.M. (1992) In vitro classification of gallstones by quantitative echography. Ultrasound in Med & Biol. 18: 553-568

Goss S A., Johnston R.L., Dunn F (1980) Compilation of emperical ultrasonic properties of mammalian tissues II. J Acoust. Soc. Am. 68: 93-108

Haigis W. (1989) Akustische Daten der Gewebe und Flussigkeiten des menschlichen Korpers (insbesondere von Augen und Orbita). In: Buschmann W, Trier H.G. Ophthalmologische Ultraschaldiagnostik. Berlin/Heidelberg/New York, Springer-Verlag: 394-398

Hartman P.J., Oosterveld B.J., Thijssen J.M., Rosenbusch G.J.E. (1991) Variability of quantitative echographic parameters of the liver: intra- and interindividual spread, temporal- and age-related effects Ultrasound in Med. & Biol. 17: 857-867

Jansson F., Sundmark E. (1961) Determination of the velocity of ultrasound in ocular tissues at different temperatures. Acta Ophthal. 39: 899-910

Jansson F., Kock E. (1962) Determination of the velocity of ultrasound in the human lens and vitreous. Acta Ophthal. 40: 420-433

Lizzi F.L., Katz L , St.Louis L., Coleman D.J. (1976) Applications of spectral analysis in medical ultrasonography. Ultrasonics. 14: 77-80

Ossoinig K.C. (1974) Quantitative ultrasonography - The basis of tissue differentiation. J. Clin. Ultrasound 2: 33-46

Pallikaris I., Gruber H. (1981) Determination of sound velocity in different forms of cataracts. In: Thijssen, J.M., Verbeek, A.M., eds. Ultrasonography in Ophtalmology, Doc. Ophthalmol. Proc. Series 29. The Hague: Junk: 165-169.

Poujol J. (1981) Echographie en Ophtalmologie. Paris: Masson

Rivarra A., Sanna G. (1962) Determination of the speed of ultrasound in the ocular studies of humans and swine. Ann Ottal. Clin. Ocul. 88: 672-682

Romijn R.L, Thijssen J.M., Oosterveld B.J., Verbeek A.M. (1991) Ultrasonic differentiation of intraocular melanomas: parameters and estimation methods. Ultrasonic Imaging 13: 27-55

van der Steen A.F.W., Cuypers M.H.M , Thijssen J.M., de Wilde P.C.M. (1991) Influence of histochemical preparation on acoustic parameters of liver tissue: a 5 MHz study. Ultrasound in Med. & Biol. 17: 879-891

van der Steen A.F.W., de Korte C.L., Thijssen J.M. (1993a) Ultrasonic spectroscopy of the porcine eye lens. Submitted Ultrasound in Med. & Biol.

van der Steen A.F.W., Thijssen J.M., van der Laak J.A.W.M., Ebben G.P.J., de Wilde P.C.M. (1993b) A new method for correlation of acoustic spectroscopic microscopy (30 MHz) and light microscopy. in press J. Microscopy

Thijssen J.M., Verbeek A.M. (1981) Computer analysis of A-mode echograms from choroidal melanoma. In: Thijssen J.M., Verbeek A.M. eds. Ultrasonography in Ophthalmology, Doc. Ophthalmol. Proc. Series 29. The Hague: Junk: 123-129.

Thijssen J.M., Mol H.J.M., Timmer M.R. (1985) Acoustic parameters of ocular tissues. Ultrasound Med Biol. 11: 157-161

Thijssen J.M., Verbeek A.M., Romijn R.L., de Wolff-Rouendaal D., Oosterhuis, J.A. (1991) Echographic differentiation of histological types of intraocular melanoma. Ultrasound Med. Biol. 17: 127-138

Trier H.G., Reuter R. (1973) Digital computer analysis of time-amplitude ultrasonograms from the human eye. I. Signal acquisition. J.Clin.Ultrasound. 1:150-154

Trier H.G., Decker D., Lepper R.D., Irion K.M., Reuter R., Kottow M., Müller-Breitelkamp R., Otto K.J. (1983) Ocular tissue characterization by RF-signal analysis: summary of the Bonn/Stuttgart *in vivo* study. In: Hillman, J.S., Le May, M.M., eds. Ophthalmic Ultrasonography, Doc. Ophthalmol. Proc. Series 38. The Hague: Junk: 455-466

Verbeek A.M., Bayer A.L., Thijssen J.M. (1981) Echografic diagnosis after intraocular silicon oil injection. In: Thijssen, J.M., Verbeek, A.M., eds. Ultrasonography in Ophtalmology, Doc. Ophtalmol. Proc. Series 29. The Hague: Junk: 59-66

Wells, P.N.T. (1977) Biomedical Ultrasonics. London: Academic Press

Yamamoto Y. et al. (1960) A study on the measurements of ocular axial length by ultrasound echography. Acta Soc. Ophthal. Jap. 64: 1333-1341

CHAPTER VI

EFFECTS OF TISSUE PROCESSING TECHNIQUES IN ACOUSTIC (1.2 GHz) AND LIGHT MICROSCOPY

A F W van der Steen J M Thijssen G P J Ebben P C M de Wilde

ABSTRACT

In this study the influence of various tissue processing and staining techniques on the acoustic properties of liver tissue was investigated A qualitative study was performed by using the ultrasound attenuation as the imaged parameter of a combined optical/acoustic microscope with a 1 2 GHz transducer Images were made of three sets of adjacent liver sections (6 μm in thickness) which were prepared in ten different ways fixed by alcohol or formalin, stained by haematoxylin-eosin (HE) toluidine blue (TB) or non-stained, sectioned by a cryostat or by a paraffin microtome It was concluded that the images obtained from cryostat sections were of much higher quality than those from paraffin sections Images obtained from sections that were sectioned while embedded in paraffin displayed no detail at all No consistent effect was noticed with respect to staining by HE or TB Alcohol fixed sections gave more detailed images than formalin fixed sections Formalin fixation in combination with cryostat sectioning yielded many cytoplasmic vacuoles

INTRODUCTION

Light microscopy is the most common type of microscopy used for studying biological tissues Acoustic microscopy at frequencies above 1 GHz is another promising type of microscopy which principally displays other features of the tissue Conventional light microscopy displays frequency dependent light absorption whereas acoustic microscopy is capable of displaying ultrasound attenuation, velocity and layer thickness The resolution of light microscopy is limited by the wavelength of visual light ($\pm$400 650 nm) Nowadays acoustic microscopes are available up to 4 2 GHz so it is possible in principle to reach at least 4 times this resolution (Jipson & Quate 1978, Hafsteinsson & Rizvi 1984) and when it is possible to increase this frequency even better resolutions can be achieved A lateral resolution of 0 6 μm has already been achieved (Kanngiesser & Anliker 1992)

A great advantage of light microscopy compared to acoustic microscopy is that fixation sectioning and staining techniques have been optimized for centuries for light microscopy Moreover, pathologists are used to dealing with the information revealed by light microscopy Histological techniques that are applicable for acoustic microscopy still have to be developed Measuring fresh tissue entails a lot of problems such as drying of the tissue before measurement (Daft *et al* 1989) autolysis (Bamber *et al* 1977, Crosby & Mackay 1978) and the accompanying

production of gaseous inclusions (Bamber & Nassiri 1985) Bamber *et al* (1979) performed a study at lower frequencies on the influence of various fixatives on the acoustic parameters of various tissues Litniewski & Bereiter Hahn (1990) performed an investigative study on fixation by glutaraldehyde on image quality Some investigative studies are reported about the influence of freezing and thawing of tissue (Kessler 1973, Frizell *et al* 1979, Parker 1983, Foster *et al* 1984, D'Astous & Foster 1986) Kolodzijczyk *et al* (1988) performed a study on the image quality of acoustic microscopy of sectioning tissue while embedded in paraffin and while embedded in dried gelatin Van der Steen *et al* (1991, 1992, Chapter VII) performed a quantitative study on the influence of formalin fixing, paraffin embedding and subsequent staining by haematoxylin-eosin (HE) on the acoustic properties of liver tissue at 5 MHz

In the present study the influence of various histological techniques of tissue processing and staining on the image quality obtained with a scanning acoustic microscope at 1 2 GHz is investigated This acoustic microscope is constructed according to the Lemons & Quate principle (Lemons & Quate 1974) Three series each of 10 conjugant sections were prepared in ten different ways fixed with alcohol or formalin, sectioned by a cryostat or while embedded in paraffin and stained by haematoxylin eosin (HE) toluidine blue (TB) or non-stained

METHODS

Tissue processing and staining

Thirty sections of liver tissue obtained from three White New Zealander rabbits were prepared in ten different ways and then measured Six adjacent sections of 6 μm in thickness were sectioned from fresh liver tissue using a cryostat Three of these sections were fixed in a 4 % buffered formalin solution and three of them in a 70% ethyl alcohol solution From both types of tissue one section remained unstained, one was stained by haematoxylin eosin (HE) and one was stained by toluidine blue (TB)

The remaining tissue was formalin fixed, dehydrated by an alcohol xylol series and embedded in paraffin Then another four sections were cut using a paraffin microtome The tissue was positioned in such a way that the obtained sections were again adjacent to each other and to the cryostat sections Three of these sections were deparaffinized and then hydrated again, the fourth section remained paraffinized One of the hydrated sections was stained with a HE solution and one was stained with a TB solution One of the hydrated sections remained unstained

From each section corresponding regions were selected for measurements
In this way it was possible to investigate almost the same region under different procedures of tissue processing

Acoustic microscopic investigations

The tissues were investigated using a scanning acoustic microscope (ELSAM, Leitz Inc , Wetzlar FRG) at a frequency of 1 2 GHz The principle of this microscope is shown in fig 1 The sample was positioned on a glass slide in the focal zone of the transducer An acoustic tone burst was generated by the ultrasonic transducer, which was used both as a transmitter and a receiver A time segment of 20 ns was gated from the received signal and a peak detection was performed in this segment Since 20 ns correspondents to 15 μm two way travel distance in water and the sections were 6 μm thick, the reflection of the surface of the tissue the backscattering from the tissue and the surface reflection of the glass plate were all within this

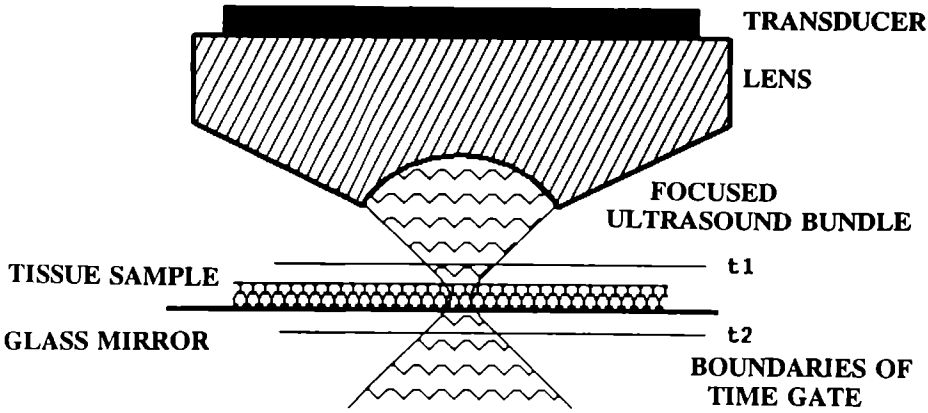

Fig 1 Principle of the mechanism of the ELSAM scanning acoustic microscope A transducer that is used both as a transmitter and a receiver produces an ultrasound burst The ultrasound beam is focused by a lens on the surface of a glass plate On the glass plate there is a tissue sample Then a period of 20 ns (t_1 to t_2) is gated around the focus of the transducer This period contains the front reflection of the sample, the backscattering of the sample and the glass plate reflection A peak detection is performed within this period

window The reflection of the glass plate is much stronger than the reflection of the surface of the tissue and the backscattering from the tissue, therefore the peak detected signal corresponded to reflection of the glass plate Since the ultrasound travelled through the tissue twice, the measured signal corresponded to the attenuation of the tissue

It is not possible to give an exact transformation from the grey scale of the image to the ultrasound attenuation for a few reasons. Firstly there is no simple analytical function describing the relation between input and output voltage of the ELSAM receiver In addition this relation varies with the amplification of the receiving system (Litniewski & Bereiter-Hahn 1990). Secondly the sections cannot be made perfectly flat (Daft & Briggs 1989, Daft *et al* 1989, Okawai *et al* 1989, 1990), and the local thickness cannot be perfectly measured in a simple way (Hildebrand *et al* 1989, Litniewski & Bereiter-Hahn 1990) Variation in section thickness influences the estimation of the attenuation

An XY-scan was made over a region of approximately 0 5 mm x 0 5 mm of each section, and an image of 512 x 512 points was generated from the received signals on a video monitor The images were optimized by controlling the offset and gain of the receiver

LIGHT MICROSCOPIC INVESTIGATIONS

light microscopic images were obtained in two ways; the first was an light reflection image provided by the Elsam microscope It was possible to produce an image of exactly the same region both optically and acoustically

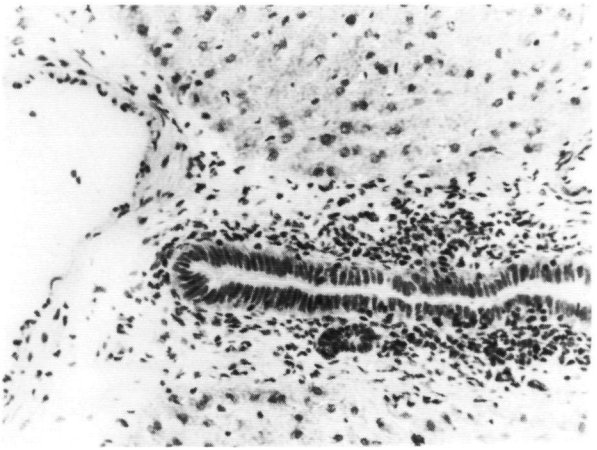

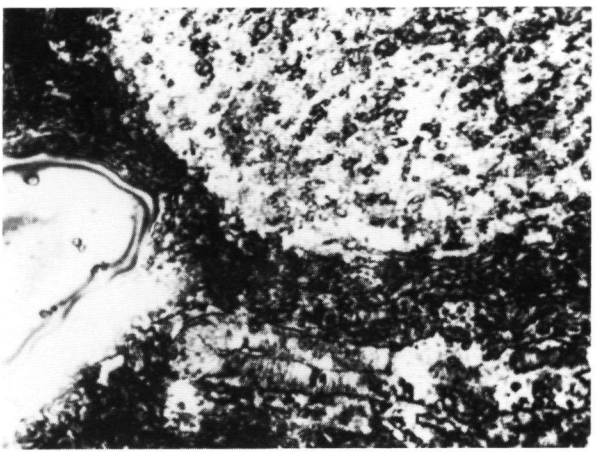

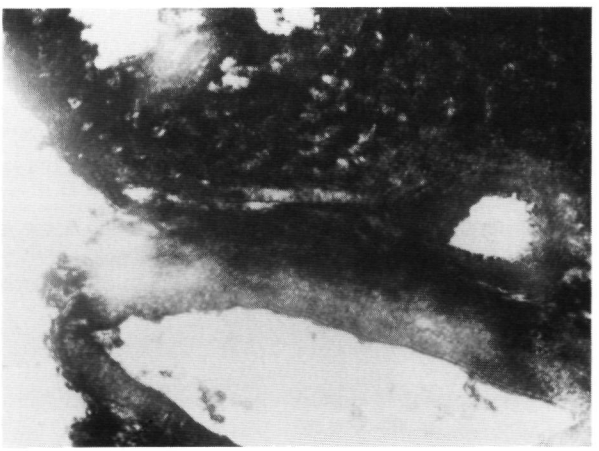

On the next day all sections were stained again with haematoxylin eosin, then dehydrated using a alcohol xylol series and mounted permanently Now the same regions that were investigated acoustically and in optical reflection were selected and an optical transmission image (i e standard light microscopy) was produced

RESULTS

Some representative micrographs of tissue sections obtained by acoustical and light examples of the microscopy are presented in Figs 2 and 3 Fig 2A shows an optical microscopic transmission image of a 6 μm thick alcohol fixed and HE stained cryostat section On the left a vein can be seen In the right upper corner parenchymal tissue is depicted and in the lower right corner a bile duct is visible The region around the bile duct mainly consists of fibrous tissue

Fig 2B shows an acoustic double transmission image of the same section The first striking result is that the collagen rich fibrous tissue is clearly contrasted from the rest of the image Collagen has a high attenuation as compared to other tissue and is dominant in acoustic images of soft tissue (O'Brien 1977, Daft *et al* 1986, O'Donnell *et al* 1981) The nuclei in the parenchymal cells and leucocytes in the lumen of the vein are visualized as small dark rings with a light spot in the centre This may be interpreted as a high ultrasound attenuation by the nuclear membrane The nuclei in the fibrous tissue and in the bile duct lining epithelium are clearly displayed in the optical image but cannot be found in the acoustic image Conversely the basal membrane around the bile duct is visualized in the acoustic image, but cannot be traced in the optical image

Fig 2C shows an acoustic double transmission image of a formalin fixed, paraffin embedded and sectioned, deparaffinized, HE stained section of the same region as is displayed in Figs 2A and 2B Using the information obtained from the other sections it is possible to recognize the various regions in the section but almost no contrast at all was obtained in the section

Fig 3A shows an optical microscopic transmission image of a formalin fixed, TB-stained cryostat section of 6 μm thickness In the centre a bile duct is seen and in the upper left corner there is a small vein Around the biliary duct and the vein collagen rich fibrous tissue is present, which is surrounded by parenchymal tissue The parenchyma displays many vacuoles that are filled with water

Fig 3B shows an acoustic double transmission image of the same section The vacuoles are also visible in this image The perivascular and periductal fibrous tissue is clearly distinguishable from the remainder of the image

Fig 2 Three examples of images of similar sections (opposite page)
A an optical microscopic transmission image of an alcohol fixed, HE stained cryostat section
B an acoustical double transmission image of the same section
C an acoustical double transmission image of a formalin fixed paraffin embedded sectioned, deparaffinized HE-stained section which was adjacent to the section displayed in Fig A and B
The same region is displayed in figure A , B and C

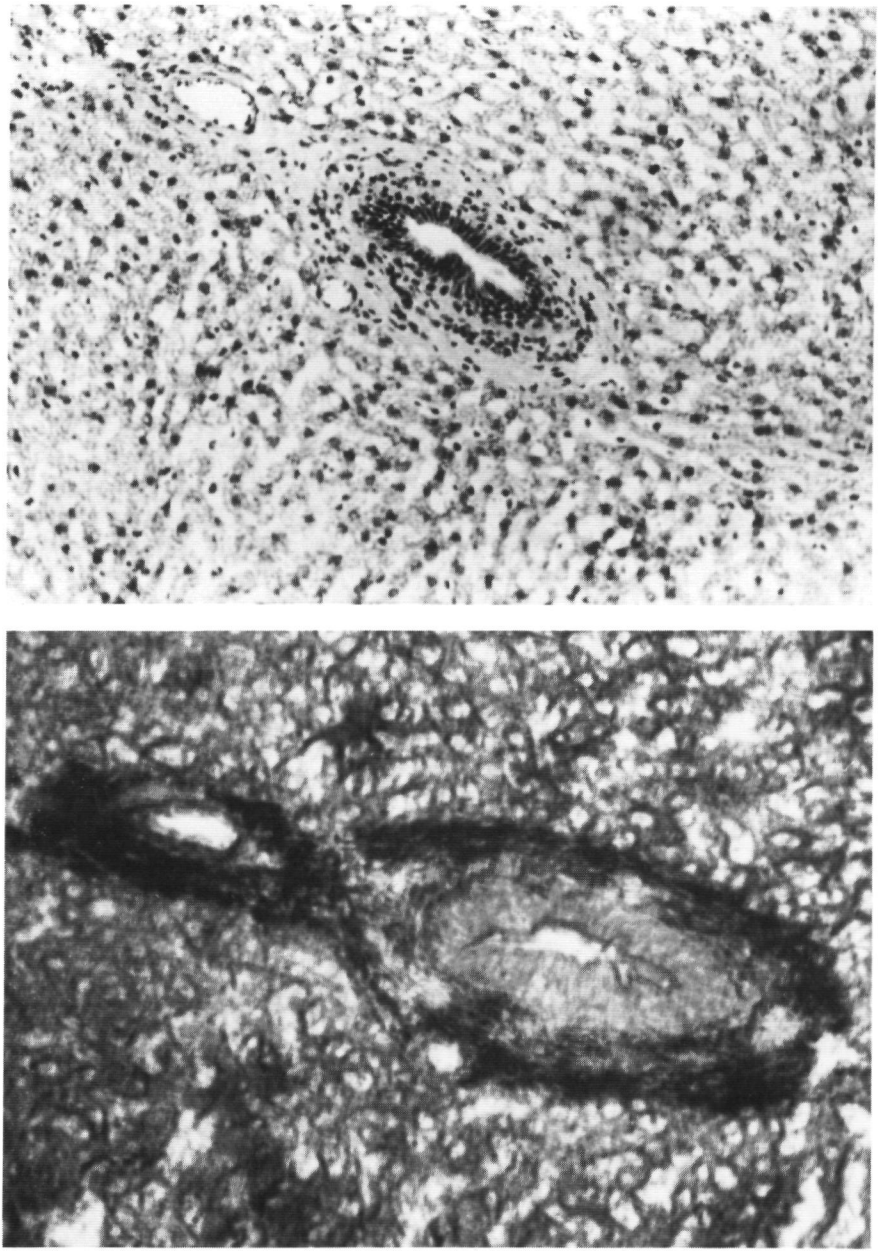

Fig.3. Four examples of images of similar sections.
A. an optical microscopic transmission image of a formalin fixed, TB-stained cryostat section.
B. an acoustical double transmission image of the same section.

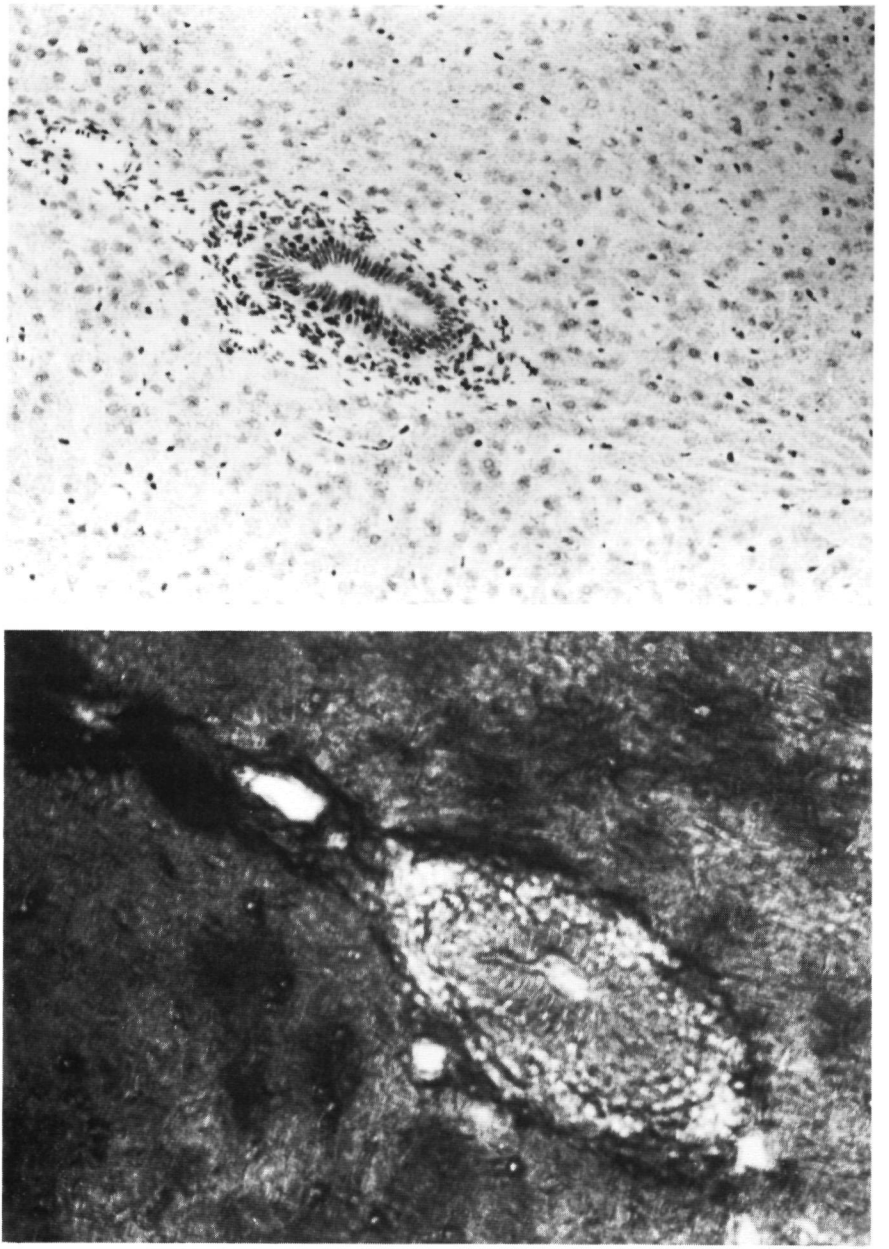

C. an optical microscopic transmission image of a alcohol fixed, TB-stained cryostat section.
D. an acoustical double transmission image of the same section.
The same region is displayed in figure A., B., C. and D.

Fig. 3C shows an optical microscopic transmission image of a alcohol fixed, TB-stained cryostat section of 6 μm thickness of the same region as is displayed in Figs. 3A. and 3B. The mentioned vacuoles are not present in this image.

Fig. 3D. shows an acoustic double transmission image of the same section. Here the vacuoles are again absent. The contrast of the perivascular and periductal collagen rich fibrous tissue is less pronounced than the contrast in the formalin fixed section (fig 3b)

DISCUSSION

In the present study, various tissue processing techniques used for light microscopy were evaluated for their applicability in acoustic microscopy Fig. 2. clearly shows that the acoustic microscopic images obtained from the cryostat sections produce images that are much more detailed compared to sections that were sectioned while embedded in paraffin; even after deparaffinizing, the acoustic contrast had practically disappeared. For the cryostat sections no chemical dehydration was applied, nor were the sections penetrated by materials that are acoustically very different from tissue This finding is consistent with the study performed by Kolodzijczyk *et al* (1988) who compared sectioning while embedded in paraffin with sectioning while embedded in dried gelatin. Since the cycle of paraffin embedding damaged the tissue acoustically to such an extent that it was not suitable for acoustic microscopy, the paraffin sections have not been evaluated further with respect to fixing and staining.

Fig 3. reveals that, in combination with cryostat sectioning, alcohol fixation yielded a higher image quality than formalin fixation. Fixation in formalin combined with cryostat sectioning caused the appearance of many water-filled vacuoles, which were also clearly visible in the optical images of the sections (Fig 3A.). It is hypothesized that the procedure of formalin fixation and then freezing induces crystals to grow, which damaged the tissue either during sectioning or after thawing After alcohol fixation this phenomenon is less provocative Formalin fixation itself retains the acoustic bulk properties substantially better than alcohol fixation (Bamber *et al.* 1979). Thus our findings indicate that there is a considerable discrepancy between the aim of studying the original acoustic properties of a tissue and the goal to obtain a detailed image of the tissue sample

Staining of the tissue by HE and TB revealed no consistent effect. In one series it could be seen that HE staining gave more detail than TB staining; both gave more detail than no staining. In the other two series these effects were not consistently present. Overall we can conclude that the paraffin embedding cycle should be avoided at all times for acoustic microscopy.

When acoustic microscopy is made applicable for routine pathologic investigations cryostat sectioning is required and appropriate staining techniques should be developed or sophisticated.

WORKS OF REFERENCE

D'Astous F T , Foster F.S (1986) Frequency dependence of ultrasound attenuation and backscatter in breast tissue Ultrasound in Med. & Biol. 12. 795-808

Bamber J.C., Fey M.J., Hill C.R., Dunn F. (1977) Ultrasonic attenuation and backscattering by mammalian organs as a function of time after excision.Ultrasound in Med. & Biol 3. 15-20

Bamber J.C., Hill C.R., King J.A , Dunn F. (1979) Ultrasonic propagation through fixed and unfixed tissues. Ultrasound in Med. & Biol. 5: 159-165

Bamber J.C., Nassiri D.K (1985) Effect of gaseous inclusions of the frequency dependence of ultrasonic attenuation in liver. Ultrasound in Med. & Biol. 11: 293-298

Crosby B.C., Mackay R.S. (1978) Some effects of time post-mortem on ultrasonic transmission through tissue under different modes of handling. IEEE Trans. BME. 25: 91-92

Daft C.M.W., Weaver J.M.R., Briggs G.A.D. (1986) Tissue characterization with microscopic resolution. 1986 IEEE Ultrasonics symposium 945-948

Daft C M.W., Briggs G.A.D. (1989) The elastic microstructure of various tissues. J. Acoust. Soc. Am. 85: 416-422

Daft C.M.W., Briggs G.A.D., O'Brien W.D. jr. (1989) Frequency dependence of tissue attenuation measured by acoustic microscopy. J. Acoust. Soc. Am. 85: 2194-2201

Foster F.S., Strban M., Austin G. (1984) The ultrasonic macroscope:initial studies of breast tissue. Ultrasonic Imaging 6: 243-261

Frizell L.A., Carstensen E.L., Davis J.D. (1979) Ultrasonic absorption in liver tissue. J. Acoust Soc. Am. 65: 1309-1312

Hafsteinsson H., Rizvi S.S.H (1984) Acoustic microscopy - Principles and applications in the studies of biomaterial microstructure. Scanning Electron Microscopy III: 1237-1247

Hildebrand J.A., Rugar D. (1984) Measurement of cellular elastic properties by acoustic microscopy. J. of Microscopy 134: 245-260

Jipson V., Quate C.F. (1978) Acoustic microscopy at optical wavelenghts. Applied Physics Letters 32: 789-791

Kanngiesser H., Anliker M. (1992) Ultrasound microscopy of biological structures with weak reflecting properties. In: Ermert H and Harjes HP (eds) Acoustical Imaging vol 19. Plenum Press, New York. 517-522

Kessler L.W. (1973) VHF ultrasonic attenuation in mammalian tissue. J. Acoust. Soc. Am. 53: 1759-1760

Kolodziejczyk E., Saurel J.M., Bagnol J., Attal J., Fernandez-Graf M.R., Saied A. (1988) Transmission acoustic microscopy of tissue sections (1 GHz). Histoacoustics and acoustic staining. Histochemistry 88: 165-169

Lemons R.A., Quate C.F. (1974) Acoustic Microscope-scanning version. Appl. Phys. Lett 24: 163-165

Litniewski J., Bereiter-Hahn J. (1990) Measurements of cells in culture by scanning acoustic microscopy. J. of Microscopy 185: 95-107

O'Brien W.D. (1977) The role of collagen in determining ultrasonic propagation properties in tissue. in Acoustic Holography Plenum (ed. LW Kessler) vol. 7: 37-50

O'Donnell M., Mimbs J.W., Miller J.G. (1981) Relationship between collagen and ultrasonic backscatter in myocardial tissue. J. Acoust. Soc. Am. 69: 580-588

Okawai H., Tanaka M., Dunn F., Chubachi N., Honda K. (1989) Quantitative display of acoustic properties of the biological tissue elements. In Acoustical imaging vol. 17 (edited by Shimizu H., Chubachi N. & Kushibiki) Plenum Press New York and London, 193-201

Okawai H., Tanaka M., Dunn F. (1990) Non-contact acoustic method for the simultaneous measurement of thickness and acoustic properties of biological tissues. Ultrasonics 28: 401-410

Parker K.J. (1983) Ultrasonic attenuation and absorption in liver tissue. Ultrasound in Med. & Biol. 9: 363-369

van der Steen A.F.W., Cuypers M.H.M., Thijssen J.M., de Wilde P.C.M. (1991) Influence of histochemical preparation on acoustic parameters of liver tissue, a 5 MHz study. Ultrasound in Med. & Biol. 17: 879-891

van der Steen A.F.W., Cuypers M.H.M., Thijssen J.M., Ebben G.P.J., de Wilde P.C.M. (1992) Preparation techniques in acoustic and optical microscopy of biological tissues, a study at 5 MHz and 1.2 GHz. In: Ermert H & Harjes HP (eds) Acoustical Imaging vol 19. Plenum Press, New York. 529-533

CHAPTER VII

INFLUENCE OF HISTOCHEMICAL PREPARATION ON ACOUSTIC PARAMETERS OF LIVER TISSUE, A 5 MHz STUDY

A.F.W. van der Steen, M.H.M. Cuypers, J.M. Thijssen, P.C.M. de Wilde

ABSTRACT

In this study the influence of various histological techniques on the acoustic parameters of liver tissue was investigated.
Radiofrequency (rf) echographic data were obtained in vitro from 21 liver samples taken from 8 white New Zealander rabbits. The samples were measured in four different subsequent histological tissue processing conditions (freshly excised, 4 % buffered formalin fixed, after it went through a paraffin cycle and after staining with Haematoxylin and Eosin).
The acoustic parameters that were obtained from the rf-data were velocity of sound, slope of the attenuation coefficient versus frequency between 1.9 and 6.9 MHz, attenuation coefficient at 4.4 MHz, slope of the backscattering spectrum between 1.9 and 6.9 MHz, intercept of the backscattering spectrum.
It was found that fixation by formalin preserves the acoustic properties of the tissue to a reasonable extent. Embedding in paraffin and deparaffinizing induces large changes in the acoustic properties of the tissue.
As an alternative, freezing prior to cutting, rather than the paraffin cycle was investigated also in 10 liver samples obtained from 4 New Zealander rabbits. This method produced no significant changes of the acoustic parameters and should therefore be preferred in acoustic microscopy.

INTRODUCTION

A great number of studies has been performed on the *in vitro* estimation of acoustic parameters (e.g. Chivers & Parry 1978, Goss *et al.* 1978, Bamber & Hill 1979, Goss *et al.* 1980, Nicholas 1982, van der Steen *et al.* 1991, Chapter II). A great variation in the values of the estimated acoustic parameters has become evident. This may be ascribed to differences in the experimental protocols. One of the experimental problems that arise is the difference in time between excision of the tissue and the measurements (Bamber *et al.* 1977, Crosby & Mackay 1978). This problem can be solved by tissue fixation immediately after excision. The only way to investigate the influence of fixation is to measure the same tissue samples first fresh and then after fixation.

Bamber *et al.* (1979) investigated the influence of various fixatives on the acoustic properties of bovine liver, spleen and brain and human liver of varying time post mortem. In their study it was concluded that formalin and potassium dichromate preserve the acoustic properties to an acceptable level of consistency.
Kremkau *et al.* (1981) investigated the influence of 10 % formalin fixation on the acoustic properties of human brain up to 5 hours after autopsy.

Recently some work has been done on the estimation of the scatterer size from the spectra of the rf-signals (Lizzi *et al.* 1986, Ueda *et al.* 1985, Romijn *et al.* 1989a, Romijn *et al.* 1989b, Insana *et al.* 1990, Coleman *et al.* 1990). These studies showed good results for simulations and measurements on tissue mimicking phantoms. The results of the *in vivo* measurements on intraocular tumours could not be correlated with histological structures . A plausible explanation is that the frequencies employed in diagnostic echography equipment is too low for a proper correlation study.

For this reason there is a quest for higher resolution and thus for higher frequencies. If one wants to find correlations, the same or adjacent sections should be investigated both acoustically and optically. This is only possible if a cutting technique is found which allows one to produce slices which can be used for both optical and acoustic microscopy. Two techniques are commonly used for optical microscopy: 1. freezing the samples prior to slicing, or 2. embedding the samples in paraffin prior to slicing. The influence of freezing on the acoustic properties of biological tissue is studied in a few papers (Kessler 1973, Frizell *et al.* 1979, Parker 1983, Foster *et al.* 1984, D'Astous & Foster 1986). The results of these studies were merely indicative. No studies are known to the authors about the influence on the acoustic properties of the application of a paraffin cycle Still it has been used for acoustic microscopy (Okawai *et al.* 1989, Okawai *et al.* 1990).

In the present study we investigated the influence on the acoustic parameters of liver tissue of various histological techniques that can be used for the preparation of tissues for both optical and acoustic microcopy.

The same regions of the same tissue samples were measured under four histological conditions. The samples were measured fresh (i.e. between 0 5 and 1.0 hour post mortem) and after fixation by 4 % buffered formalin Then they were embedded in paraffin, rehydrated and measured, then stained by Haematoxylin and Eosin and measured again.

The influence of freezing was also investigated. In this part of the study the same regions of the same samples were measured formalin fixed and after freezing and thawing

The investigated parameters were velocity of sound, slope of the attenuation coefficient versus frequency between 1.9 and 6.9 MHz, attenuation coefficient at 4.4 MHz, slope of the backscattering spectrum between 1.9 and 6.9 MHz, intercept of the backscattering spectrum.

METHODS

Tissue processing

First the influence of the tissue processing needed for slicing embedded in paraffin was investigated. For this study 24 liver samples of 8 white New Zealander rabbits (4 to 5 months old, weight 2.5 to 3.0 kilogram) were measured under four different successive histological conditions:
- fresh (i.e. less then 1 hour after the rabbit was sacrificed)

- fixed in 4 % buffered formol solution for 1 week
- after the application of a paraffin cycle
- Haematoxylin and Eosin stained

The livers were excised within ten minutes after sacrifice of the rabbits. By clamping the large vessels before excision care was taken that air could not enter the livers. The livers were transported to the laboratory in a degassed physiological saline solution. There they were put in a large container filled with the same solution and then manually cut into slices of approximately 5 mm thickness using a chopper and a microtome blade. The chopper is a mold consisting of two parallel copper plates at a distance of 2 cm. Each plate has forty parallel grooves in it at mutual separations of 1 mm.

Three slices were selected from each liver and transported in a small container to the measurement watertank. All measurements were performed at room temperature (20 ± 2 °C) Both the watertank and the container were filled with a degassed physiological saline solution. It may be stressed that there was no contact with air between the excision of the liver and the measurements. The transportation and cutting took twenty minutes. The measurements on three slices took half an hour. After the measurements the slices were fixed in a degassed physiological saline solution, with 4 % buffered formalin addition, for at least one week After that period the slices were cooled to 6 °C for at least 24 hours to dissolve gas which may have been formed by autolysis (Frizell *et al.* 1979, Cloostermans *et al.* 1986) Then the slices were stabilized at room temperature for 20 minutes and measured again After this procedure the slices were dehydrated, embedded in paraffin, deparaffinized for 48 hours and then hydrated again during 72 hours. Where possible the fluids used were degassed and physiological. The slices were cooled again to 6 °C for 24 hours, stabilized at room temperature for 20 minutes and then measured again.

Finally the slices were stained in a degassed Haematoxylin Eosin solution for 72 hours at room temperature and conserved for 24 hours at 6 °C. After this they were stabilized at room temperature for 20 minutes and measured again.

The influence of freezing was also investigated For this purpose 10 liver samples, obtained from 4 rabbits (same race and age as in the former study), were investigated under 2 successive histological conditions:

- fixed in 4 % buffered formol solution for 1 week
- after subsequent freezing and thawing.

The livers were removed as has been described above. They were cut after one day of fixation, fixed for one week and then measured. Then they were frozen to -30 °C for 1 minute and then warmed up to -10 °C. After 10 minutes they were thawed again After this they were measured again. Prior to each measurement the samples were stored at 6 °C for 24 hours and stabilized at room temperature for 20 minutes.

Instrumental setup

The instrumental setup that was used is shown in Fig. 1. An externally triggered pulser (Aerotech Laboratories, UTA 3) sent an electrical pulse to a focused broadband transducer (Panametrics, V308, central frequency 5 MHz, diameter 23 mm, -10 dB bandwidth 5 MHz, focused at 6 cm). The received signal was amplified by a receiver (Panametrics, 5052 PR). The receiver was only used at fixed gain +40 dB. The stepper attenuator at the input of the receiver was used at 0 dB, -20 dB and -30 dB. After this the signal was low pass filtered by a 5th order Bessel filter (-3 dB at 15 MHz) and then digitized by an externally triggered transient

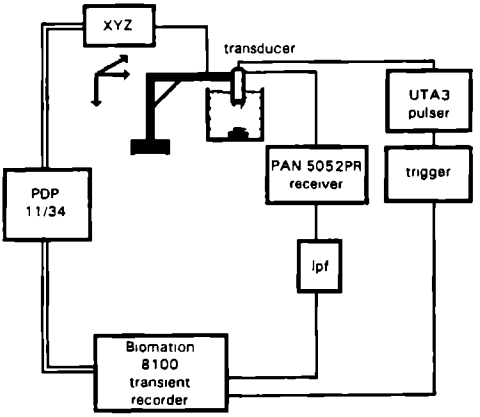

Fig 1 The instrumental set up that is used during this study

recorder (Biomation, 8100) at a sampling rate of 20 MHz. The transient recorder was interfaced to a computer (Digital Equipment Corporation, PDP 11/34) in which the data were stored. The computer also controlled a XYZ translation system (Marzhauser GmbH, $\Delta x_{min}=\Delta y_{min}=1$ μm, $\Delta z_{min}=0.1$ μm) in which the transducer was mounted.

Before the beginning of the experiments an extensive study was performed on the limitations of the used equipment. The main conclusions from this study were:
- The Marzhauser XYZ translation system reproduces very well.
- The Panametrics receiver reproduces well if the controls are all in the same position. The difference between the -30 dB and the -20 dB position of the attenuator at the input is frequency independent It's pulser does not produce enough power to be used in the backscattering measurements. For this reason the Aerotech pulser was used in the whole series of measurements.
- The Biomation transient recorder only accurately digitizes signals below 10 MHz Even at these low frequencies the controls have to be kept in the same position and the digitized signals have to be averaged as follows (Elsley 1980). To the signal 23 different offset levels are added, varying from -0.11 to +0.11 times full scale of the ADC. At each offset level the signal is averaged 4 times. In this way each signal is averaged 92 times at each acquisition.

DATA ACQUISITION

The slice of liver was put on a glass block mounted on the bottom of the watertank. The glass block was mounted in such a position that the liver was in the focal zone of the transducer and the surface of the block was parallel to the movements of the XY-plane of the XYZ-translation system. There was a plastic ring with a stretched polyethylene membrane (thickness 3 μm, total mass 2.5 g) put on top of the slice. For the fixed, paraffinized and stained slices there was another ring (mass 4 g) put on top of it to enhance the flattening of the tissue The attenuation of the membrane was measured to be less than 0.1 dB in the applied frequency range.

The principle of the acquisition procedure is illustrated in Fig. 2. First the backscattering was measured (trace 1), using the receiver at 0 dB attenuation. A scan was made in the XY-plane. This so-called C-scan covered 100 measurement positions in a 5 * 20 rectangle. The distance between the points was 500 μm in X direction and 300 μm in Y direction (total area 2.5 by 6.0 mm).

A second C-scan was made, using the receiver at -20 dB attenuation (trace 2). In this way the glass plate reflection was acquired through the liver. Then the liver was removed and a third acquisition was made of the glass plate reflection at -30 dB attenuation as a reference (trace 3). For all histological conditions the same parts of the liver specimens were examined.

DATAPROCESSING

From the signals the following parameters of the liver were obtained:
- velocity of ultrasound
- slope of the attenuation coefficient versus frequency
- attenuation coefficient at central frequency (4.4 MHz)
- slope of backscattering spectrum
- intercept of backscattering spectrum with 0 MHz axis.

VELOCITY

The local velocity c(x,y) was estimated from the time of flight measurements of the glass plate reflection with tissue $t_2(x,y)$, the membrane reflection $t_1(x,y)$ and the reference glass plate reflection $t_0(x,y)$ and the known velocity in the physiological saline solution c_0 (1500 m/s (measured)).
It was calculated from:

$$c(x,y) = c_0\left(1 + \frac{t_0(x,y) - t_2(x,y)}{t_2(x,y) - t_1(x,y)}\right) \quad [m/s] \qquad (1)$$

The difference in arrival times $t_0(x,y)$-$t_2(x,y)$ was estimated by the Spectral Phase Difference (SPD) method (Verhoef *et al.* 1985). The glass plate reflections were gated out, then Fourier transformed into the frequency domain. The obtained phase spectra were unwrapped, subtracted and subsequently a linear fit was made through this phase difference spectrum. The slope of this line yielded the difference in arrival time.

Since this method can only be applied when the two reflections are similar, this method could not be used to measure the difference in arrival time $t_2(x,y)$-$t_1(x,y)$. The estimation of this time difference was done by centroid estimation of the peak of the envelope of the glass plate and membrane reflection (Kontonassios & Ophir 1987).
First the sample point with maximum amplitude (t_{sm}) was selected. Then the exact location of the maximum was calculated from 9 successive sample points:

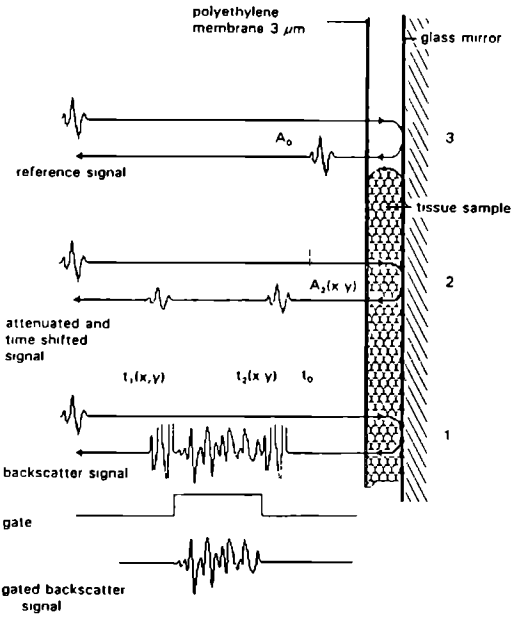

Fig 2 Scheme of data acquisition during the experiments Data are acquired in three traces The backscatter parameters are calculated from trace 1 The velocity, thickness and attenuation are calculated from trace 2 and 3

$$t_{max} = \frac{\sum_{i=i_m-4}^{i_m+4} i \cdot A(i)}{\sum_{i=i_m-4}^{i_m+4} A(i)} \quad [s] \tag{2}$$

Both the SPD and the centroid method yield a sub-sampling period accuracy.

The local thickness of the slice d(x,y) was calculated from:

$$d(x,y) = c(x,y) \cdot (t_2(x,y) - t_1(x,y)) \quad [m] \tag{3}$$

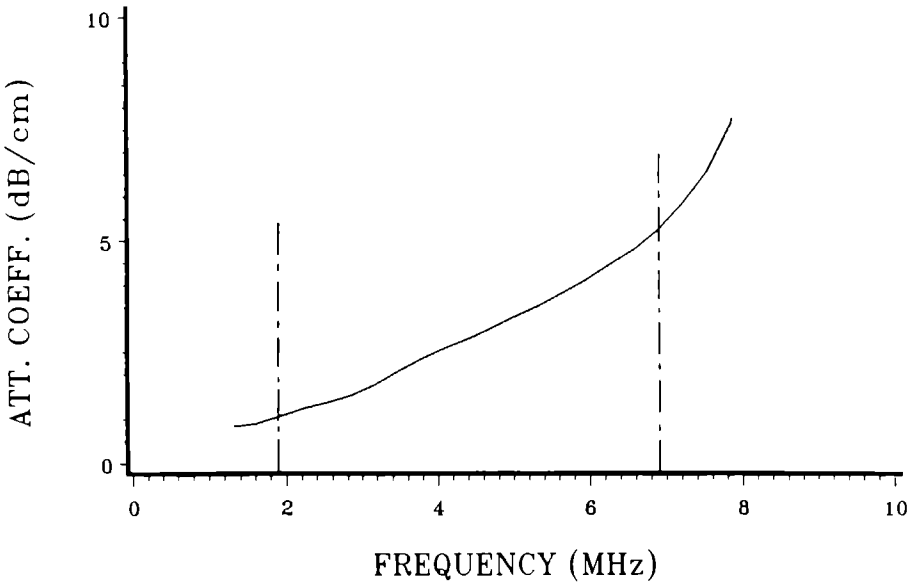

Fig 3 Attenuation coefficient versus frequency The spectrum is characterized by means of a least square fit between 1 9 and 6 9 MHz

ATTENUATION

The attenuation of ultrasound in biological tissues is frequency dependent, and a general model description of the tissue transfer function A_t is given by:

$$A_t(f, 2z) = 10^{-\alpha(f)2z/20} \quad \textbf{(4)}$$

where $\alpha(f)$ = attenuation coefficient [dB/cm]
f = frequency of the ultrasound [MHz]
2z = the acoustic path lenght through the tissue [cm]

The attenuation was obtained using the substitution method. This method has been shown to be robust with respect to influences by beam diffraction (Verhoef *et al.* 1985). In short: the glass plate reflection was measured with and without the tissue interposed. Then the reflections were gated from the rf-signals, using a double shaped cosine bell window (Bloomfield 1976) and Fourier transformed into the frequency domain.
The amplitude spectrum $P_t(f,z)$ of the reference echo can be described by:

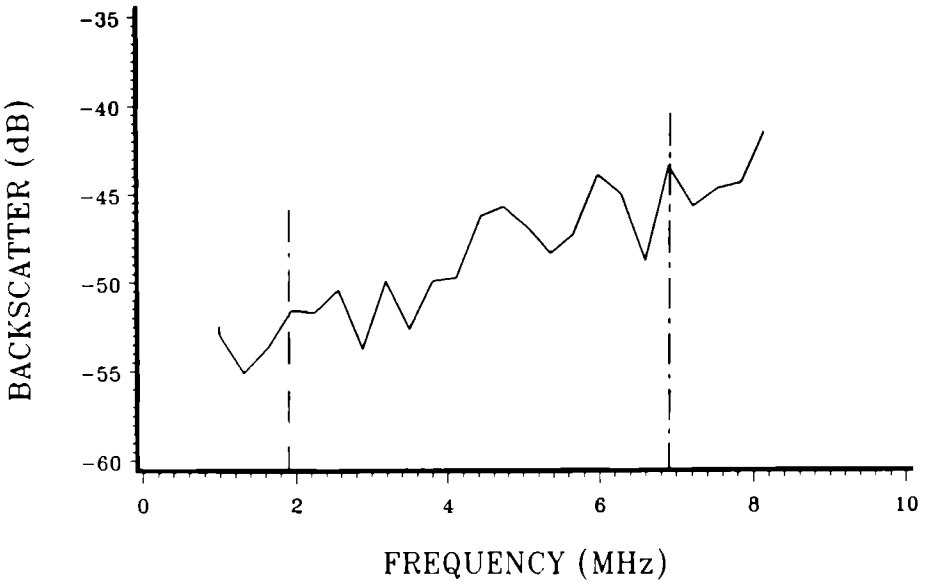

Fig 4 Backscattering spectrum The backscattering spectrum is characterized by means of a least square fit between 1 9 and 6 9 MHz

$$P_r(f,z) = V(f) \cdot A_{ph}(f,2z) \quad H_{pr}(f,z) \cdot R_g \tag{5}$$

and the amplitude spectrum $P_t(f,z)$ of the echo with the tissue interposed by.

$$P_t(f,z) = V(f) \cdot A_{ph}(f,2(z-d)) \cdot A_t(f,2d) \quad H_{pr}(f,z) \cdot R_g \tag{6}$$

where V(f) = the electroacoustic roundtrip function of the pulser, transducer and receiver
$A_t(f,2d)$ = transfer function of the tissue as described above
$A_{ph}(f,2z)$ = transfer function of the physiological saline solution
$H_{pr}(f,z)$ = the diffraction factor, the Fourier transform of the impulse response $h_{pr}(t,z)$ of the transducer-plane reflector configuration
R_g = reflectivity coefficient of the glass plate

If $H_{pr}(f,z)$ is identical for both the echo's then the attenuation coefficient follows from:

$$\alpha(f) = 20 [\, \log P_r(f,z) - \log P_t(f,z) \,] / 2d \quad [dB/cm] \tag{7}$$

For our measurements this was the case because the transducer had a relative long focal zone. Both the reference echo and the echo with tissue interposed were within this zone.

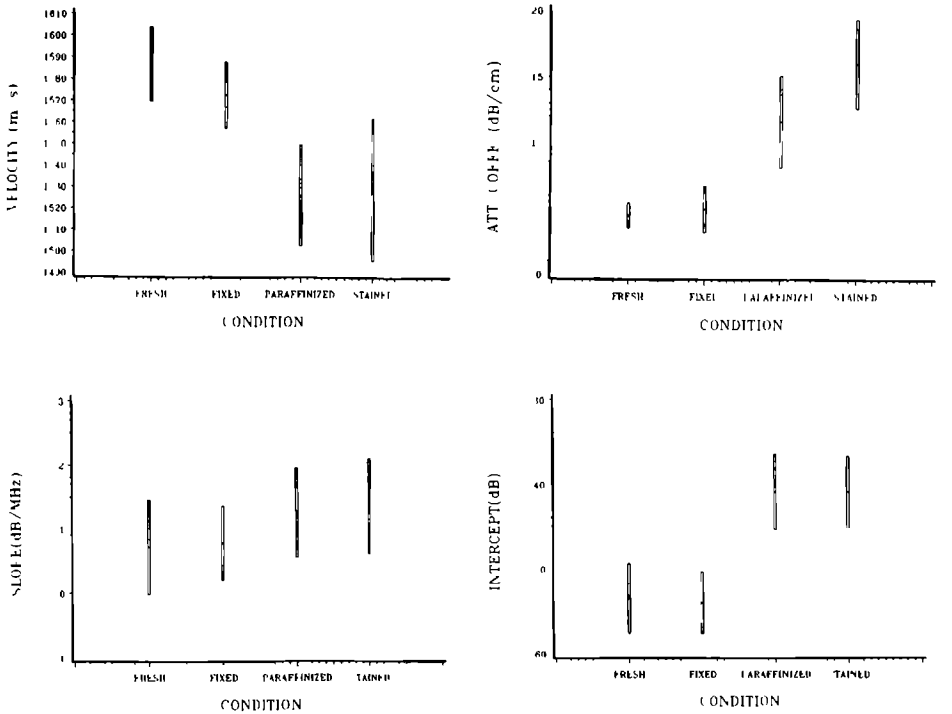

Fig 5 The influence of fixation with formalin, application of the paraffin cycle and Haematoxylin and Eosin staining on various acoustical parameters The parameters are A velocity, B attenuation coefficient at 4 4 MHz C backscattering spectral slope and D backscattering spectral intercept Given values are averages plus minus standard deviations versus histological state Data are obtained from Tables I and IV to VI

As can be seen from Fig 3 the attenuation coefficient displays a nearly linear dependency with frequency. A linear least square fit was performed to the data over the -10 dB bandwidth of the transducer (1 9 - 6 9 MHz) The slope of this fit represents the attenuation coefficient slope The value this fit at 4 4 MHz was taken as the attenuation coefficient at 4 4 MHz

BACKSCATTERING

The most simple acoustic model for biological tissue is a homogeneous and isotropic medium with a particular mass density, sound velocity and attenuation coefficient in which scattering structures are positioned at random The scattering is caused by a local difference in the acoustic impedance relative to that of the surrounding medium If the characteristic dimension σ of the scattering structures is small as compared to the wavelength ($k\sigma << 1$)

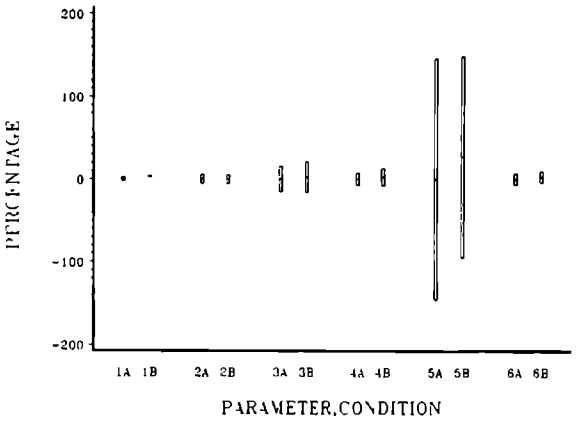

Fig 6 The relative change in the acoustic parameters introduced by freezing and thawing again The parameters are 1 velocity, 2 slice thickness, 3 attenuation coefficient slope, 4 attenuation coefficient at 4 4 MHz, 5 backscattering spectral slope and 6 backscattering spectral intercept Given values are average percentage relative to normal and standard deviations Conditions are A after formalin fixation, B after freezing and thawing again

Rayleigh scattering will occur, which is known to yield a backscattering coefficient which is proportional to f^4 (Morse & Ingard 1968):

$$\mu_{bs} \propto R_0^2 n k^4 r^6 \tag{8}$$

where μ_{bs} = backscattering coefficient
R_0 = amplitude reflection coefficient of the scatterers
r = radius of the scatterers [m]
n = number of scatterers per unit volume
k = $2\pi f/c = 2\pi/\lambda$ = wave number [m^{-1}]

If however the scatterers are larger, the backscattering coefficient can be described in terms of the amplitude reflection coefficient R_0 and a correlation function C describing the distribution of the impedance inhomogeneities within the medium (Romijn *et al.* 1989, Ueda & Ozawa 1985)

$$\mu_{bs} = \frac{2k^3 R_s^2 \sigma^2}{\pi} \int_0^\infty \gamma C(\gamma) \sin(2k\sigma\gamma)\, d\gamma \tag{9}$$

where σ = characteristic dimension of the scattering structure (correlation length) [m]
$\gamma = l/\sigma$ [m^{-1}], l = distance in 3D space [m]
R_s^2 = variance of the amplitude reflection coefficient (= $R_0^2 N\sigma^3(1-N\sigma^3)$)
$N\sigma^3$ = volume concentration in case of suspension of particles
N = number of inhomogeneities per unit volume

To obtain the backscattering coefficient the measured backscattering signal has to be corrected for attenuation, diffraction and focusing effects and system properties A method to correct for these effects is described by Romijn *et al* (1989) The backscattering coefficient of a tissue is calculated from the power backscattered by the tissue, $S_t^2(k,F)$, and a reflection by a perfect reflecting plate $S_p^2(k,F)$ both in focus of the transducer It is described by

$$\mu_{bs}(k,F) = \frac{2}{\pi d (T_a^2/F^2)} \quad \frac{R_p^2 \quad S_t^2(k,F)}{S_p^2(k,F)} \qquad \textbf{(10)}$$

where R_p = reflection amplitude coefficient of the reflector
F = focal distance [m]
T_a = transducer radius [m]
d = thickness of window in phantom [m]

OBTAINING OF $S_t(K\ F)$ $S_p(K,F)$ AND R_p

The backscattering was obtained from the rf signal acquired at the highest gain First a window of maximum length was gated, excluding both the membrane reflection and the glass plate reflection Then as many windows as possible, of 64 sampling points, with 50 % overlap, were gated, again using a double shaped cosine bell (Bloomfield 1976) Windows which contained specular reflections were omitted Specular reflections were presumed to be present in windows when the ADC saturated In this case the rf signal had a level of approximately 10 dB above average backscattering level Each remaining window was Fourier transformed into the frequency domain resulting in the amplitude spectrum $S_t(k\ F)$

Each spectrum was normalized through division by a reference spectrum ($R_p(k,F)$ which was obtained from the surface reflection of a tissue mimicking phantom (approximately 10 % gelatin in deionized water) acquired at a position corresponding to the centre of the backscattering window The reflection coefficient R_p of the phantom was obtained relative to a glass plate reflection by dividing the maximum amplitude of the phantom spectrum by the maximum amplitude of a spectrum from a glass plate reflection By using a phantom reflection instead of a stainless steel or glass reflection it was possible to keep the same receiver and transient recorder gain settings for both the backscattering and the reference measurements resulting in an identical V(f) Since the transducer is not sharply focused it was possible to acquire all the backscattering data in the focal zone of the transducer For this reason it was permitted to correct with the spectrum of a surface reflection and not with the spectrum obtained from the backscattering of a tissue mimicking phantom

After this procedure the normalized spectra were corrected for attenuation with A(f,2z) obtained in the former paragraph Then all the spectra obtained from one rf-line were averaged and subsequently the spectra of 10 adjacent measurement positions were averaged, thus obtaining 10 averaged spectra out of 100 positions After this the logarithm of the averaged spectra were taken and subsequently it is multiplied by 20 yielding a logarithmic spectrum with decibel scale (Fig 4)

From these averaged spectra, the backscattering parameters were obtained by a linear least squares fit over the -10 dB bandwidth of the transducer (1 9 6 9 MHz) From this fit the slope and the intercept at 0 MHz were obtained as tissue characterizing parameters

Table I *Velocity in four different conditions of the tissue Given values are average, standard deviation, inter slice standard deviation, intra slice standard deviation, and number of specimens All values are in m/s*

	μ	SD	SD_{INTER}	SD_{INTRA}	n
fresh	1586.6	17.3	17.0	5.1	21
fixed	1572.4	15.3	14.1	6.6	21
paraffin	1525.9	23.5	22 0	9.5	21
stained	1528.6	33 2	32.1	11.1	19

Table II *Slice thickness in four different states of the tissue Given values are the same as in Table I All values are in mm*

	μ	SD	SD_{INTER}	SD_{INTRA}	n
fresh	5.41	0.54	0.54	0.09	21
fixed	6.28	0.72	0.72	0.13	21
paraffin	5.92	0.62	0.62	0.15	21
stained	5.46	0.74	0.73	0.18	19

Table III *Attenuation coefficient slope in four different states of the tissue Given values are the same as in Table I All values are in dB/(cm · MHz)*

	μ	SD	SD_{INTER}	SD_{INTRA}	n
fresh	0.88	0.51	0.21	0.47	21
fixed	1.22	0.47	0.27	0.39	21
paraffin	3.16	0.90	0 52	0.74	21
stained	4.27	1 07	0.53	0.94	19

The obtained values were not normalized to the sample volume, so the displayed values are derived from the backscattering spectrum relative to a plane reflector, and not the backscattering coefficient This measure is often used in practice (e.g. Lizzi *et al.* 1983, Romijn *et al.* 1990, Rijsterborgh *et al.* 1990).

STATISTICS

The mentioned parameters were calculated in 4 conditions of the liver for 100 points in 21 slices obtained from a total of 8 rabbits. Three slices could not be processed because of technical problems during measurements or because the tissue was not flat enough. In this case the membrane reflection was not received by the transducer, so the front echo of the tissue could not be located. Two more measurements failed after the application of the paraffin cycle.

The effect of freezing was investigated with 2 states for 100 points in 10 slices obtained from 4 rabbits. Two slices were rejected for the same reasons as mentioned above

Table IV *Attenuation coefficient at 4 4 MHz in four different states of the tissue Given values are the same as in Table I All values are in dB/cm*

	μ	SD	SD_{INTER}	SD_{INTRA}	n
fresh	4.47	0.97	0 64	0.75	21
fixed	4.96	1.80	0.91	1 57	21
paraffin	11.62	3.50	2.79	2.21	21
stained	16.01	3 37	2.07	2 71	19

Table V *Backscatter spectral slope in four different states of the tissue Given values are the same as in Table I All values are in dB/MHz*

	μ	SD	SD_{INTER}	SD_{INTRA}	n
fresh	0.71	0.74	0.44	0.64	21
fixed	0.77	0.58	0.33	0.50	21
paraffin	1.24	0.70	0 45	0.57	21
stained	1.34	0.75	0.50	0.59	19

Table VI *Backscatter spectral intercept in four different states of the tissue Given values are the same as in Table I All values are in dB*

	μ	SD	SD_{INTER}	SD_{INTRA}	n
fresh	-53.5	4.1	2.6	3.4	21
fixed	-54.0	3 7	2.2	3 1	21
paraffin	-41.0	4.5	3 4	3.2	21
stained	-41.0	4.2	2.8	3.4	19

For each parameter the following statistics were calculated (Armitage 1973)

1 average over all livers
2 standard deviation over all livers
3 inter slice standard deviation
4 intra slice standard deviation

After this processing it was investigated whether the different histological techniques cause significant differences in the parameters using a paired t-test.

Table VII *Significance of the changes in the parameters introduced by the various histological techniques. Significances over a 1 % level are underlined*

	vel	thick	att.sl	att.fc	bs sl	bs int
fresh to fixed	0.0044	0.0001	0.0001	0.0093	0.5742	0.4190
fixed to para.	0.0001	0.0001	0.0001	0.0001	0.0005	0.0001
para. to stain	0.7377	0.0001	0.0001	0.0001	0.4912	0.4196
fixed to freeze-thawed	0.5514	0.1883	0.7823	0.1202	0.2868	0.0943

RESULTS

The results of the experiments on the influence of fixation, the paraffin cycle and staining are summarized in the Tables I to VI. Table I gives the velocity, Table II the slice thickness, Table III the attenuation coefficient slope, Table IV the attenuation at 4.4 MHz, Table V the backscattering spectral slope and Table VI the backscattering spectral intercept.

The results of the experiments on the influence of freezing after fixation are summarized in Fig. 6. in which change of the parameters relative to fixed are given for the same parameters as mentioned above.

Table VI gives the p-values and statistical significance ($p=0.01$) of the changes introduced by the various histological techniques.

Tables I and VII and Fig. 5A. reveal that velocity decreases slightly (but statistical significant) with fixation. It decreases much more when the slices are paraffinized. The spread in the values also increases considerably.

The thickness of the slices also varies with histological processing (Table II). For this reason, and also because an inter individual spread is observed of about 10 % in the thickness of slices which were cut in exactly the same way, one should really measure the thickness of the specimen or else inaccuracies are introduced in the measurements of attenuation and some time of flight estimates of the velocity. Even the intra individual spread is of the order of 2 % so a method in which the thickness is estimated at each point should be recommended.

There is a relative small but statistically significant increase in attenuation through fixation (Table III and IV, Fig 5B.). The attenuation increases dramatically after the tissue is paraffinized and rehydrated. Staining also introduces a rise in attenuation. The attenuation coefficient at 4.4 MHz and the slope of the attenuation coefficient show the same tendency. The relative standard deviations of the attenuation at 4.4 MHz are small as compared to those of the slope measurements.

Fixation causes no statistically significant change in the backscattering parameters (Table V, VI and VII, Fig 5C. and 5D.). The paraffin cycle causes a statistical significant rise in both the spectral intercept and the slope. Staining yields no significant difference in the backscattering parameters.

Fig. 6. shows that the changes introduced by freezing are very small. none of them is significant at a one per cent level (Table VII).

DISCUSSION

Many studies have been performed on the estimation of acoustic parameters *in vitro* Tissue samples were investigated under various histological conditions (fresh, after storage for some time period fixed by various fixatives, nonfixed etc) Since the experimental protocols vary a great deal it is not possible to estimate the influence of fixation from the data of these experiments The only way to estimate the influence of various histological techniques is to study tissue samples that are prepared in various ways with exactly the same protocol

Bamber *et al* (1979) investigated the influence of various fixatives on bovine liver, spleen and brain and human liver of varying time post mortem and they found that fixation by 4 % formalin decreased the velocity by 1 5 % and increased the attenuation by 30 % In our study we found a decrease of the velocity of 0 9 % and an increase of the slope of the attenuation coefficient of 38 % and an increase of the attenuation coefficient at 4 4 MHz of 11 % These values are statistically significant at a 1 % level but small as compared to their standard deviations and the change introduced by the paraffin cycle For the backscattering he found a decrease of about 35 % In our study no significant change has been found

Kremkau *et al* (1981) reported a decrease of velocity of 10 m/s (0 6 %) caused by fixation by 10 % formalin in human brains which was measured fresh within 5 hours after autopsy They found large spreads in their attenuation measurements, so their study is inconclusive at this point

Two preparation techniques needed for slicing of sections were investigated in the present study The results of the present study revealed that the paraffin cycle has a great influence on all parameters The velocity of sound in the chemicals used during the paraffin cycle differs much from the velocity in tissue (paraffin 2185 m/s (measured), alcohol 1207 m/s (Weast ed 1971), xylene substitute 1246 m/s (measured)), so the velocity will change if any of the chemicals would not totally be removed

Paraffin has an extreme high attenuation as compared to tissue (approximately 10 dB/(cm MHz) (measured) versus approximately 0 8 dB/(cm MHz)) Therefore, when a very small amount of paraffin remains in the tissue, attenuation measurements will be useless The large rise of the attenuation resulting from the paraffin cycle might be taken as a sign of this However, since absorption is active on a molecular level, denaturation of biomolecules may be another likely explanation

From the backscattering measurements it can be seen that both the intercept and the slope of the backscattering spectrum increase due to the paraffin cycle The slope of the backscattering spectrum is a measure for the size of the scatterers (Nicholas 1982, Ueda & Ozawa 1985, Lizzi *et al* 1986 Wagner *et al* 1987, Romijn *et al* 1989, Insana *et al* 1990) Since the slope has an inverse relationship with the scatterer size, it is highly presumable that the scattering is induced by smaller particles after paraffinizing of the tissue However, one should be very careful with this conclusion because the backscattering spectra display a lot of scalloping, so the slope cannot be estimated with a high precision (Table V)(Romijn *et al* 1989) There are two possible explanations for the increase of the intercept and the slope of the backscattering spectrum after application of the paraffin cycle there are remains of paraffin in the tissue, or the paraffin cycle causes damage to the tissue, from the acoustic point of view Both explanations yield the same conclusion the paraffin cycle is not suitable for acoustic microscopy

The other technique that has been investigated is slicing with a cryostat In the present study it is shown that this procedure yields no significant changes in the acoustic bulk parameters

of the tissue. It is very important that gaseous inclusions caused by autolysis are removed as much as possible by cooling (Cloostermans *et al.* 1986, Bamber & Nassiri 1985) Freese & Mackow (1968) found that attenuation and backscattering from beef and fish tissue increased markedly by freezing and then thawing the tissue. Frizell (1979) showed that this can easily be explained by gaseous inclusions. He found similar results for the attenuation. After this observation he removed gaseous inclusions in some specimens by cooling down and pressurizing the tissues. He compared the results obtained from pulse echo methods with results using the transient thermoelectric method. After degassing he found similar results for both methods.

Kessler 1973 and Parker 1983 mentioned that the acoustic properties of fresh and freeze-thawed tissues are similar. Foster *et al.* (1984) investigated one specimen and found that freeze thawing decreased the attenuation by 4 % and the velocity was not affected. d'Astous & Foster (1986) investigated one specimen and found a change in the attenuation of 6% and a change in backscattering of 9 % They concluded that these values were not significant.

If one wants to compare optical with acoustic microscopy one should use a cryostat. Although this way of slicing provides a lower level of consistency of the tissue than slicing with a paraffin microtome, and thus yields some morphological artifacts, the acoustic properties of the tissue do not change significantly Therefore, the cryostat technique should be applied in future studies.

The influence of HE-staining after the application of a paraffin cycle was also investigated in this study. The staining had a major influence only on the attenuation parameters. The influence of staining after freezing is not reported here. It is currently being studied with a Scanning Acoustic Microscope at a frequency of 1.2 GHz.

CONCLUSIONS

Fixation with formalin preserves the acoustic properties of tissue to reasonable extent. The paraffin cycle has a very sizeable effect on all the investigated acoustic parameters. From this study it can be concluded that it should be avoided at all times. The acoustic properties of tissue are not affected by freezing. If one wants to compare optical with acoustic microscopy one should use a cryostat.

WORKS OF REFERENCE

Armitage P (1973) Statistical methods in medical research. Oxford: Blackwell Scientific Publications

D'Astous F.T., Foster F.S. (1986) Frequency dependence of ultrasound attenuation and backscatter in breast tissue. Ultrasound in Med. & Biol. 12: 795-808

Bamber J.C., Fey M.J., Hill C.R., Dunn F. (1977) Ultrasonic attenuation and backscattering by mammalian organs as a function of time after excision. Ultrasound in Med. & Biol. 3: 15-20

Bamber J.C., Hill C.R. (1979) Ultrasonic attenuation and propagation speed in mammalian tissues as a function of temperature. Ultrasound in Med. & Biol. 5: 149-157

Bamber J.C., Hill C.R., King J.A., Dunn F (1979) Ultrasonic propagation through fixed and unfixed tissues. Ultrasound in Med. & Biol. 5: 159-165

Bamber J C., Nassiri D.K. (1985) Effect of gaseous inclusions of the frequency dependence of ultrasonic attenuation in liver. Ultrasound in Med. & Biol. 11: 293-298

Bloomfield P. (1976) Fourier analysis of time series:an introduction. New York: John Wiley. 80-85

Chivers R.C., Parry R.J. (1978) Ultrasonic velocity and attenuation in mammalian tissues. J. Acoust. Soc. Am. 63· 940-953

Cloostermans M.J.T.M, Mol H., Verhoef W.A., Thijssen J.M. (1986) *In vitro* estimation of acoustic parameters of the liver and correlations with histology. Ultrasound in Med. & Biol. 12: 39-51

Coleman D.J., Silverman R.H., Rondeau M.J., Lizzi F.L., Mclean I.W., Jacobiec F.A. (1990) Correlations of acoustic tissue typing of malignant melanoma and histopathologic features as a predictor of death. Am. J. of Ophthalm. 110: 380-388

Crosby B.C., Mackay R.S. (1978) Some effects of time post-mortem on ultrasonic transmission through tissue under different modes of handling. IEEE Trans. BME. 25: 91-92

Elsley R.K. (1980) Accurate ultrasonic measurements with the Biomation 8100 transient recorder. In Ultrasonic Materials Characterization (Edited by H. Berger and M. Linzer) NBS/NSF Special Publication 596, Washington D.C.: U.S. Govt. Printing Office: 311-317

Foster F.S., Strban M., Austin G. (1984) The ultrasonic macroscope:initial studies of breast tissue. Ultrasonic Imaging 6: 243-261

Freese M., Makow D. (1968) Ultrasonic backscatter in fresh and thawed animal tissue. J Fish. Res. Bd., Canada 25: 605-607

Frizell L.A., Carstensen E.L, Davis J.D. (1979) Ultrasonic absorption in liver tissue J. Acoust. Soc. Am. 65: 1309-1312

Goss S.A., Johnston R.L., Dunn F. (1978) Comprehensive compilation of emperical ultrasonic properties of mammalian tissues. J. Acoust. Soc. Am. 64: 423-457

Goss S.A., Johnston R.L., Dunn F. (1980) Compilation of emperical ultrasonic properties of mammalian tissues II. J. Acoust. Soc. Am. 68: 93-108

Insana M.F., Wagner R.F., Brown D.G., Hall T.J. (1990) Describing small-scale structure in random media using pulse-echo ultrasound. J. Acoust. Soc. Am. 87: 179-192

Kessler L.W. (1973) VHF ultrasonic attenuation in mammalian tissue. J. Acoust. Soc. Am. 53: 1759-1760

Kontonassios T., Ophir J. (1987) Variance reduction of speed of sound estimation in tissues using the beam tracking method. IEEE Trans. UFFC. 34: 524-530

Kremkau F.W., Barnes R.W., McGraw C.P. (1981) Ultrasonic attenuation and propagation speed in normal human brain. J. Acoust. Soc. Am. 70: 29-38

Lizzi F.L., Greenebaum M., Feleppa E.J., Elbaum M., Coleman D.J. (1983) Theoretical framework for spectral analysis in ultrasonic tissue characterization. J. Acoust. Soc. Am. 73: 1366-1373

Lizzi F.L., Ostromogilsky M., Feleppa E.J., Rorke M.C., Jaremko M.M. (1986) Relationship of ultrasonic spectral parameters to features of tissue microstructure. IEEE Trans. UFFC. 33: 319-329

Morse P.M., Ingard K.U. (1968) Theoretical Acoustics. New York: McGraw-Hill Inc.. chap. 8

Nicolas D. (1982) Evaluation of backscattering coefficients for excised human tissues: results, interpretation and associated measurements. Ultrasound in Med. and Biol. 8: 17-28

Okawai H., Tanaka M., Dunn F., Chubachi N., Honda, K. (1989) Quantitative display of acoustic properties of the biological tissue elements. In Acoustical imaging vol. 17 (edited by Shimizu H., Chubachi N. and Kushibiki) Plenum Press New York and London: 193-201

Okawai H., Tanaka M., Dunn F. (1990) Non-contact acoustic method for the simultaneous measurement of thickness and acoustic properties of biological tissues. Ultrasonics 28: 401-410

Parker K.J. (1983) Ultrasonic attenuation and absorption in liver tissue. Ultrasound in Med. & Biol. 9: 363-369

Rijsterborgh H., Mastik F., Lancée C.T., van der Steen A.F.W., Sassen L.M.A., Verdouw P.D., Roelandt J., Bom N. (1990) Ultrasonic myocardial integrated backscatter and myocardial wall thickness in animal experiments. Ultrasound in Med. & Biol. 16: 29-36

Romijn R.L., Thijssen J.M., Beuningen, G.W.J. van. (1989) Estimation of scatterer size from backscattered ultrasound: a simulation study. IEEE Trans. UFFC. 36: 593-606

Romijn R.L., Thijssen J.M., Oosterveld B.J., Verbeek A.M. (1991) Ultrasonic differentiation of intraocular melanomas: parameters and estimation methods. Ultrasonic Imaging

van der Steen A.F.W., Rijsterborgh H., Mastik F., Lancée C.T., van Hoorn W.M., Bom N. (1991) The influence of attenuation on measurements of ultrasonic myocardial integrated backscatter during cardiac cycle (an *in vitro* study). Ultrasound in Med. & Biol. 17: 879-891

Ueda M., Ozawa Y. (1985) Spectral analysis of echoes for backscattering coefficient measurement. J. Acoust. Soc. Am. 77: 38-47

Verhoef W.A., Cloostermans M.J.T.M., Thijssen J.M. (1985) Diffraction and dispersion effects on the estimation of ultrasound attenuation and velocity in biological tissues. IEEE Trans. BME. 32: 521-529

Wagner R.F., Insana M.F., Brown D.G. (1987) Statistical properties of radiofrequency and envelope detected signals with application to medical ultrasound. J. Opt. Soc. Am. 4: 910-922

Weast R.C. ed. (1971) Handbook of Chemistry and Physics. Cleveland Ohio: The Chemical Rubber Co.: E-41

CHAPTER VIII

A NEW METHOD FOR CORRELATION OF ACOUSTIC SPECTROSCOPIC MICROSCOPY (30 MHz) AND LIGHT MICROSCOPY.

A.F.W. van der Steen, J.M. Thijssen, J.A.W.M. van der Laak, G.P.J. Ebben, P.C.M. de Wilde

ABSTRACT

In this study a powerful method has been developed to investigate the correlation between light microscopic and acoustic properties of biological tissues. Liver specimens were sectioned, alternating in thickness between 250 μm and 10 μm. The thick ones were investigated acoustically, the thin ones by means of light microscopy. In these sections markers were placed that can be detected and located, both optically and acoustically. By means of these markers it was possible to find and reconstruct corresponding regions in the acoustic and optical section (2.5 x 2.5 mm).
From the sections that were investigated acoustically, parameter images were reconstructed. The acoustic parameters were the attenuation at 30 MHz, the slope of the attenuation spectrum between 10 and 50 MHz, the backscattering at 30 MHz, the slope of the backscattering spectrum between 10 and 50 MHz and the local ultrasound velocity. They were obtained in the frequency range from 10 up to 50 MHz, yielding a lateral resolution of about 50 μm.
The sections for light microscopy were stained according to the Goldner trichrome staining technique. The histological composition of the optical sections was obtained quantitatively, using digital image segmentation techniques. The percentage collagen rich fibrous tissue content, the percentage luminal structure, the percentage interstitial spaces and the number of nuclei were calculated in regions of 250 x 250 μm. These histological features were correlated with the acoustic parameters obtained from the corresponding regions in adjacent sections. In this way it was possible to find the histological components responsible for acoustic parameters.

INTRODUCTION

During the last two decades, many papers were issued on tissue characterization by means of ultrasound. Several of these pilot studies claimed promising results for application in clinical settings. However, the lack of correlation between the acoustic parameters and histological details shows that there is a need for good tissue models. In order to develop these, the tissue components which are fundamental to the acoustic characteristics of tissues and to the texture of echographic images should first be identified.

Several *in vitro* studies have been reported on the correlation between histological components and acoustic bulk parameters of biological tissues mainly on liver tissue (Pauly & Schwan 1971, Field & Dunn 1973, Johnston *et al* 1979, Bamber & Hill 1981, Bamber *et al* 1981, Pohlhammer & O'Brien 1981, Zimmerman & Smith 1983, Nicholas & Nicholas 1983, Cloostermans *et al* 1986) In addition, some *in vivo* studies on patients have been reported in which the histological verification of diffuse liver diseases was based on biopsies (Kuc 1980, Kuc & Taylor 1982, Narayama & Ophir 1983, Wilson *et al* 1983, Maklad *et al* 1984, Robinson *et al* 1984 Garra *et al* 1987, Parker *et al* 1988, Hartman *et al* 1993 Oosterveld *et al* 1993)

Recently, the technology of ultrasonic imaging has been considerably improved and it is possible nowadays to make parametric images at higher frequencies, yielding better resolution Acoustic microscopes have been developed to operate at frequencies up to 4 GHz, resulting in higher resolutions than those of light microscopes (Jipson & Quate 1978, Hafsteinsson & Rizvi 1984) These acoustic microscopes, however are limited in the number of parameters which can be imaged New microscopic techniques have been developed for imaging other acoustic parameters which are also being used in diagnostic tissue characterization and classification (Foster *et al* 1984 Daft *et al* 1986, Daft *et al* 1989 Briggs 1992) These microscopes make it possible to perform correlation studies of the optical and acoustic parameters of biological tissues

So far only qualitative comparisons between acoustic and optical images have been reported (e g d'Astous & Foster 1986) For quantitative studies two main problems arise First, most of the standard tissue processing techniques used in light microscopy are not suited for acoustic microscopy because they considerably influence the acoustic parameters of the tissue Van der Steen *et al* developed tissue processing techniques that are acceptable for both light and acoustic microscopy (van der Steen *et al* 1991, van der Steen *et al* 1992a van der Steen *et al* 1992b, Chapters VI VII) Second, in order to estimate the acoustic parameters of biological tissues, thicker sections are needed than those used in light microscopy Consequently it is not possible to observe the same sections both acoustically and optically

The method described in this study enables one to correlate the acoustic parameters of a section with the quantitative histological features of an adjacent section A sectioning technique is used that produces sections alternating in thickness between 250 μm and 10 μm The histological parameters are assessed by digital red green-blue (RGB) segmentation of light microscopic video images acquired after a special histological Goldner trichrome staining technique The acoustic techniques employed are discussed as well as a method for finding the corresponding region in adjacent sections Finally a statistical technique is proposed to find correlations between the acoustic parameters and the histological features and to then eliminate the influence of one parameter on the correlation between others The method is illustrated with the results for a representative slice of liver tissue

METHODS

TISSUE PROCESSING

Liver tissue samples obtained from White New Zealander rabbit were fixed for 24 hours in a degassed, physiological saline solution (0 9 % NaCl) with 4 % buffered formalin addition (buffered with 0 5 mM di-Sodium tetraborate and 0 02 M Boric acid) This procedure has

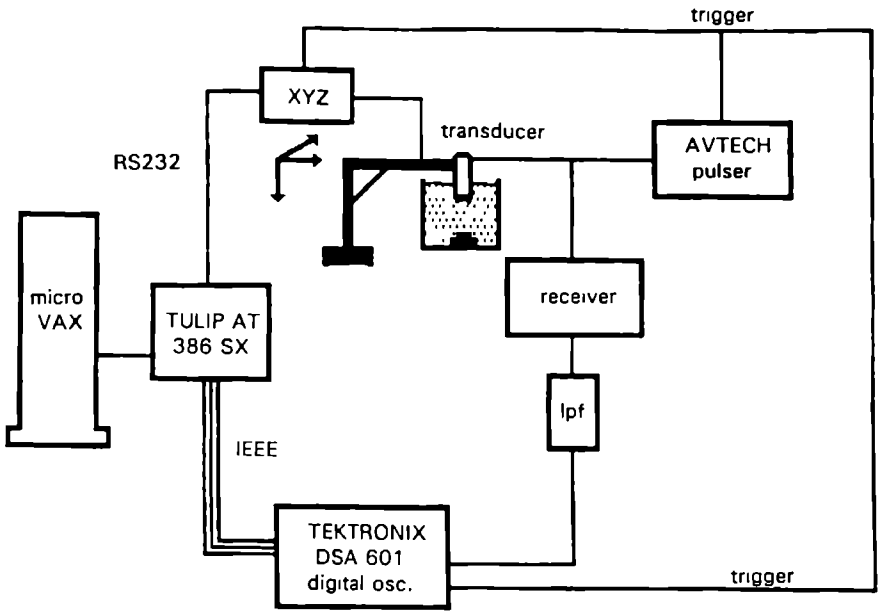

Fig 1 Instrumental set up used for acoustical investigation of the sections

no major influence on the acoustic properties of the tissue (van der Steen *et al.* 1991, van der Steen *et al.* 1992a, Chapters VI-VII). Immediately after excision the liver was lamellated to obtain a faster penetration of the fixative. After 24 hours the tissue was cut into small blocks of approximately 1 x 1.5 x 1 cm. In these blocks two parallel markers were inserted by piercing them with two strings of black silk surgical suture material (ethicon[1] 0.7 metric, 6-0, c-1), which were first soaked in Indian ink. The distance between the markers in the various blocks varied from 6 to 8 mm, the diameter of the markers was about 75 μm. These markers could be identified both optically and acoustically. After this procedure the tissue was embedded in polyacrylamide to enhance the consistency of the tissue during sectioning. This material does not penetrate the tissue (Chrambach & Rodbard 1971, Hausen & Dreyer 1981), and therefore it did not affect the acoustic properties of the tissue. The tissue was then sectioned, perpendicular to the markers with a freeze sled microtome (Leitz Weltzlar Inc.). Adjacent sections alternated in thickness between 250 μm and 10 μm. The thick ones were investigated acoustically and the thinner ones with a light microscope. The latter sections were stained by a trichrome staining technique according to Goldner (Romeis 1968). This staining resulted in sections with red parenchymal tissue, green collagen-rich fibrous tissue and dark red nuclei.
The sections for acoustic investigation were both transported to the acoustic setup and measured in a degassed physiological saline solution.

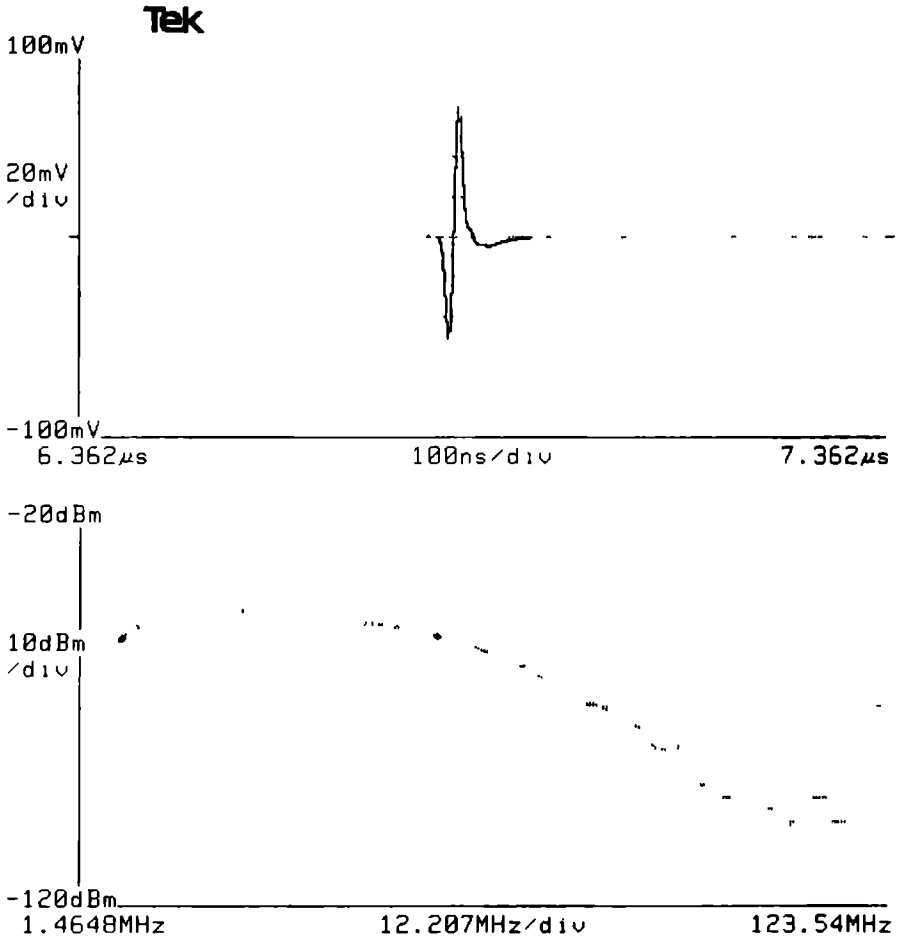

Fig 2 Glass mirror reflection (upper panel) and its spectrum (lower panel) The cursors in the spectrum are placed at the -6 dB points of the spectrum (8 and 55 MHz)

ACOUSTIC

INSTRUMENTAL SETUP

The instrumental setup that was used is shown in Fig. 1. An externally triggered pulser (Avtech AVG-3-C) transmitted an electrical pulse (duration 5 ns half power, amplitude stepwise selectable from -50 V up to -500 V) to a broadband PVDF transducer (Fulmer IFS 125, central frequency 30 MHz, -6 dB frequency range 10-55 MHz, aperture diameter 3 mm, focused at

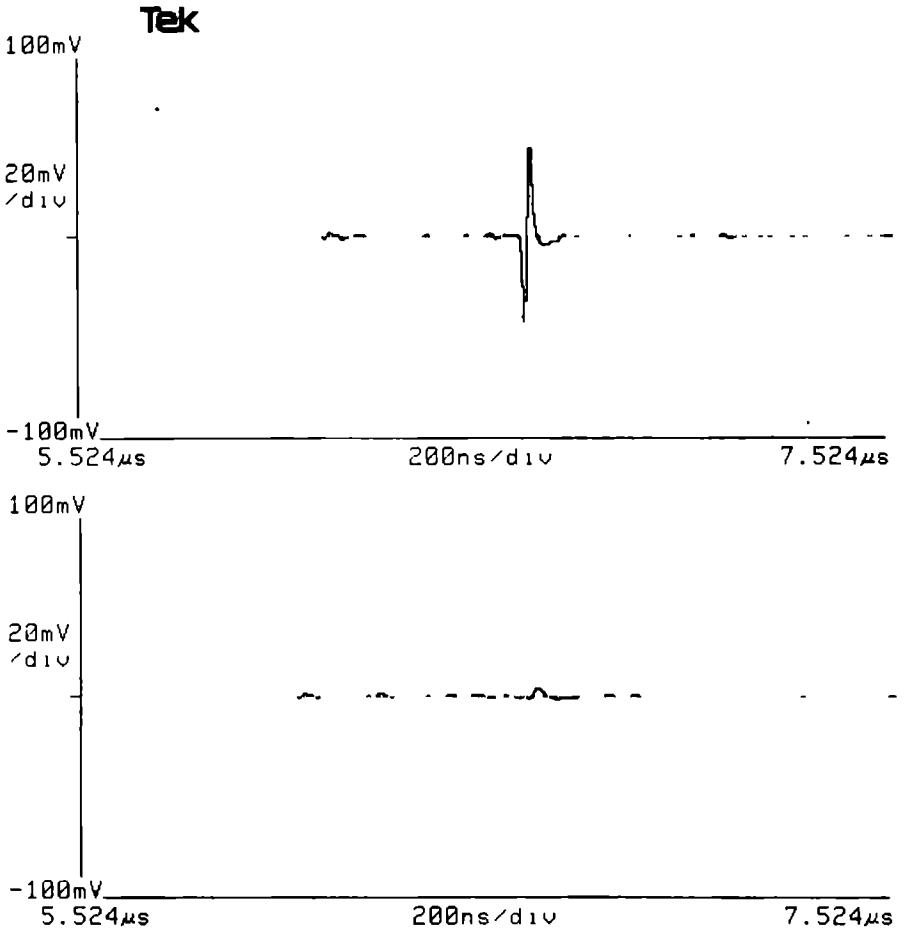

Fig 3 Glass mirror reflection with the tissue interposed The reflection in the upper panel is acquired above liver tissue and the lower one above a marker The reflection in the latter one has totally vanished

5 mm) The theoretical resolution, i.e. the point spread function of the transmitted sound pulse in the focus was 20 μm x 50 μm, depth x width. The received signal was preamplified by a custom made broadband receiver (gain 20 dB, -6 dB bandwidth more than 150 MHz, input impedance 600 Ω) that was connected to the transducer with a cable of 6 cm length. The preamplified signal was low pass filtered (7th order Bessel, K&L Inc , cut off frequency 70

MHz) to prevent aliasing, and digitized to 8 bits by a digital oscilloscope (Tektronix DSA 601) at a sampling rate of 250 MS/s. (The number of effective bits in the used frequency range was between 7.0 and 7.2 without averaging of the signal.) Fig. 2. shows the reflection and its log power spectrum of a glass mirror at the focus of the transducer, with a electrical transmission pulse of 100 V. The digital oscilloscope was interfaced by means of an IEEE GPIB bus to a 386 SX IBM compatible PC (Tulip B.V., The Netherlands) with a 80387 coprocessor A rewritable, removable optical disk (Ricoh 9200 E II, capacity 600 Mbyte/disk) was connected to the PC. The PC was interfaced by means of an RS232 interface to the controller (custom made) of an XYZ-translation system (Marzhauser GmbH, F R.G., $\Delta x_{min}=\Delta y_{min}=$ 1μm, Δz continuously adjustable) in which the transducer was mounted. On the X and Y directions of the system, optical transducers were assembled for a position feedback (Heidenhain, F.R G., MT60K $\Delta x=\Delta y=0$ 5μm). This position feedback gave the opportunity to perform measurements on the fly, as described in the section Data Acquisition.
The acquisition PC was interfaced by means of a local area network (DECNET, Digital Inc.) to a Microvax 3200 (Digital Inc), on which the data processing was performed.

DATA ACQUISITION

The tissue section for acoustic measurements was placed on a glass block mounted in the bottom of a watertank filled with a physiological saline solution The surface of the block was parallel to the movements of the XY-plane of the XYZ-translation system. The transducer position was vertically adjusted, until the section was in the focal zone of the transducer. The section was covered by a 3 μm thick polyethylene membrane that was stretched in a plastic ring. This membrane flattened the tissue specimen and prevented it from moving during the measurements. The attenuation of the membrane was measured to be less than 0 2 dB in the applied frequency range. Measurements were performed at room temperature (20 $\pm$ 2 °C)

The position of the two markers (see Tissue processing) was assessed prior to the measurements. The silk suture displayed a very high ultrasonic attenuation when it was insonified along the fibre orientation. The centres of the markers were found by determining the positions of a total disappearance of the glass block reflection (Fig 3.) For an exact location the information in the lower frequency components of the ultrasound pulse are of importance, since the lateral resolution of these components is in the order of the size of the markers The markers could be relocated acoustically with a reproducibility of 25 μm. Once the two markers were located, 3 C-scans (100 x 100 points, $\Delta x=\Delta y=25\mu$m) were performed on a region midway between the two markers. The first C-scan was made while using a transmission pulse of -500 V (Fig. 4., scan 1), the second with a transmission pulse of -100 V (Fig. 4., scan 2) and the third, after removal of the section, also with a transmission pulse of -100 V (Fig. 4., scan 3).

The measurements were performed on the fly, which means that the transducer moved continuously and did not stop at the measurement points. The lateral displacement of the transducer between transmitting and receiving of the pulse due to this movement was approximately 5 nm, which is negligible. This was enabled by appropriate use of the positioning feedback and of the triggering facilities of the digital oscilloscope: the XYZ table was allowed to move with uniform velocity. When it reached a each measurement position, which was detected by the XYZ-controller, the controller gave a trigger pulse to the pulser and to the oscilloscope. Then the rf-signal was acquired and stored directly in the RAM of the PC. After each full scan line of 100 traces had been recorded, the data were transferred from the RAM to the hard disk,

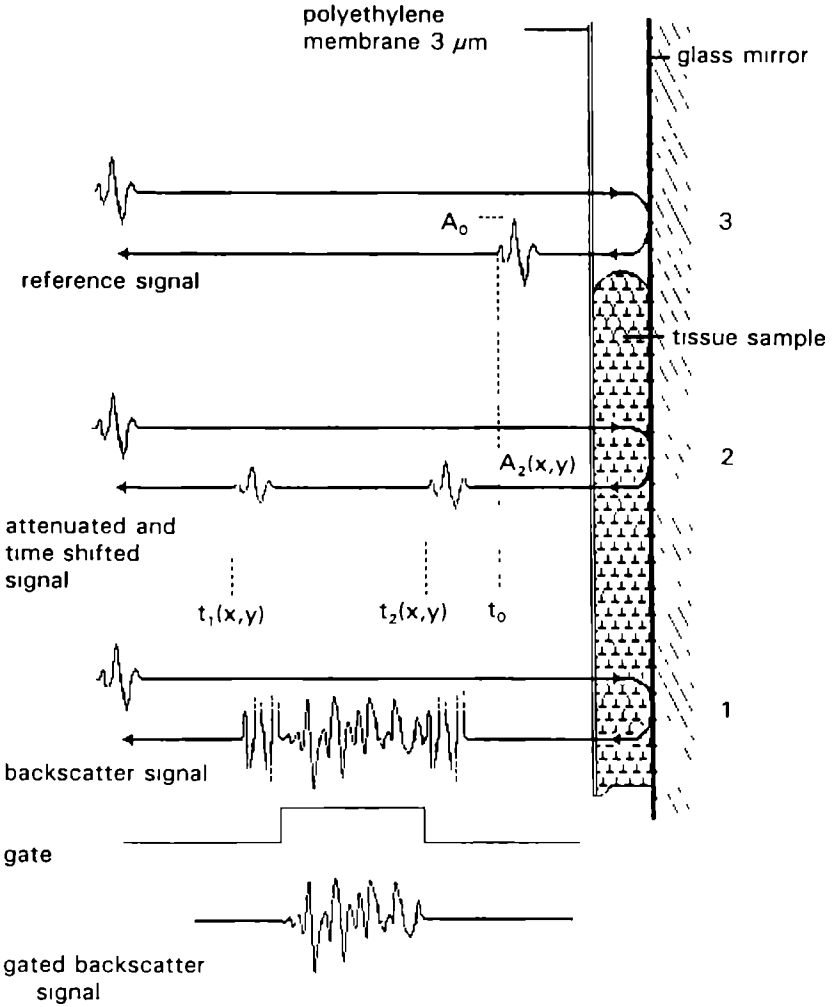

Fig 4 The three rf signals used for calculation of the acoustical parameters
Trace 1 was recorded using the pulser at an amplitude of - 500 V From this trace the backscatter parameters were obtained Trace 2 and 3 were recorded using the pulser at an amplitude of -100 V These traces provide information about the location and the spectra of the echo peaks with and without the tissue interposed From the times of flight of the reflection of the glass plate reflection and the membrane reflection the local ultrasound velocity and the local thickness were obtained From difference in spectra of the glass plate reflection with and without the tissue interposed the spectral attenuation was obtained These three rf-signals were obtained in a 100 x 100 matrix

or to the optical disk Then the next line of the 100 line raster was scanned, etc Measuring on the fly was 85% faster than measuring in start-stop mode One full two dimensional C-scan of 100 x 100 traces was performed in 16 minutes

DATA PROCESSING

From the rf signals the following parameters were obtained

- velocity of ultrasound
- slope of the attenuation coefficient versus frequency between 10 and 50 MHz
- attenuation coefficient at central frequency (30 MHz)
- slope of the backscattering spectrum between 20 and 40 MHz
- backscattering at 30 MHz

An extensive description of the acoustic data processing to obtain these parameters has been reported in a previous paper (van der Steen *et al* 1991, Chapter VII) In short

VELOCITY

The local velocity c(x y) was estimated from the time of flight measurements of the glass plate reflection with a tissue section interposed $t_2(x,y)$, the membrane reflection $t_1(x,y)$, which were obtained from measurement 2 (Fig 4) and the reference glass plate reflection $t_0(x\ y)$, i e measurement 3 (Fig 4) and the known velocity in the physiological saline solution c_0 (1500 m/s (measured)) It was calculated from

$$c(x\ y) = c_0\left(1 + \frac{t_0(x\ y) - t_1(x\ y)}{t_2(x\ y) - t_1(x,y)}\right) \quad [m/s] \tag{1}$$

The difference in arrival times $t(x,y)$ $t_2(x,y)$ was estimated by the spectral phase difference (SPD) method (Verhoef *et al* 1985) The estimation of the time difference $t_2(x\ y)$ $t_1(x\ y)$ was done by centroid estimation of the peak of the envelope of the glass plate reflection and the membrane reflection (Kontonassius & Ophir 1987)
The local thickness of the section d(x,y) was calculated from

$$d(x,y) = c(x\ y)\quad (t_2(x,y) - t_1(x,y))/2 \quad [cm] \tag{2}$$

ATTENUATION

The attenuation was obtained using the substitution method This method has been shown to be robust with respect to influences of beam diffraction (Verhoef *et al* 1985) The glass plate reflection was measured with and without the section interposed Then the reflections were gated from the rf signals using a double shaped cosine bell window (Bloomfield 1976) and Fourier transformed into the frequency domain The attenuation coefficient versus frequency, $\alpha(f)$ follows from

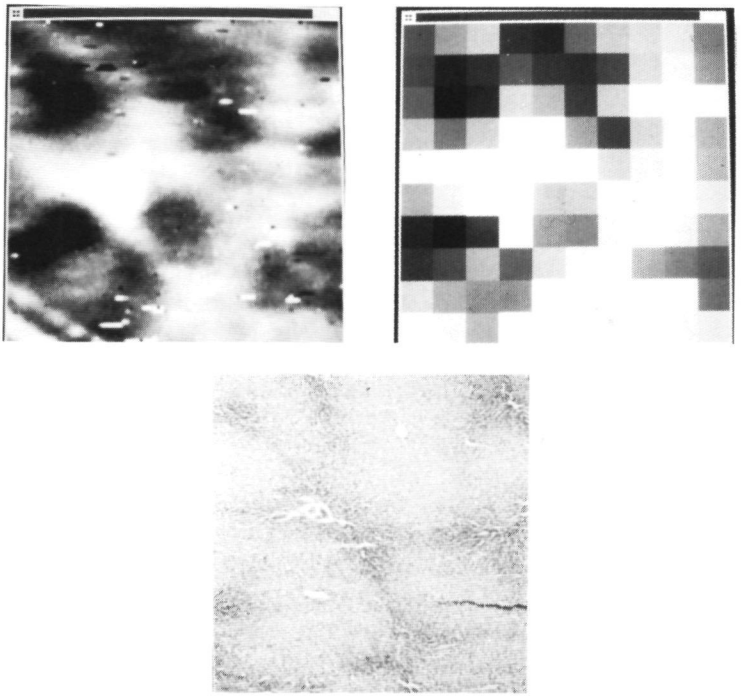

Fig. 5. The averaging of the acoustical parameters.

A. Acoustical parameter image (attenuation slope) of a liver section (2.5 x 2.5 mm).

B. Averaged image, used for the correlation study.

C. Light microscopic image of the same region in an adjacent light microscopic section. Note the correpondence of regions containing collagen (green in the optical image) with region of high attenuation.

$$\alpha(f) = 20\,[\log P_r(f) - \log P_t(f)\,] / 2d \quad [dB/cm] \tag{3}$$

where $P_r(f)$ = amplitude spectrum of the reference glass plate reflection
$P_t(f)$ = amplitude spectrum of the glass plate reflection with the tissue interposed.

A linear least square fit was performed on the data between 10 to 50 MHz. The slope of this spectrum represents the attenuation coefficient slope. The value of this fit at 30 MHz was taken as the attenuation coefficient at 30 MHz.

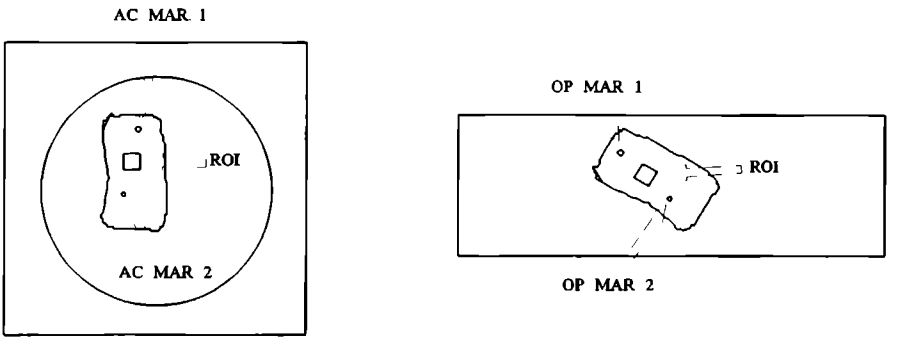

Fig 6 Illustration of the collocation of the acoustical and optical fields
A The section for acoustical investigation was placed in the measurement bath at an arbitrary angle The locations of the markers (AC MAR) were recorded and a central region between the markers was investigated
B In the section for light microscopy the location of the markers (OP MAR) were again recorded From these and the location of the acoustical markers, the location, rotation and size of the region of interest within the optical section was calculated

BACKSCATTERING

The backscattering was obtained from the rf-signal acquired at the highest gain setting First a window of maximum length was gated, excluding both the membrane reflection and the glass plate reflection Then as many windows as possible of 33 sample points with 50 % overlap were gated, again using a double shaped cosine bell. Windows that contained specular reflections were omitted Specular reflections were presumed to be present in windows in which the ADC saturated. In this case the rf-signal had a level of approximately 10 dB above average backscattering level Each remaining window was Fourier transformed into the frequency domain Each spectrum was normalized through division by the spectrum of a glass plate reflection which was acquired with the glass plate at the position of the centre of the window investigated. This was valid because the section was quite thin (250 μm) and the spectrum of the sound field hardly changes when this close to the focus

Then the spectra were corrected for the measured attenuation $\alpha(f)$ After these corrections the spectra became depth independent and they were averaged along each rf-line. Then the logarithm of the spectra was taken and subsequently it was multiplied by 20, yielding a logarithmic spectrum with decibel scale A linear least square fit of the backscattering spectrum between 10 and 50 MHz was taken. From this fit the slope and the intercept at 30 MHz were obtained as parameters

Imaging of parameters

The parameters were calculated as described above in 10000 points and then for each parameters 100 x 100 pixel parameter images were reconstructed as follows. The range of the parameter was normalized to a grey level range from 0 to 255 (i.e. 8 bits) and encoded in a 100 x 100 pixel image. Fig 5A. is a parameter image (attenuation at 30 MHz, range 25 to 50 dB/cm) of an arbitrary liver section of 250 μm thickness. For the correlation study the parameters were averaged over 10 x 10 points. Since the thickness of the section was about 250 μm and the points were acquired 25 μm apart, this resulted in an image of 100 cubic voxels, as is shown in Fig. 5B. A light microscopic image, obtained after a trichrome staining according to Goldner (section tissue processing) of a similar region in an adjacent section is shown for comparison in Fig. 5C

Optical

Instrumental setup

The heart of the optical setup was a VIDAS^{plus} system (Kontron Inc., F R G.) It consisted of an IBM compatible 80386 32 bit 16 MHz host processor, containing a 387 math coprocessor, 2 Mbyte RAM, 4 MByte image memory, 86 MByte Winchester hard disk, MIAP 1 image processor, and AD and DA converters for RGB and monochrome images. The same optical disk used for acoustic data acquisition was connected to the system during optical image acquisition and processing On this hardware an image processing package was installed (IBAS2.0) The images were acquired by a CCD RGB camera (Sony 3CCD CA-325AP) mounted on a light microscope (Axioskop, Zeiss) The stage of this microscope was provided with two transducers for positional feedback (Sony MSH 707, accuracy 1 μm).

Data acquisition

The marker holes in the sections for light microscopy were found by visual inspection and localized by means of the positional feedback device. The centre of the markers could be localised optically with a reproducibility of 10 μm. The black suture had washed out of most sections during tissue staining, but the remaining holes were easily identified due to the residual presence of Indian ink. By correlating the positions of the markers in the optical section with those in the acoustic section, it was possible to find the same 2.5 x 2.5 region of interest in both sections. Since both the acoustic and optical sections were positioned on glass plates in arbitrary positions, these regions common were aligned by rotation with respect to each other over arbitrary angles (Fig 6.) During histochemical processing, the thin optical sections were sometimes stretched or squeezed slightly (0 to 2 %), so that the size of the optical and acoustic section was not always exactly the same. This was taken into account when the averaged acoustic C-scan parameter images were projected on the optical section images from the positions of the acoustic and optical markers. From the region of interest within the optical section a 10 x 10 matrix of RGB images was acquired, each of approximately 325 x 325 pixels, covering an area of approximately 250 μm x 250 μm

Segmentation

After acquisition, the optical images were segmented. The percentage area that was occupied by collagen rich fibrous tissue, interstitial spaces, luminal structures, nuclei and parenchymal tissue, and the number density of nuclei were estimated as follows:

(It should be kept in mind that there are three grey level images for each field: one representing the local red intensity, one for the local green intensity, and one for the local blue intensity.)

Collagen: (Fig 7) The local average over the red, the blue and the green intensities was subtracted from the local green intensity. This resulted in the image depicted in Fig. 7B.

Subsequently, all pixels with a value exceeding a threshold determined by a user were selected (Fig. 7B.), resulting in a binary image. This threshold was first chosen in a representative field image and was then used as a global threshold for all 100 fields. A binary closing operation (Serra 1982) followed by a binary opening operation was used to remove the small objects from the binary image and to smooth the contours of the collagen boundaries (Fig. 7D.). The area that was occupied by collagen was then measured and the percentage collagen in the observed region was calculated.

Lumina and interstitial spaces: A histogram was calculated from each of the red, the green and the blue image. In all three images, pixels with a grey value of more than 80 % of the maximum grey value in the image were selected, resulting in three binary images.

The three binary images were first closed and in the red image objects smaller than 150 pixels were removed All objects in the resulting binary red image having any overlap with an object in both the binary green image and the binary blue image were selected A division was then made between large and small optically empty spaces: the spaces larger than 350 pixels were classified as being luminal, and the spaces smaller than this were classified as being interstitial spaces The areas of both types of optically empty spaces were measured and the percentage areas of luminal structures and of interstitial spaces were calculated.

Fig 7 Illustration of the segmentation of collagen (left side of opposite page)

- *A The original light microscopic image with green collagen and red parenchymal tissue*
- *B The average of the red, the green and the blue intensity is subtracted from the green intensity image*
- *C A global threshold is manually set*
- *D The final result The resulting binary image is smoothed by a binary open operation and followed by a binary closing operation*

Comparison of a and d reveals a successful segmentation of the collagen-rich fibrous tissue

Fig 8 Illustration of the segmentation of nuclei (right side of opposite page)

- *A The original light microscopic image*
- *B The image after thresholding and inspection of the overlap with the binary green and blue image*
- *C The image after rejection of the objects which did not fulfil the morphological selection criteria for nuclei*
- *D A monochrome grey value representation of the original red image with the cellular structures that were identified as being nuclei depicted in pseudocolor (green)*

Comparison of a and d reveals a successful segmentation of the nuclei

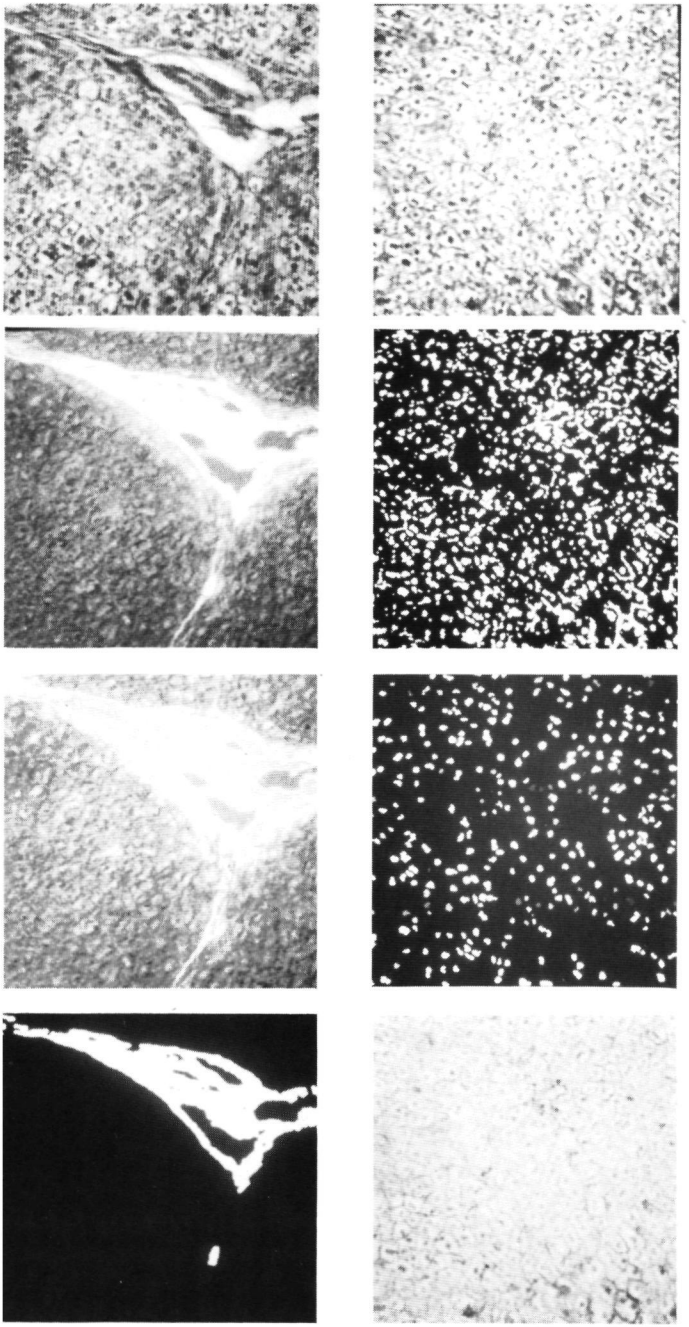

If in these two procedures a pixel was selected as being both collagen and empty space it was counted as being collagen.

Nuclei: (Fig. 8.) In the red intensity image, all pixels with a value below a global threshold, chosen by a human observer, were selected (Fig. 8B.). The resulting image was processed by a binary open operation, and objects not fulfilling morphological selection criteria for nuclei were removed (Fig. 8C.).
The number of nuclei and the percentage area occupied by nuclei were then calculated

CORRELATION OF ACOUSTIC AND LIGHT MICROSCOPY

The above described histological features of tissues were obtained in 100 fields of 250 x 250 μm The average of the acoustic parameters were calculated in corresponding fields in an adjacent section. This averaging is illustrated in Figs. 5A. and 5B This averaging was necessary to obtain regions of the same size for the acoustic and light microscopic parameters. The fields were chosen this size because the thickness of the acoustic sections was 250 μm, thus obtaining cubic voxels of 250 x 250 x 250 μm.

The Pearson correlation coefficients between the histological parameters and the acoustic parameters of an adjacent acoustic section were obtained.
Furthermore, a correction of the contribution of a parameter to a correlation between two others was assessed
This was done by calculating the partial correlation coefficients according to (Snedecor & Cochran 1979):

$$r_{ab \cdot c} = \frac{r_{ab} - r_{ac} * r_{bc}}{\sqrt{(1 - r_{ac}^2)(1 - r_{bc}^2)}} \qquad (4)$$

where. r_{ab} = the correlation coefficient of a and b
$r_{ab.c}$ = the correlation coefficient of a and b with c partialled out

If a correlation between two parameters is still present after partialling out a third parameter, then this correlation was not caused by a correlation between the third parameter and the first two If the correlation disappears, then the correlation can be explained from the correlation between the third parameter and both the first and the second. A clear example of this will show up in the section Results.

RESULTS

In table I the values of the acoustic and histological parameters of a representative section of liver tissue are presented. The values are represented as mean and standard deviations of the values in 100 fields of the section The average values of the histological parameters of particular interest (area collagen, area lumina) are low (1.2 % each). The standard deviations of the acoustic parameters appear to be relatively low, but it should be born in mind that the values that were used for the calculation of the averages were already averages of 100 data

Table I *Values for the parameters in a representative slice of liver. The values are represented as mean and standard deviation of 100 fields within the sections*

parameter	mean	SD
area collagen [%]	1 2	5 5
area lumina [%]	1 2	2 7
area interstitial spaces [%]	0 7	0 5
number of nuclei	30	12
velocity [m/s]	1593 2	6 7
attenuation slope [dB/(cm MHz)]	1 99	0 17
attenuation at 30 MHz [dB/cm]	41 7	3 3
backscatter slope [dB/MHz]	0 39	0 11
backscatter at 30 MHz [dB]	32 3	1 7

points (see section Imaging and Figs 5A and 5B)

Table II gives the results of the correlation study for the same representative piece of liver tissue. There is a high and statistically significant correlation between the attenuation parameters and the collagen content as well as a high correlation between the attenuation parameters and the percentage area occupied by lumen. Fig 5 is an illustration that subscribes this observation: the highest attenuation was found in regions that contain collagen. Furthermore, there is a high correlation between area lumen and collagen content, the reason for which is quite obvious since most of the luminal structure is surrounded by collagen. When the area lumen is partialled out (Table III) there is still a high correlation between collagen and attenuation. When the collagen content is partialled out (Table IV) the correlation between area of luminal structure and attenuation disappears. This means that the correlation between lumen and attenuation can be explained from the contribution of collagen but has no contribution of any significance by itself.

DISCUSSION

A powerful tool has been developed to investigate the correlation of light microscopic and acoustic properties of biological tissues. Until now only qualitative studies and quantitative studies at a much lower resolution have been performed.

This method is illustrated here with an example of a slice of liver tissue, but it is of general applicability and can be extended to other biological tissues. For this other staining and segmentation techniques are likely to be necessary, but many are available, requiring only minor adaptations to the methods. When selecting a staining technique, it is important that it is stable and reliable. This can be a problem, since most of the commonly used staining techniques are developed and optimized for paraffin sections and not for sections cut in frozen condition required for acoustic microscopy (van der Steen *et al* 1991, van der Steen *et al* 1992a, van der Steen *et al* 1992b, Chapter VI-VII). Furthermore, stained tissue is commonly subjected only to qualitative interpretation. When automatic segmentation is applied, much

Table II *The Pearson correlation coefficients and p-values of area collagen, area lumen, ultrasound velocity, attenuation slope and the attenuation at 30 MHz of a section of liver tissue.*

	area collagen	area lumen	velocity of sound	atten slope	atten. central freq
area collagen	1 000 0.0	0.672 <0.001	-0.119 0 237	0.805 <0.001	0.818 <0.001
area lumen		1.000 0.0	-0 216 0 031	0.524 <0.001	0.502 <0.001
velocity of sound			1 0000 0.0	-0.310 0.002	-0.105 0.299
atten. slope				1.0000 0.0	0.956 <0.001
atten. centr.freq.					1.0000 0.0

Table III *Partial correlation coefficients and p-values of area collagen and the acoustic parameters after partialling out the area lumen*

	area collagen	velocity of sound	atten. slope	atten central freq.
area collagen	1.000 0 0	0.036 0.727	0.718 <0.001	0.750 <0.001

Table IV *Partial correlation coefficients and p-values of area lumen and the acoustic parameters after partialling out the area collagen*

	area lumen	velocity of sound	atten. slope	atten. central freq.
area lumen	1.000 0.0	-0.184 0.068	-0.040 0.694	-0.112 0.272

higher demands are made regarding the quality and the consistency of the staining technique.

A present limitation of the method is that it only works for tissues that do not substantially change within 250 μm in depth. This problem could be solved by investigating thinner acoustic sections However, this requires a highly accuracy XYZ-translation system. The calculation of the velocity of sound is especially demanding in this respect. The system used in this study has a variation in the Z-direction of approximately 3 μm when a scan is made in the XY-plane. This yields an accuracy of velocity estimation in one measurement point of 1 % for sections of 250 μm thickness and an accuracy of 2.5 % for sections of 100 μm thickness.

The accuracy in determining the attenuation is largely dependent on the accuracy of the AD converter and the actual degree of attenuation. With a presumed attenuation of 1 dB/(cm · MHz), a section of 250 μm and an AD-converter using 7 bits effectively, the attenuation at 30 MHz can be estimated in a single point with an error of 6 %. With a section 100 μm thick, the error increases to 15 %. It should be mentioned that in this study all acoustic parameters were averaged over 100 statistically independent points before any statistics were calculated. This resulted in an improvement in the accuracy of the statistics by a factor equal to the square root of 100 = 10.

The method provides possibilities to calculate correlations between histological and acoustic parameters in biological tissues Furthermore, it is possible to eliminate the influence of one parameter to a correlation between two others by means of calculating partial correlation coefficients. This is especially important when various histological features often coincide. This is shown here for the effect of correlation between the presence of collagen and lumina on the correlation between lumina and attenuation and the correlation between collagen and attenuation. At first sight, there seems to be a high correlation between the presence of lumina and attenuation, but after partialling out the collagen content, this correlation totally disappears. Conversely, there is a high correlation between the collagen content and attenuation, but partialling out the presence of lumina does not make this correlation disappear This means that the correlation between the area lumina and the attenuation can be fully explained from the correlation between collagen and attenuation, but has no significance by itself.

An extensive study of the correlation between local acoustic parameters and histology in liver tissue has already been performed, using the method described in this paper (van der Steen *et al.* 1993, Chapter IX)

WORKS OF REFERENCE

D'Astous F.T., Foster F.S. (1986) Frequency dependence of ultrasound attenuation and backscatter in breast tissue. Ultrasound in Med. & Biol. 12: 795-808

Bamber J.C., Hill C.R. (1981) Acoustic properties of normal and cancerous human liver. I. Dependence on pathological condition. Ultrasound in Med. & Biol. 7: 122-133

Bamber J.C., Hill C R., King J.A (1981) Acoustic properties of normal and cancerous human liver II. Dependence on tissue structure. Ultrasound in Med. & Biol. 7: 135-144

Bloomfield P. (1976) Fourier analysis of time series:an introduction pp.80-85. John Wiley, New York

Briggs G.A.D (1992) Acoustic microscopy. Clarendon Press, Oxford

Chrambach A., Rodbard D. (1971) Polyacrylamide gel electrophoresis. Science 172: 440-451

Cloostermans M.J.T.M., Mol H., Verhoef W.A., Thijssen J.M., Kubat K. (1986) *In vitro* estimation of acoustic parameters of the liver and correlations with histology. Ultrasound in Med. & Biol. 12: 39-51

Daft C.M.W., Weaver J.M.R., Briggs G.A.D. (1986) Tissue characterization with microscopic resolution. 1986 IEEE Ultrasonics symposium: 945-948

Datt C.M.W., Briggs G.A.D., O'Brien W.D. jr. (1989) Frequency dependence of tissue attenuation measured by acoustic microscopy. J. Acoust. Soc. Am. 85: 2194-2201

Fields F., Dunn F. (1973) Correlation of echographic visualizability of tissue with biological composition and state. J. Acoust. Soc. Am. 54: 809-812

Foster F.S., Strban M., Austin G. (1984) The ultrasonic macroscope: initial studies of breast tissue. Ultrasonic Imag 6: 243-261

Garra B.S., Insana M.F., Shanker T.H., Russell M.A. (1987) Quantitative estimation of liver attenuation and echogenicity: normal state versus liver disease. Radiology 162: 61-67

Hafsteinsson H., Rizvi S.S.H. (1984) Acoustic microscopy - Principles and applications in the studies of biomaterial microstructure. Scanning Electron Microscopy III: 1237-1247

Hartman P.C., Oosterveld B.J., Thijssen J M., Rosenbusch G.J.E, van den Berg J. (1993) Detection and differentiation of diffuse liver disease by quantitative echography. Invest. Radiol. 28: 1-6

Hausen P., Dreyer C. (1981) The use of polyacrylamide as an embedding medium for immunohistochemical studies of embryonic tissues. Stain. Tech. 56: 287-293

Jipson V., Quate C.F. (1978) Acoustic microscopy at optical wavelenghts. Applied Physics Letters 32: 789-791

Johnston R.L., Goss S.A., Maynard V., Brady J.K., Frizell L.A., O'Brien W.D. Jr., Dunn F. (1979) Elements of tissue characterization . I. Ultrasonic propagation properties. In Ultrasonic Tissue Characterization II (Edited by M. Linzer), Washington D.C.: 19-27

Kontonassios T., Ophir J. (1987) Variance reduction of speed of sound estimation in tissues using the beam tracking method. IEEE Trans. UFFC. 34: 524-530

Kuc R (1980) Clinical application of an ultrasound attenuation coefficient estimation technique for liver pathology characterization IEEE Trans. Biomed. Eng. BME-27: 312-319

Kuc R., Taylor K.J.W. (1982) Variation of acoustic attenuation coefficient slope estimates for *in vivo* liver. Ultrasound in Med. & Biol. 8: 403-412

Maklad N.F., Ophir J., Balsara V. (1984) Attenuation of ultrasound in normal liver and diffuse liver disease *in vivo*. Ultrasonic Imag. 6: 117-125

Narayama P.A., Ophir J. (1983) On the frequency dependence of attenuation in normal and fatty liver. IEEE Trans. Sonics Ultrasonics SU-306: 379-383

Nicholas D., Nicholas A.W. (1983) Two dimensional diffraction scanning of normal and cancerous human hepatic tissue *in vitro*. Ultrasound in Med. & Biol. 9: 283-295

Oosterveld B.J., Thijssen J.M., Hartman. P.C., Rosenbusch G.J.E (1993) Detection of diffuse liver disease by quantitative echography: dependence in a priori choice of parameters. Ultrasound in Med. & Biol. 19: 21-26

Parker, K.J. Asztely M.S., Lerner R.M., Schenk E.A., Waag R.C. (1988) *In vivo* measurements of ultrasonic attenuation in normal and diseased liver. Ultrasound in Med. & Biol. 14: 127-136

Pauly H., Schwan H.P. (1971) Mechanism of absorption of ultrasound in liver tissue. J. Acoust. Soc. Am. 50: 692-699

Pohlhammer J., O'Brien Jr. W.D. (1981) Dependence of the ultrasonic scatter coefficient on collagen concentration in mammalian tissue J. Acoust. Soc. Am. 69: 283-285

Romeis B. (1968) Microscopische Technik. R. Oldenbourg Verlag, Munich

Robinson D.E., Wilson L.S., Bianchi T. (1984) *In vivo* characterization of beams for ultrasonic attenuation measurements. Ultrasonic Imag. 6: 217 (Abstract)

Serra J. (1982) Image analysis and mathematical morphology. Academic Press, London

Snedecor G.W, Cochran W.G. (1979) Statistical methods. 6th edition 10th printing, Iowa State University Press, Iowa

van der Steen A.F.W., Cuypers M.H.M., Thijssen J.M., de Wilde, P.C.M. (1991) Influence of histochemical preparation on acoustic parameters of liver tissue: a 5 MHz study. Ultrasound in Med. & Biol. 17: 879-891

van der Steen A.F.W., Thijssen J.M., Ebben G.P.J., de Wilde P.C.M. (1992a) Effects of tissue processing techniques in acoustic (1.2 GHz) and light microscopy. Histochemistry 97: 195-199

van der Steen A.F.W., Cuypers M.H.M., Thijssen J.M., Ebben G.P.J, de Wilde P.C.M. (1992b) Preparation techniques in acoustic and optical microscopy of biological tissues, a study at 5 MHz and 1.2 GHz. In: Ermert H and Harjes HP (eds) Plenum Press, New York. Acoustical Imaging vol 19: 529-533

Verhoef W.A., Cloostermans M.J.T.M., Thijssen J.M. (1985) Diffraction and dispersion effects on the estimation of ultrasound attenuation and velocity in biological tissues. IEEE Trans. BME. 32: 521-529

Wilson L.S., Chen C.F., Robinson D.E. (1983) *In vivo* measurement of sound velocity in liver by pulse echo techniques. Ultrasonic Imag. 5: 168 (Abstract)

Zimmerman K.P., Smith J.C. (1983) Ultrasound velocity in fixed human liver: empirical anova and regression modelling on histologically assessed abnormalities. Ultrasonic Imag. 5: 280-294

CHAPTER IX

CORRELATION OF HISTOLOGY AND ACOUSTIC PARAMETERS OF LIVER TISSUE ON A MICROSCOPIC SCALE

A.F.W. van der Steen, J.M. Thijssen, J.A.W.M. van der Laak,
G.P.J. Ebben, P.C.M. de Wilde

ABSTRACT

The correlation of several acoustic parameters with histological features was investigated in healthy White New Zealander rabbit liver (n=10). Thin sections (10 μm) were studied by means of a light microscope in combination with a digital image processing system. Adjacent thick sections (250 μm) were studied by means of a custom designed acoustic microscope. Markers of black silk suture material that could be identified both optically and acoustically, enabled the spatial correlation of both imaging modalities. Acoustic images were reconstructed from the velocity of ultrasound, the attenuation at the central frequency (30 MHz), the attenuation spectral slope, the backscattering spectral slope and the backscattering at the central frequency. The measurements comprised the frequency range from 10 to 50 MHz, yielding a resolution of approximately 50 μm. From the thin sections (10 μm) the local histological composition was obtained by digital segmentation techniques. The features that were segmented are: the collagen rich fibrous tissue content, the area lumina, the area interstitial spaces, the number density of nuclei and the area parenchymal tissue. Correlation techniques revealed that the main feature responsible for attenuation is collagen. There was a fair correlation between area lumina and attenuation, but this was caused by a high correlation between the collagen that surrounds the lumina, and the attenuation. No correlation was found between any histological feature and backscattering parameters or velocity.

INTRODUCTION

The quantitative analysis of echographic data, generally called "ultrasonic tissue characterization", has been used in many clinical pilot studies. The analysis comprised acousto-spectrographic parameters, i.e. the frequency dependent characteristics of the attenuation coefficient (Berger *et al.* 1987, Parker *et al.* 1988, Kuc *et al.* 1979, Garra *et al.* 1987, Hartman *et al.* 1993, Oosterveld *et al.* 1991, Romijn *et al.* 1991) and of the backscattering (Lizzi *et al.* 1988, Coleman *et al.* 1985, Feleppa *et al.* 1986, Romijn *et al.* 1989a,b, Thijssen *et al.* 1991, Oosterveld *et al.* 1993 & Hartman *et al.* 1993) Some studies were based on the analysis of the texture of conventional B-mode echograms (e.g. Nicholas *et al.* 1986, Garra *et al.* 1987,

Romijn *et al.* 1991, Hartman *et al.* 1993, Thijssen *et al* 1993). Although these studies yielded promising results by retrospective classification of patients by using the histological diagnosis, a thorough understanding of the relation between the quantitative ultrasound data and the histological structural characteristics of healthy and diseased tissues is still lacking. Global explanations were obtained by *in vitro* studies. (e.g Pauly & Schwan 1971, Fields & Dunn 1973, Johnston *et al.* 1979, Bamber & Hill 1981, Bamber *et al.* 1981, Pohlhammer & O'Brien 1981, Zimmerman & Smith 1983, Nicholas & Nicholas 1983, Cloostermans *et al.* 1986) Some of these studies revealed correlations between bulk parameters and histological composition (Bamber *et al.* 1981, Cloostermans *et al.* 1986); none of them reveals correlations between local acoustic parameters and local histological features Further research is needed to gain a more basic understanding of the experimental results which should be based on the histological characteristics of tissues

Recently a method has been developed to identify the histological features, responsible for acoustic tissue characterization parameters (van der Steen *et al.* 1993, Chapter VIII). The method comprises the comparison of the local histological features in a thin section (10 μm) to the local acoustic parameters in an adjacent thick section (250 μm) Similar regions are found in these two sections by markers that can be localized both acoustically and optically By using the positioning feedback system of both the acoustic and optical systems, it was possible to investigate similar areas in both sections In this way a mapping is possible and the correlations between the acoustic properties and the histological composition is feasible on a microscopic scale.

METHODS

The methods described in Chapter VIII (cf van der Steen *et al* 1993) were applied to pieces of White New Zealander rabbit liver From these tissues sections of 250 μm thickness were investigated acoustically, and adjacent sections of 10 μm thickness were investigated by means of light microscopy. The acoustic examination revealed the local ultrasound velocity, the attenuation at 30 MHz, the attenation spectral slope between 10 and 50 MHz, the backscattering at 30 MHz and the backscattering slope between 20 and 40 MHz The light microscopic examination revealed the area collagen, the area lumen, the number density nuclei the area interstitial spaces and the area parenchymal tissue.

SELECTION CRITERIA

After segmentation the sections that were to be used in the final correlation study were selected. Sometimes the staining of the sections was too different from the standard staining, so that these sections were not suited for our segmentation algorithms, and had to be rejected Another reason for rejection was the following: During the correlation study it was shown that the correlation of the acoustic parameters with collagen was predominant. If the collagen was to sparse, the correlations with collagen could not be estimated with a high accuracy. Since the sections were taken from healthy young animals, collagen was often hardly present. If the area of collagen was less than 0.15 % of the optical section, the section was not used for the correlation study. The number of sections was reduced from twenty to ten by this selection.

Table I *The Pearson Correlation Coefficient of the acoustical parameters and the histological features to the histological features The values that are given are the averaged correlation coefficient and the boundaries of the 95 % confidential interval Correlations that are significant to a 5 % level are marked by an asterisk*

	collagen	lumina	interstitial spaces	number of nuclei	parenchymal tissue
attenuation centr freq	0 72* (0 56, 0 83)	0 36* (0 22,0 49)	-0 03 (-0 12,0 07)	-0 00 (-0 13,0 12)	-0 52* (-0 68,-0 31)
slope of att spectrum	0 71* (0 55, 0 81)	0 40* (0 25,0 52)	0 01 (-0 08,0 09)	-0 04 (-0 18,0 10)	-0 55* (-0 70,-0 34)
backscatter centr freq	0 08 (-0 04, 0 20)	0 04 (-0 07 0 15)	0 06 (-0 05,0 17)	0 07 (-0 07,0 21)	-0 05 (-0 17,0 06)
slope of bs spectrum	-0 12* (-0 23,-0 01)	-0 08 (-0 18,0 02)	-0 14* (-0 24,-0 02)	-0 06 (-0 15,0 02)	0 10 (-0 00,0 20)
velocity	0 07 (-0 05,0 20)	-0 03 (-0 21 0 14)	-0 01 (-0 15,0 13)	0 12 (-0 05,0 29)	0 01 (-0 16,0 17)
collagen	1 00	0 59* (0 47 0 76)	-0 02 (-0 13,0 09)	-0 12 (-0 24,0 01)	-0 80* (-0 89,-0 66)
lumina	0 59* (0 47,0 76)	1 00	0 02 (-0 16,0 21)	-0 20* (-0 38,-0 01)	-0 95* (-0 97,-0 92)
interstitial spaces	-0 02 (-0 13,0 09)	0 02 (-0 16,0 21)	1 00	0 11 (-0.02,0 24)	-0 14 (-0 33,0.05)
number of nuclei	-0 12 (-0 24,0 01)	-0 20* (-0 38,-0 01)	0 11 (-0 02,0 24)	1 00	0 20* (0 03,0 35)
parenchymal tissue	-0 80* (-0 89,-0 66)	-0 95* (-0 97, 0 92)	-0 14 (-0 33,0 05)	0 20* (0 03,0 35)	1 00

CORRELATION

The pearson correlation coefficients and partial correlation coefficients between the acoustic and histological parameters were calculated according Chapter VIII These correlations were calculated for each liver and then averaged over ten slices of livers. Since the Pearson correlation coefficient is limited to an upper value of 1 and a lower value of -1, it displays an asymmetric distribution. The Fisher-Z transform was applied to the correlation coefficients before averaging, and the inverse Fisher-Z transform after averaging. The Fisher-Z transform is described by Snedecor & Cochran (1979):

Table II *The Pearson Correlation Coefficient between the acoustical parameters and the histological features after partialling out the area lumina. The values are presented as in Table I*

	collagen	interstitial spaces	number of nuclei	parenchimal tissue
attenuation centr. freq	0.57* (0.40,0.71)	-0.06 (-0.16,0.04)	0.06 (-0.05,0.15)	-0.44* (-0.61,-0.21)
slope of att spectrum	0.55* (0.42,0.66)	-0.03 (-0.12,0.06)	-0.01 (-0.11,0.10)	-0.43* (-0.58,-0.23)
backscatter centr. freq	0.05 (-0.05,0.16)	0.05 (-0.06,0.17)	0.07 (-0.05,0.18)	-0.05 (-0.12,0.01)
slope of bs spectrum	-0.07 (-0.18,0.03)	-0.13* (-0.24,-0.01)	-0.09 (-0.19,0.00)	0.11* (0.01,0.22)
velocity	0.07 (-0.04,0.19)	-0.07 (-0.20,0.05)	0.10 (-0.08,0.28)	0.06 (-0.12,0.00)

Table III *The Pearson Correlation Coefficient between the acoustical parameters and the histological features after partialling out the area collagen. The values are presented as in table I*

	lumina	interstitial spaces	number of nuclei	parenchymal tissue
attenuation centr. freq	-0.06 (-0.20,0.08)	-0.01 (-0.10,0.08)	0.11* (0.01,0.21)	0.07 (-0.06,0.21)
slope of att spectrum	-0.01 (-0.14,0.13)	0.03 (-0.06,0.12)	0.04 (-0.08,0.16)	0.01 (-0.11,0.14)
backscatter centr. freq	0.02 (-0.06,0.11)	0.07 (-0.04,0.18)	0.08 (-0.04,0.21)	-0.04 (-0.13,0.06)
slope of bs spectrum	-0.02 (-0.11,0.08)	-0.12 (-0.24,-0.00)	-0.10 (-0.20,0.00)	0.04 (-0.05,0.14)
velocity	-0.12 (-0.28,0.05)	-0.03 (-0.16,0.10)	0.12 (-0.05,0.29)	0.13 (-0.04,0.31)

$$Z = 0.5 \cdot \ln\left(\frac{1+r}{1-r}\right) \qquad (1)$$

The average correlation coefficients are presented with 95 % confidential limits.

Table IV *The Pearson Correlation Coefficient between the acoustical parameters and the histological features after partialling out the area parenchymal tissue The values are presented as in table I*

	collagen	lumina	interstitial spaces	number of nuclei
attenuation centr freq	0 47* (0 33,0 58)	-0 29* (-0 41 -0 16)	-0 12 (-0 25,0 01)	0 06 (-0 04,0 17)
slope of att spectrum	0 42* (0 34,0 51)	-0 26* (-0 37, 0 15)	-0 10 (-0 22,0 02)	0 00 (-0 10,0 11)
backscatter centr freq	0 02 (-0 08,0 13)	-0 03 (-0 10 0 02)	0 05 (-0 07,0 17)	0 07 (-0 04,0 18)
slope of bs spectrum	-0 04 (-0 15,0 08)	0 09 (-0 02 0 19)	-0 11 (-0 24,0 02)	-0 09 (-0 19,0 01)
velocity	0 09 (-0 06,0 23)	-0 06* (-0 12 -0 01)	-0 06 (-0 19,0 07)	0 11 (-0 07,0 28)

RESULTS

Table I gives the averaged correlations between all acoustic parameters and light microscopic features There is a high positive correlation between the attenuation parameters and the collagen content and area lumina There is a high negative correlation between the attenuation parameters and the area parenchymal tissue The number of nuclei and the interstitial spaces seem to have no contribution to the acoustic parameters. There is hardly any correlation between histology and backscattering parameters. There is also no correlation between velocity and histological features There is a high correlation between the attenuation parameters. There is also a high positive correlation between the area lumina and the collagen content and a high negative correlation between the area parenchymal tissue and the area lumina and area collagen.

Table II gives the averaged correlations after partialling out the area lumina. The correlation between the attenuation parameters and the area collagen remains, as well as the correlation between the attenuation parameters and the parenchymal tissue. There is no partial correlation between the backscattering parameters or the velocity and any histological feature.

Table III gives the averaged correlations after partialling out the collagen content All correlations that were found have disappeared and no new correlations are found.

Table IV gives the averaged correlations after partialling out the parenchymal tissue. The correlation between attenuation and collagen remains, and a slight negative correlation between the area lumina and the attenuation is found.

DISCUSSION

In this study the correlation between local spectral acoustic parameters and local histological features in liver was investigated by a method developed by van der Steen *et al.* (1993) (Chapter VIII) This method correlates the acoustic properties of a 250 μm thick section of biological tissue to the light microscopic features of an adjacent 10 μm thick section.
The correlations are presented as averages and 95 % confidence limits. In the tables the statistically significant averages are marked by asterisks. Although many values appear to be statistically significant, the averages close to zero are considered not relevant for investigating the local correspondence between histological and acoustic tissue characteristics

High correlations were found between the attenuation parameters and collagen content and area lumina There was also a high correlation between collagen content and the area lumina ($r = 0\ 59$). This is not surprising, because the lumina are generally surrounded by collagen This means that the fields that contain collagen are likely to contain lumina as well After partialling out the area lumina there still was a high correlation between the attenuation and the collagen content After partialling out the collagen content, the correlation between area lumina and attenuation totally disappears. This means that the correlation between lumina and attenuation can be fully explained from the correlation between collagen and attenuation and between collagen and lumina, and had no contribution of its own Bamber *et al.* (1981) found a positive, though barely significant correlation between global collagen content and bulk attenuation ($r=0\ 35$, $p=0.07$). Cloostermans *et al.* (1986) found a positive correlation ($r = 0\ 63$)

A similar argumentation is valid for the correlation between area parenchymal tissue and the attenuation parameters. The negative correlation disappears when the collagen is partialled out. The parenchymal tissue as such has no influence on the attenuation If the parenchymal tissue is partialled out, a slight, though significant correlation appears between attenuation and area lumina

In this study no correlation was found between backscattering parameters and the collagen content. Bamber *et al.* (1981) and Cloostermans *et al* (1986) found the same results for bulk backscattering and global values of collagen content in human liver. Bondestam *et al.* (1992) found no correlation between collagen content and backscattering in the liver of living burbot fish. Pohlhammer & O'Brien (1981) found a positive dependency of the ultrasonic scatter coefficient on collagen concentration in various mammalian tissues. This scatter coefficient was however defined as a summation of reflection, refraction, diffraction and scattering, so a direct relationship to the backscattering coefficient as measured in this study is questionable.

A first possible explanation for the lack of correlation is that the influence of collagen is eliminated by the influence of the lumina. However, if this would be the case, a positive correlation should appear if the area lumina was partialled out, but this was not observed. It should be kept in mind that the frequencies used in this study are up to ten times the frequencies used in clinical studies. For this reason some of the collagen structures in liver could be identified as scatterers in clinical studies, but are effective as specular reflectors in this study, and therefore did not contribute to the backscattering intensity.

There was also no significant correlation of the local ultrasound velocity to any histological feature under study This was also found by Bamber *et al.* (1981) and Cloostermans *et al* (1986) for bulk parameters. This observation implies that variation in the velocity is caused by other features, or that the features responsible for the velocity variation, vary so much within

the sample volume (250 μm)^3 that the resolution of our imaging method is not good enough to detect them.

The nuclear density had no influence on any acoustic parameter. Some caution should be exercised with this conclusion, because it may be possible that the nuclear density varies significantly within 250 μm in the tissue, in which case the employed method is not able to produce a consistent result (van der Steen *et al.* 1993, Chapter VIII).

WORKS OF REFERENCE

Bamber J.C., Hill C.R. (1981) Acoustic properties of normal and cancerous human liver. I. Dependence on pathological condition. Ultrasound in Med. & Biol. 7: 122-133

Bamber J.C., Hill C.R., King J.A (1981) Acoustic properties of normal and cancerous human liver. II. Dependence on tissue structure. Ultrasound in Med. & Biol. 7: 135-144

Berger G., Laugier P., Fink M., Perrin J. (1987) Optimal precision in ultrasound attenuation estimation and application to the detection of Duchenne's muscular dystrophy carriers Ultrasonic Imag. 9: 1-17

Bondestam S., Alanen A., Toikkanen S. (1992) Correlations of liver echo intensity with cytology and chemical measurements of fat, water and protein content in live burbots (Lota lota). Ultrasound in Med. & Biol. 18: 75-80

Cloostermans M.J.T.M., Mol H., Verhoef W.A., Thijssen J.M., Kubat K. (1986) In vitro estimation of acoustic parameters of the liver and correlations with histology. Ultrasound in Med. & Biol. 12: 39-51

Coleman D.J., Lizzi F.L., Silverman R.H. *et al.* (1985) A model for acoustic characterization of intraocular tumours. Invest. Ophthalmol. Vis. Sci. 26: 545-550

Feleppa E.J., Lizzi F.L., Coleman D.J., Yaremko M.M. (1986) Diagnostic spectrum analysis in ophthalmology: a physical perspective. Ultrasound in Med. & Biol. 12: 623-631

Fields F., Dunn F (1973) Correlation of echographic visualizability of tissue with biological composition and state. J. Acoust. Soc. Am. 54: 809-812

Garra B.S., Insana M.F., Shawker T.H., Russell M.A. (1987) Quantitative estimation of attenuation and echogenicity: normal state versus diffuse liver disease. Radiology 162: 61-67

Johnston R L., Goss S.A., Maynard V., Brady J.K., Frizell L.A., O'Brien W.D. Jr., Dunn F. (1979) Elements of tissue characterization. 1. Ultrasonic propagation properties. In Ultrasonic Tissue Characterization II (Edited by M. Linzer), Washington D.C.: 19-27

Hartman P.C., Oosterveld B.J., Thijssen J.M., Rosenbusch G.J.E., van den Berg, J. (1993) Detection and discrimation of diffuse liver disease by quantitative echography - A retrospective assesment. Invest. Radiol. 28: 1-6

Kuc R., Schwartz M. (1979) Estimating the acoustic attenuation coefficient slope for liver from reflected ultrasound signals. IEEE Trans. Sonics Ultrason. SU-26: 353-362

Lizzi F.L., King D.L., Rorke M.C. (1988) Comparison of theoretical scattering results and ultrasonic data from clinical liver examinations. Ultrasound in Med. & Biol. 14: 377-385

Nicholas D., Nicholas A.W. (1983) Two dimensional diffraction scanning of normal and cancerous human hepatic tissue *in vitro*. Ultrasound in Med. & Biol. 9: 283-295

Nicholas D., Nassiri D.K., Garbutt P., Hill C.R. (1986) Tissue characterization from ultrasound B-scan data. Ultrasound in Med. & Biol. 12: 135-143

Oosterveld B.J., Thijssen J.M., Hartman P.C , Romijn R.L., Rosenbusch G J.E (1991) Ultrasound attenuation and B-mode texture analysis of diffuse liver disease: methods and preliminary results. Physics in Med. & Biol. 36: 1039-1064

Oosterveld B.J., Thijssen J M., Hartman P.C., Rosenbusch G.J.E. (1993) Detection of diffuse liver disease by quantitative echography: dependence on a prior choice of parameters. Ultrasound in Med. & Biol. 19. 21-26

Parker K.J., Asztely M.S., Lerner R.M., Schenk E.A., Waag R.C. (1988) In-vivo measurements of ultrasound attenuation in normal or diseased liver. Ultrasound in Med. & Biol. 14: 127-136

Pauly H , Schwan H P. (1971) Mechanism of absorption of ultrasound in liver tissue J Acoust. Soc. Am. 50: 692-699

Pohlhammer J., O'Brien W.D. Jr. (1981) Dependence of the ultrasonic scatter coefficient on collagen concentration in mammalian tissue J. Acoust. Soc. Am. 69. 283-285

Romijn R.L., Thijssen J.M., van Delft J.L., De Wolf-Rouendaal D., van Best J., Oosterhuis J.A. (1989a) *In vivo* ultrasound backscattering estimation for tumor diagnosis: An animal study. Ultrasound in Med. & Biol. 15: 471-479

Romijn R.L , Thijssen J.M., van Beuningen G.W.J. (1989b) Estimation of scatter size from backscattered ultrasound. a simulation study. IEEE Trans. Ultrasonics Ferroel. Freq. Control 36· 593-606

Romijn R L, Thijssen J.M., Oosterveld, B.J., Verbeek A.M. (1991) Ultrasonic differentiation of intraocular melanomas: parameters and estimation methods Ultrasonic Imaging 13. 27-55

van der Steen A F W., Thijssen J.M., van der Laak J.A.W.M., Ebben G.P.J , de Wilde P.C.M. (1993) A new method for correlation of acoustic spectroscopic microscopy (30 MHz) and light microscopy. (in press) J. Microscopy

Thijssen J.M., Oosterveld B.J., Hartman P.C., Rosenbusch G.J.E. (1993) Correlations between acoustic and texture parameters from RF and B-mode liver echograms. Ultrasound in Med. & Biol 19: 13-20

Verhoef W A., Cloostermans M.J.T.M., Thijssen J.M. (1985) Diffraction and dispersion effects on the estimation of ultrasound attenuation and velocity in biological tissues. IEEE Trans. BME. 32. 521-529

Zimmerman K P., Smith J.C. (1983) Ultrasound velocity in fixed human liver· emperical anova and regression modeling on histologically assessed abnormalities Ultrasonic Imag. 5: 280-294

CHAPTER X

SUMMARY AND GENERAL DISCUSSION

INTRODUCTION

This thesis describes several applications for which *in vitro* ultrasound can be an aid to understanding phenomena which occur in *in vivo* tissue characterization The thesis consists of three parts In the first part (Chapter I) ultrasonic tissue characterization and *in vitro* ultrasound are placed in a historical and functional context In the second part (Chapters II-V) measurements on various fresh tissues are described The results of these studies give further insight in the acoustic properties of myocardium (Chapter II), gallstones (Chapter III), eye lenses (Chapter IV) and the total eye (Chapter V) The third part of the thesis (Chapters VI IX) is concerned with the correlation between acoustic and light microscopy First the development of preparation methods which can be used for both acoustic and light microscopy is discussed (Chapters VI and VII) Then a method is proposed to correlate the acoustic and histological parameters of biological tissues (Chapter VIII) Finally, this method is applied to liver tissue (Chapter IX)

In this chapter the general methods and basic results are summarized and the significance of the conclusions is discussed It is described how the results can be of use in clinical practice and an outline is given of future research which remains to be performed

GENERAL METHODS

In all studies presented in this thesis the acoustic parameters were obtained *in vitro* in a similar way

The acoustic parameters which were measured are spectral parameters based on attenuation, velocity and backscattering The attenuation parameters (Chapters II-IX) and ultrasound velocity (Chapters III-IX) were obtained using the substitution method the reflection of a rigid body was acquired with and without a piece of tissue interposed The spectral difference of the reflections yielded the frequency dependent attenuation of the tissue, the time shift of the reflection yielded the ultrasound velocity in the tissue The backscattering parameters (Chapters II III and VI-IX) were obtained after correction of the backscattered signal for the frequency dependent properties of the instrumental setup and the attenuation In Chapter III a method is introduced to estimate the attenuation from a decrease of the central frequency of the backscattering spectrum with increasing depth

MYOCARDIUM

In Chapter II the dependence of ultrasonic integrated backscatter and attenuation in myocardium on wall thickness in a state of acute ischemia is described Other studies revealed that the variation during cardiac cycle of myocardial integrated backscatter changes in myocardium in a state of acute ischemia *in vivo* When left ventricular myocardium is compressed *in vitro*,

the ultrasonic integrated backscatter increases, and the ultrasonic attenuation decreases. Since the measurements of integrated backscatter are combined measurements of two phenomena i e backscattering and attenuation, the influence of varying attenuation during cardiac cycle should be taken into account for the modelling of integrated backscatter as a tissue identification parameter.

The magnitude of the variation in attenuation is such that it is potentially as a parameter for detection of acute ischemia. It is possible to measure attenuation *in vivo* in several ways. One way is the measurement of the reflectivity of left ventricular blood during cardiac cycle. A problem which occurs here is that the reflectivity of the left ventricular blood may not be constant during cardiac cycle (e.g. due to the creation and annihilation of rouleaux of red blood cells). Another way is the method proposed for the differentiation of different classes of gallstones in chapter III. It is a method which uses the information from the frequency shift which occurs when the spectrum is taken from windows of backscattering at increasing depths. A merit of this method is that it does not suffer from temporal changes in disturbance by intervening tissues, caused by heartbeat or respiration.

GALLSTONES

In Chapter III a method is described to discriminate between various classes of human gallstones by means of quantitative echography and B-mode characteristics. A significant difference between the group of stones containing mainly cholesterol, which are suitable for treatment with extra-corporeal shock wave lithotripsy or oral bile-acid dissolution, and the group of stones containing mainly calcium, which cannot be treated, was found for the velocity of sound ($p < 0.01$), the attenuation coefficient slope per unit of time ($p < 0.10$), the slope of the backscattering spectrum ($p < 0.05$) and the 4 5 MHz intercept ($p < 0.01$). The latter three parameters were assessed by *in vivo* applicable methods. This means that it should be possible to differentiate, *in vivo*, on the basis of acoustic parameters, especially when a multi parameter approach is used. This should be tested in a clinical study.

EYES

In Chapter IV measurements of local acoustic parameters of the porcine eye lens are described, as well as their correlation with chemical and optical parameters, obtained from literature. The acoustic properties are not constant throughout the lens, but were found to follow a systematical gradient. Axial and equatorial profiles of the ultrasound velocity, the attenuation spectral slope and the attenuation at 20 MHz are similarly-shaped as profiles of the protein content in the eye lens of mammals other than pig. In literature, no protein profiles were found for porcine lenses. These were measured and had a similar shape as the mammals mentioned (not reported in this thesis). The correlation between the local acoustic parameters and the local protein content is so high, that the method is suited to measure protein content acoustically. Measurements of human lenses revealed similar results. This may give an opportunity to study aging, based on acoustic parameters. A method should be developed to measure the acoustic parameters *in vivo*. Again, the method introduced in Chapter III (measurement of the product of attenuation and velocity based on frequency shift in backscattering spectra) could be useful,

all the more so because the attenuation and velocity are positively correlated in the eye lens ($r > 96$ %). A problem here is that the method is based on the measurement of scattering from the lens and during our study it was shown that this scattering is low in amplitude. Another method could be the measurement of difference in reflectivity of the anterior and posterior lens capsule.

In previous studies it was demonstrated that it is possible to differentiate between different eye melanomas based on acoustic parameters. These melanomas are diagnosed by means of data obtained by a transducer located at the front of the eye, while the melanoma is at its back. The ultrasound beam is disturbed by the eye itself. To estimate the distortion an acoustic model of the eye should be constructed. For this reason the acoustic properties of porcine and human eye tissues were measured (at room temperature). The results are described in Chapter V. The values for the acoustic parameters of both types of eyes were found to be in the same range, so the porcine eye is a reasonable model for the human eye. After measurement of the mass density an acoustic model of the eye can be constructed. It can be optimized by taking the effects of temperature and age into account. An age dependent effect is suggested in the study, but remains inconclusive because of the limited number of observations.

PREPARATION

The effects of various histochemical preparation techniques on the acoustic parameters of biological tissues were investigated extensively and are reported in Chapter VI and VII

Chapter VI describes a qualitative study of the influence on acoustic parameters of liver tissue, performed at 1 2 GHz. It was concluded that images obtained from cryostat sections were of much higher quality than those from paraffin sections Images obtained from sections, which were sectioned while embedded in paraffin, displayed no detail at all

Chapter VII describes a quantitative study of the influence on acoustic parameters of liver tissue, performed at 5 MHz It was found that fixation by formalin preserves the acoustic properties of the tissue to a reasonable extent. Embedding in paraffin and deparaffinizing induces large changes in the acoustic properties of the tissue. As an alternative, freezing prior to cutting, rather than the paraffin cycle was also investigated. This method produced no significant changes.

The investigations resulted in a preparation method which is suited for both acoustic and light microscopy, which is necessary for the studies described in Chapters VIII and IX The tissue is fixed in formalin and then cut in frozen condition. Fixation is necessary since it is a basis for most standard staining techniques and because it prevents autolysis. By using a freeze sled microtome instead of a standard cryostat, it is possible to section tissues at thicknesses varying from 10 up to 250 μm. Freezing and then thawing does not affect the acoustic properties of tissues, so sectioning of non-fixed tissues is possible. This gives way to application of immunohistochemical staining techniques in combination with acoustic measurements

One of the observations in the qualitative preparation study (Chapter VI) is that acoustic microscopy of cryostat sections reveals high contrast images. At the used frequency (1.2 GHz), the light microscopic images reveal more detail. However, it was found that the acoustic images give additional and sometimes even complementary information. Furthermore, acoustic microscopes are already available at frequencies up to 4 GHz, resulting in a resolution below the optical wavelengths. It is shown that even unstained sections reveal a high acoustic contrast, although staining does enhance this contrast. The study remains inconclusive as to which of

the staining techniques gives higher quality images. Optimizing the staining techniques is worthwhile, if acoustic microscopy at high frequencies (>1 GHz) is to be used in clinical practice (e.g. in pathology)

CORRELATION

In Chapter VIII a method is described which was developed to investigate the correlation between light microscopic and acoustic properties of biological tissues. This should give further insight into the acoustic interactions between ultrasound and biological tissues. Tissues are fixed and sectioned in conformity with the methods evolving from Chapters VI and VII. By means of markers which can be localized both optically and acoustically, corresponding regions can be found in adjacent sections, one of which is investigated acoustically and the other by means of light microscopy. The histological composition of the optical sections was obtained quantitatively, using digital image segmentation techniques. Of several staining techniques (v Gieson, Masson, Goldner, Azan, Laguesse) the trichrome staining according to Goldner is shown to be optimal for staining liver tissue, when quantitative colour information is used for automatic segmentation of tissue components For studying other tissues, other staining techniques might be optimal. In principle this does not change the method. The used frequencies (10 up to 55 MHz) yield an acoustic resolution of about 50 μm. The actual resolution at which tissue properties can be studied by the method is 250 μm A limitation of the method is that some properties cannot easily be extrapolated to lower (i.e. diagnostic) frequencies. Attenuation has proven to vary almost linear with frequency in most biological tissues and velocity is hardly frequency dependent, so these parameters will cause no problems. However the backscattering from biological tissues and its frequency dependence may change with frequency in this range.

In Chapter IX the method described in chapter VIII is applied to White New Zealander rabbit liver. Correlation techniques revealed that the main feature responsible for attenuation is collagen. There was a fair correlation between area lumina and attenuation, but this was caused by a high correlation between the collagen, which surrounds the lumina, and the attenuation No correlation was found between any histological feature and backscattering parameters or velocity.

The method could be applied to study the acoustic properties of melanomas. A pilot study was already performed on human skin melanomas which were subcutaneously implanted in nude mice (not reported in this thesis). Again, the staining techniques mentioned above were considered and the Trichrome staining according to Goldner was applied. However, this staining technique revealed no optimal distinction between necrosis and collagen and for this reason the study remained inconclusive. Other staining techniques should be used for this purpose. Immunohistochemical techniques to stain endothelium are suggested, so the correlation between vascularization and acoustic properties can be investigated. These staining techniques should be applied to non-fixed material. The segmentation techniques for this staining have already been optimized and show good results.

CONCLUDING REMARKS

Summarizing, this thesis demonstrates that *in vitro* ultrasound can be a very useful tool for ultrasonic tissue characterization. The various parts of the thesis are situated at different stages on the way from fundamental insight to clinical application. The gallstone study is ready for a clinical follow-up. The myocardium study provides more insight into the phenomena under study and gives an indication for a new tissue identification parameter. The applicability of this parameter should be investigated first, again *in vitro*. The lens study shows that there may be possibilities for application in aging studies. The total eye study can be used as an input for a model to correct for distortion effects. The qualitative preparation study reveals that high frequency acoustic microscopy may be useful in pathology. The correlation study developed gives possibilities to gain insight into acoustic properties in detail. It can be applied for many tissues. The information can be used for application in acoustic tissue models. This part of the thesis is more fundamental and has some way to go to clinical practice.

SAMENVATTING

In dit proefschrift worden diverse toepassingen beschreven waar *in vitro* ultrageluid onderzoek een hulpmiddel kan zijn voor het begrijpen van fenomenen die van belang zijn voor *in vivo* weefselidentificatie Het proefschrift bestaat uit drie delen In het eerste deel (Hoofdstuk I) worden weefselidentificatie met ultrageluid en *in vitro* ultrageluid in hun historische en functionele context geplaatst In het tweede deel (Hoofdstuk II V) worden *in vitro* metingen aan verse weefsels beschreven De resultaten van deze onderzoeken verbeteren het inzicht in de akoestische eigenschappen van myocardium (Hoofdstuk II), galstenen (Hoofdstuk III) ooglenzen (Hoofdstuk IV) en het gehele oog (Hoofdstuk V) Het derde deel (Hoofdstuk VI IX) gaat over de relatie tussen akoestische en lichtmicroscopie van biologische weefsels Allereerst wordt het ontwikkelen van prepareermethoden besproken die zowel voor lichtmicroscopie als akoestische microscopie gebruikt kunnen worden (Hoofdstuk VI en VII) Dan wordt een methode voorgesteld om akoestische en histologische parameters van biologische weefsels te correleren (Hoofdstuk VIII) Tot slot wordt deze methode toegepast op leverweefsel (Hoofdstuk IX)

In alle studies die beschreven worden in dit proefschrift werden de akoestische parameters *in vitro* verkregen op overeenkomstige wijze De akoestische parameters waren spectrale parameters gebaseerd op verzwakking snelheid en backscattering De verzwakkingsparameters (Hoofdstuk II IX) en de snelheid (Hoofdstuk III-IX) zijn met behulp van de substitutiemethode verkregen de reflectie van een sterke reflector werd gemeten met en zonder weefsel tussen de transducer en de reflector De ratio van de spectra van de reflecties geeft de frequentieafhankelijke verzwakking in het weefsel, en de verplaatsing van de reflectie in de tijd levert de ultrageluidsnelheid op De backscattering parameters (Hoofdstuk II III en VI-IX) werden verkregen na correctie van het teruggestrooide ultrageluid signaal voor de frequentieafhankelijke eigenschappen van de meetopstelling en de verzwakking In Hoofdstuk III wordt een methode geintroduceerd waarbij de verzwakking geschat wordt uit de afname van de centrale frequentie van het backscattering spectrum met toenemende doordringdiepte

In Hoofdstuk II wordt beschreven hoe integrated backscatter en verzwakking van vroeg ischemisch myocardium *in vitro* afhangen van de wanddikte In andere studies was *in vivo* al aangetoond dat de variatie van integrated backscatter uit het myocardium gedurende de hartcyclus verandert als het myocardium ischemisch wordt Als het myocardium van de linker ventrikel *in vitro* wordt samengedrukt neemt de integrated backscatter toe en de verzwakking af Omdat het meten van integrated backscatter een combinatie is van meting van backscattering en verzwakking, dient er rekening gehouden te worden met de invloed van variatie van verzwakking gedurende de hartcyclus bij de modelvorming van integrated backscatter als weefselidentificatieparameter De variatie van de verzwakking is zelfs zo groot dat deze gebruikt zou kunnen worden voor detectie van acute ischemie

In Hoofdstuk III wordt een methode beschreven waarmee onderscheid gemaakt kan worden tussen verschillende klassen humane galstenen Deze zijn gebaseerd op quantitatieve echografie en B Mode eigenschappen Een significant verschil tussen cholesterol stenen die geschikt zijn voor behandeling door middel van vergruizing of medicamenten en calcium stenen, die met deze methoden niet te behandelen zijn is gevonden voor de ultrageluidsnelheid, de verzwakking per tijdseenheid de helling van het backscattering spectrum en de backscattering bij 4 5 MHz De laatste drie parameters zijn bepaald met methoden die ook *in vivo* toepasbaar zijn Dit betekent

dat het *in vivo* mogelijk moet zijn om te differentieren tussen al dan niet behandelbare stenen op grond van akoestische parameters, zeker als een multiparameteraanpak gevolgd wordt

In Hoofdstuk IV worden metingen van lokale akoestische parameters van varkensooglenzen en hun relatie tot lokale chemische en optische eigenschappen beschreven De laatste zijn verkregen uit de literatuur De akoestische eigenschappen zijn niet constant in de lens maar vertonen een systematische gradient Axiale en equatoriale profielen van de ultrageluidsnelheid, de helling van het verzwakkingsspectrum en de verzwakking bij 20 MHz zijn gelijkvormig aan de profielen van het proteinegehalte in de ooglenzen van andere zoogdieren dan het varken Als de correlatie tussen het proteinegehalte en akoestische eigenschappen hoog genoeg is, geeft dit mogelijkheden om het proteinegehalte akoestisch te meten Dit kan mogelijkheden geven om veroudering akoestisch te meten

In voorgaande studies is aangetoond dat het mogelijk is om op grond van akoestische parameters onderscheid te maken tussen verschillende typen oogmelanomen De data werden verkregen met behulp van een transducer aan de voorzijde van het oog, terwijl het melanoom zich aan de achterzijde van het oog bevond De ultrageluidbundel wordt hierbij verstoord door het oog zelf Om deze verstoring te schatten dient een akoestisch model van het oog geconstrueerd te worden Om deze reden zijn de akoestische eigenschappen van mensen- en varkensoogweefsels gemeten De resultaten zijn beschreven in Hoofdstuk V De waarden voor mensen en varkens komen voor de meeste weefsels aardig overeen, dus het varkensoog is een redelijk diermodel voor het mensenoog

Het effect van histochemische prepareertechnieken op akoestische parameters van biologische weefsels is uitgebreid bestudeerd en staat beschreven in Hoofdstuk VI en VII
Hoofdstuk VI beschrijft een kwalitatieve studie naar de invloed op akoestische parameters van leverweefsel bij 1,2 GHz De belangrijkste conclusie was dat afbeeldingen die verkregen zijn van cryostaatcoupes van veel hogere kwaliteit zijn dan afbeeldingen van paraffinecoupes Er was vrijwel geen enkel detail aanwezig in afbeeldingen van paraffinecoupes

Hoofdstuk VII beschrijft een quantitatieve studie naar de invloed op akoestische parameters van leverweefsel bij 5 MHz De akoestische eigenschappen van het weefsel blijven redelijk behouden bij fixatie door middel van formaline Inbedden in paraffine en deparaffineren brengt aanzienlijke veranderingen in de akoestische eigenschappen van het weefsel met zich mee Het is ook mogelijk de paraffinecyclus te omzeilen door het weefsel te bevriezen alvorens het te snijden Bevriezen en daarna ontdooien heeft geen effect op de akoestische eigenschappen

Het onderzoek resulteerde in een prepareermethode die zowel geschikt is voor akoestische als lichtmicroscopie, hetgeen nodig is voor de studies die beschreven staan in Hoofdstuk VIII en IX Het weefsel wordt gefixeerd in formaline en vervolgens in bevroren toestand gesneden Fixatie is nodig omdat het een basis vormt voor de meeste standaard kleurtechnieken en omdat het autolyse voorkomt Door het gebruik van een vriesslede-microtoom in plaats van een standaard cryostaat is het mogelijk weefselcoupes te snijden die in dikte varieren tussen 10 en 250 μm Bevriezen en dan ontdooien tast de akoestische eigenschappen van weefsels niet aan, dus niet gefixeerde weefselcoupes snijden is ook mogelijk Dit geeft mogelijkheden voor toepassing van immunohistochemische kleurtechnieken in combinatie met akoestische metingen

Een van de observaties in de kwalitatieve studie (Hoofdstuk VI) is dat akoestische microscopie van cryostaatcoupes afbeeldingen geeft met hoog contrast Bij de gebruikte frequentie (1,2 GHz) geven de lichtmicroscopische afbeeldingen meer detail. De akoestische afbeeldingen geven echter additionele en soms complementaire informatie.

In Hoofdstuk VIII wordt een methode beschreven die ontwikkeld is om de correlatie tussen akoestische en lichtmicroscopische eigenschappen van biologische weefsels te onderzoeken. Dit verhoogt het inzicht in de akoestische interacties tussen ultrageluid en biologische weefsels. Weefsels worden getixeerd en gesneden conform methoden die voortgekomen zijn uit Hoofdstuk VI en VII. Door middel van markeringen die zowel optisch als akoestisch te detecteren zijn kunnen corresponderende gebieden gevonden worden in aangrenzende coupes, waarvan de één akoestisch onderzocht wordt, en de ander lichtmicroscopisch. De histologische samenstelling van de coupes wordt bij lichtmicroscopie quantitatief bepaald met behulp van digitale beeldsegmentatietechnieken. De akoestische resolutie is bij gebruikte frequenties (10 tot 55 MHz) ongeveer 50 μm. De resolutie waarmee de akoestische eigenschappen bestudeerd kunnen worden is 250 μm.

In Hoofdstuk IX wordt de methode die beschreven staat in Hoofdstuk VIII toegepast op leverweefsel. Uit de correlatietechnieken kwam naar voren dat collageen de belangrijkste component is die verzwakking veroorzaakt. Er was een behoorlijke correlatie tussen het oppervlakte lumen en de verzwakking, maar deze werd veroorzaakt door het collageen wat rondom de lumina aanwezig was. Er was geen correlatie tussen de onderzochte histologische parameters en snelheid of backscattering.

Samengevat demonstreert dit proefschrift dat *in vitro* ultrageluid onderzoek een erg bruikbaar hulpmiddel kan zijn voor de ontwikkeling van weefselidentificatie met ultrageluid. De verschillende delen van het proefschrift bevinden zich op verschillende plaatsen langs het pad van fundamenteel inzicht tot klinische applicatie. De galsteenstudie is klaar voor een klinische follow up. De myocardiumstudie geeft meer inzicht in de bestudeerde fenomenen en levert een nieuwe weefselidentificatieparameter. De lensstudie doet vermoeden dat er mogelijkheden zijn voor toepassingen in verouderingsstudies. De resultaten van de studie naar de akoestische eigenschappen van het gehele oog kunnen gebruikt worden als input voor een model om voor verstoring van de ultrageluidbundel door het oog te corrigeren. Uit de kwalitatieve preparatiestudie blijkt dat akoestische microscopie bruikbaar zou kunnen zijn binnen de Pathologie. De ontwikkelde correlatiemethode geeft mogelijkheden om gedetailleerd inzicht te verkrijgen in de akoestische eigenschappen van biologische weefsels. Dit kan gebruikt worden bij het opstellen van akoestische weefselmodellen. Dit deel van het proefschrift is fundamenteel en heeft nog een lange weg te gaan tot aan een klinische toepassing.

NAWOORD

"Niemand schrijft zijn eigen proefschrift alleen" zou Willy Alberti ongetwijfeld gezongen hebben als hij naast zanger wetenschapper geweest was in plaats van vader. Inderdaad zit in het 158 pagina's tellende kleinood dat voor u ligt niet slechts mijn zweet maar ook nog dat van vele anderen. Voordat ik ga uitsplitsen wil ik iedereen die denkt eraan bijgedragen te hebben van harte voor deze bijdrage bedanken.

Allereerst Han Thijssen, voor jouw alomme aanwezigheid in het hele project.

Professor van Oosterom, het was "niet uw soort fysica", dat medisch ultrageluid. Maar u heeft wel bewezen dat uw kritische blik toch een wezenlijke bijdrage kan leveren aan "ons soort fysica". Bedankt dat u de moeite genomen heeft u erin te verdiepen.

Rien Cuypers, jouw technische ondersteuning is van onschatbare waarde geweest voor dit project. Van nog veel grotere waarde echter waren jouw relativeringsvermogen en positieve werkinstelling Ik vraag me af of dit proefschrift ooit het licht had gezien als jij in het eerste Nijmeegse jaar niet aanwezig geweest was.

Wim van Hoorn, buiten de begeleiding vanuit de TU van de hartspierstudie was overleg met jou van onontbeerlijk belang bij de vele keuzes die gemaakt moesten worden bij het ontwikkelen van de akoestische microscoop.

De mannen van het XYZ-front: Robert Rutteman, Jan Willem van Dijk en Chris de Korte. Dankzij jullie hulp bleef het project in beweging, hoewel dit bijna niemand opviel.

André Goedegebure, voor jouw bijdrage aan de galsteenstudie. Na een intensieve inwerkperiode bestond mijn bijdrage aan deze studie voornamelijk uit het afremmen van jouw enthousiasme.

Leon van Erning, voor jouw CT-ondersteuning van het galsteenproject.

Chris de Korte, sinds jouw afstuderen ziet de wereldopinie omtrent de akoestische eigenschappen van de ooglens er in essentie anders uit. Nu nog hopen dat ik niet de enige ben die die mening heeft

Jeroen van der Laak, de beeldbewerking die jij onbezoldigd verricht hebt voor het project vulde de missing link tussen akoestische en lichtmicroscopie. Daarenboven was je tot op de laatste dag betrokken bij de wording van het proefschrift. Sommige dingen blijven bij.

Peter de Wilde, jij was mijn eerste confrontatie met het fenomeen "Patholoog anatoom". Ik heb veel geleerd van de besprekingen die we gevoerd hebben.

Pieter Wesseling, terloopse gesprekken en af en toe over jouw schouder meekijken hebben aan de wieg gestaan van enkele kardinale beslissingen in dit project.

Gerard Ebben, jouw creativiteit en enthousiasme zijn van grote waarde geweest tijdens het ontwikkelen van prepareertechnieken. De eerlijkheid gebiedt me te zeggen dat dezelfde eigenschappen me ook wel eens zorgen baarden toen de technieken uitgekristalliseerd waren en gewoon routinematig toegepast dienden te worden.

Martin Pahlplatz, jouw inzichten in quantitatieve microscopie waren zeker een bron van inspiratie.

Professor Ruiter, voor het stroomlijnen van de ondersteuning van het project vanuit Pathologie.

John van Oyen en Jan van den Berg van Philips Natlab, voor jullie medewerking bij de 1,2 GHz-studie

Ton de Haan en Theo de Boo van het MSA, voor jullie statistische ondersteuning en jullie vermogen om je nog eens over je experimenten na te laten denken.

De medewerkers van de fijnmechanische werkplaats en de afdeling electronica van de Instrumentele dienst, voor jullie ondersteuning bij het XYZ-gebeuren.

De medewerkers van het weefselidentificatieproject in Rotterdam: Hans Rijsterborgh, Charles Lancée en Frits Mastik. Bedankt voor jullie opvoeding en voor de ruimte die ik van jullie gekregen heb.

De medewerkers van de centrale dierenlaboratoria van het Dijkzigt en het Radboud ziekenhuis, mw. E. Pels van Eurotransplant en Ine Cornelisse van de afdeling Pathologie voor de medewerking bij het aanleveren van weefsels.

De vrouwen van de bovenste plank: Yolanda, Yvonne, Anja en Marriet. Af en toe een bezoek aan jullie hield het besef hoog dat alles wat in een ziekenhuis gebeurt mensenwerk is.

Huub Winkens, voor jouw bereidheid om als het nodig was bij te springen in mijn onderzoek met de faciliteiten van het Biochemisch Laboratorium van Oogheelkunde en voor de bereidheid mijn lekevragen aan te horen en te beantwoorden

De collega's van het Biofysisch Laboratorium van Oogheelkunde die mij de afgelopen 4 jaar vergezeld hebben in de strijd tegen de ultrasonore problemen. Niet eens zozeer vanwege de praktische bijdrage, als wel vanwege het "we"-gevoel.

Ons vader en ons moeder, omdat jullie me ook steunen als jullie het even niet meer begrijpen.

Tot slot dient nog vermeld te worden dat het onderzoek niet mogelijk geweest was zonder financiele ondersteuning van de Nederlandse Kankerbestrijding (Hoofdstuk 4 - 9), Stichting Technische Wetenschappen (Hoofdstuk 2) en Dornier Medizintechnik GmbH (Hoofdstuk 3). Hiervoor mijn welgemeende dank.

Een naam die ik uit deze opsomming nog eens naar voren wil halen is die van Hans Rijsterborgh. Hans, als begeleider van mijn afstuderen heb ik veel van jou meegekregen. Van jou heb ik geleerd hoe je meetresultaten moet objectiveren en concretiseren. Jij was een zeer goede bron van informatie, alleen al omdat je kennis niet losliet voordat je er zelf zeker van was. Buiten dit om heb jou leren kennen als een bijzonder lief mens. Ik vind het verschrikkelijk dat je geveld bent door de ziekte waar de hoofdsponsor van dit proefschrift zich hard tegen maakt. Ik hoop dat je weet dat je één van mijn voorbeelden geweest bent.

CURRICULUM VITAE

De schrijver dezes werd in Vught gebaard op zondag 23 augustus 1964 om half drie 's-middags bij een buitentemperatuur van 28 °C. Een direct verband met zijn tropenzucht is nooit onomstotelijk aangetoond. De eerste pogingen tot educationele vorming werden ondernomen op de Mariaschool te Vught. Hier werd hij geprezen om zijn schoonschrift, edoch gehekeld om zijn lage tempo. Van de beslissing dit dan maar om te keren ondervindt hij, maar vooral zijn omgeving, nog dagelijks de gevolgen

De middelbare school werd doorlopen op het Maurick College te Vught, alwaar het aantal talen waarin hij onderwezen werd gestaag afnam van zes naar twee, dit ten gunste van de meer exacte vakken. Het geheel resulteerde in 1983 in een VWO-B diploma met als laagste cijfer een 8. Op dat moment was de arbeidsmarkt al vier jaar verkend: twee jaar als pompbediende en twee jaar als expert buitenlandse bieren annex krattensjouwer bij een slijter.

Een volgende stap in zijn leven bracht hem bij de faculteit der Technische Natuurkunde van de Technische Universiteit te Delft Na vier jaar doelloos rondploeteren kreeg zijn studie richting op de afdeling Experimentele Echocardiografie van het Dijkzigt ziekenhuis te Rotterdam o l.v. prof dr.ir N. Bom. Daar verrichtte hij onderzoek aan weefselidentificatie met ultrageluid, ten behoeve van detectie van vroege ischemie in het myocardium. Dit was tevens zijn afstudeerwerk voor de vakgroep Akoestische en Seismische Technieken o l.v. prof.dr ir. A.J. Berkhout, van wie hij begin mei 1989 een diploma kreeg. De arbeidsmarkt werd gedurende zijn studieperiode verder verkend middels verkeerstellingen, interviews afnemen in louche wijken van Den Haag en vooral barkeepen. Tijdens deze periode heeft hij nog een jaar lang in het bestuur van studentenvereniging Nieuwe Delft (De Bolk) zitting gehad.

Zijn afstudeerbaan als ultrasonoor echoakoestisch biofysicus kreeg gedurende vier jaar een vervolg met een soortgelijke functie als wetenschappelijk onderzoeker aan het Biofysisch Laboratorium (o l v. dr.ir. J.M. Thijssen) van de afdeling Oogheelkunde van het Academisch Ziekenhuis Nijmegen, echter nu in het bezit van een diploma, dus wat beter bezoldigd. Hier heeft hij de spectrale akoestische microscopie van de grond getild en met een zelfgebouwde akoestische microscoop diverse biologische weefsels onderzocht Correleren met lichtmicroscopie stond hierbij hoog in het vaandel. Gedurende deze periode lag in zijn vrije tijd de nadruk meer op geld spenderen dan verdienen, hetgeen zich onder andere uitte in diverse tropenreizen. De activiteiten in Rotterdam, maar vooral die in Nijmegen hebben geresulteerd in dit proefschrift.

Na het afronden van dit proefschrift heeft de auteur nog geen nieuwe stek gevonden. Hierover in de nabije toekomst wellicht meer.

PUBLICATIONS BY THE AUTHOR

PUBLICATIONS

A.J. van den Berg, L. Klostermann, A.F.W. van der Steen (1988) Holografische interferometrie: De trillingswijzen van een carillonklok gefotografeerd. Polytechnisch Tijdschrift Elektrotechniek. 43(5): 50-54

H. Rijsterborgh, F. Mastik, C.T. Lancée, A.F W. van der Steen, J. Roelandt, N. Bom (1990) Ultrasonic myocardial integrated backscatter and myocardial wall thickness in animal experiments. Ultrasound in Med. & Biol. 16(1): 29-36

A.F.W. van der Steen, H. Rijsterborgh, F. Mastik, C.T. Lancée, W.M. van Hoorn, N. Bom (1991) Influence of attenuation on measurements of ultrasonic myocardial integrated backscatter during cardiac cycle (an in vitro study). Ultrasound in Med. & Biol. 17(9): 869-877

A.F.W. van der Steen, M.H.M. Cuypers, J.M. Thijssen, P.C.M. de Wilde (1991) Influence of Histochemical preparation on acoustical parameters of liver tissue, a 5 MHz studie. Ultrasound in Med. and Biol. 17(9): 879-891

A.F.W. van der Steen, M.H.M. Cuypers, J.M. Thijssen, G.P.J. Ebben, P.C.M. de Wilde (1992) Preparation techniques in acoustical and optical microscopy of biological tissues, a studie at 5 MHz and 1.2 GHz. in: H. Ermert, H.P. Harjes (eds.) Acoustical Imaging vol. 19: 529-533 Plenum Press New York

A.F.W. van der Steen, J.M.Thijssen, G.P.J. Ebben, P.C.M. de Wilde (1992) Effects of tissue processing techniques in acoustical (1.2 GHz) and light microscopy. Histochemistry 97: 195-199

A. Goedegebure, A F.W. van der Steen, J.M. Thijssen (1992) In Vitro classification of gall stones by quantitative echography. Ultrasound in Med. & Biol. 18(6/7): 553-568

A.F.W. van der Steen, J.M. Thijssen, J.A.W.M. van der Laak, P.C.M. de Wilde, G.P.J Ebben (1993) Quantitative correlation of acoustical and light microcopy. International Conference on "Acoustical Sensing and Imaging" IEE, London, in press

A F W. van der Steen, J.M. Thijssen, J.A.W.M. van der Laak, G.P.J. Ebben, P.C.M. de Wilde (1993) A new method for correlation of acoustical spectroscopic microscopy (30 MHz) and light microscopy. J. Microscopy, in press

A.F.W van der Steen, J.M. Thijssen, G.P.J. Ebben, J.A.W.M. van der Laak, P.C.M. de Wilde (1993) Correlation of histology and acoustical parameters of liver tissue on a microcopic scale. Ultrasound in Med. & Biol., in press

C.L. de Korte, A.F.W. van der Steen, J.M. Thijssen (1993) Acoustic velocity and attenuation of eye tissues at 20 MHz. Ultrasound in Med & Biol., in press

A.F.W. van der Steen, C.L. de Korte, J.M. Thijssen (1993) Acoustic spectography of the porcine eye lens. (submitted for publication)

C.L. de Korte, A.F.W. van der Steen, J.M. Thijssen, J.J. Duindam, C. Otto, G.J. Puppels (1994) Relation between local acoustic parameters and protein distribution in human and porcine eye lenses. (submitted for publication)

ABSTRACTS

A.F.W. van der Steen, H. Rijsterborgh, F. Mastik, C.T. Lancée, W.M. van Hoorn, N. Bom (1989) The influence of attenuation on measurements of ultrasonic myocardial integrated backscatter during cardiac cycle (an in vitro study). 8th European Workshop on Ultrasonic Tissue characterization and Echographic Imaging: 11

A.F.W. van der Steen, M H.M. Cuypers, J.M. Thijssen, P.C.M. de Wilde, P. Wesseling, D.J. Ruiter (1989) Akoestische microscopie van neoplasma's. Klinische Fysica 1989/4: 209

A.F.W. van der Steen, M.H.M. Cuypers, J.M. Thijssen, P.C.M. de Wilde, G.P.J. Ebben, D.J. Ruiter (1990) De invloed van prepareermethoden op akoestische eigenschappen van leverweefsel. Klinische Fysica 1990/4: 175-176

A.F.W. van der Steen, M.H.M. Cuypers, J.M. Thijssen, P.C.M. de Wilde, G.P.J. Ebben (1991) Akoestische microscopie van Melanomen. Klinische Fysica 1991/4: 189

A.F.W. van der Steen, M.H.M. Cuypers, J.M. Thijssen, G.P.J. Ebben, P.C.M. de Wilde (1991) Preparation techniques in acoustical and optical microscopy of biological tissues, a studie at 5 MHz and 1.2 GHz. 19th symposium on Acoustical Imaging MB 5.5

A.F.W. van der Steen, M.H.M. Cuypers, J.M. Thijssen, G.P.J. Ebben, P.C.M. de Wilde (1991) The influence of preparation of biological tissues in acoustical microscopy, studies at 5 MHz and at 1.2 GHz. 1991 IEEE Ultrasonics symposium: 158

A.F.W. van der Steen, M.H.M. Cuypers, J.M. Thijssen, G.P.J. Ebben, P.C.M. de Wilde (1991) Akoestische microscopie van biologische weefsels. Ultrasonoor Bulletin 1991/1: 16-17

J.M. Thijssen, A.F.W. van der Steen, M.H.M. Cuypers, P.C.M. de Wilde (1991) Acoustic Microscopy of neoplasms. Int. Ophthalmol. 15 supplement: 18

J.M. Thijssen, A.F.W. van der Steen, M.H.M. Cuypers, P.C.M. de Wilde (1991) Akoestische microscopie van neoplasma's. Ned. Tijdschr. Geneeskd: 135

A.F.W. van der Steen, M.H.M. Cuypers, J.M. Thijssen, P.C.M. de Wilde, G.P.J. Ebben (1992) Akoestische microscopie van oogtumoren. NOG-BOG-101 jan. 1992

A. Goedegebure, A.F.W. van der Steen, J.M. Thijssen (1992) In Vitro classification of gall stones by quantitative echography. 9th European Workshop on Ultrasonic Tissue characterization and Echographic Imaging. Ultrasonoor Bulletin special issue: 10

A.F.W. van der Steen, M.H.M. Cuypers, J.M. Thijssen, P.C.M de Wilde, G.P.J. Ebben (1992) Correlation of acoustical and light microscopy. 9th European Workshop on Ultrasonic Tissue characterization and Echographic Imaging. Ultrasonoor Bulletin special issue: 11

A.F.W. van der Steen, M.H.M. Cuypers, J.M. Thijssen, J.A.W.M van der Laak, P.C M de Wilde, G.P.J. Ebben (1992) Correlatie van akoestische en lichtmicroscopie. Klinische Fysica 1992/4: 196

A F.W van der Steen, C.L. de Korte, J.M. Thijssen (1993) De akoestische eigenschappen van de ooglens. NOG-BOG-IOI jan. 1993

A.F.W. van der Steen, J.M. Thijssen, J.A.W.M. van der Laak, P.C.M. de Wilde, G.P.J. Ebben (1993) Quantitative correlation of acoustical and light microcopy. International Conference on "Acoustical Sensing and Imaging" IEE, London

A.F.W van der Steen, C.L. de Korte, J.M. Thijssen (1993) Acoustic spectography of the porcine eye lens. 18th International Symposium on Ultrasonic Imaging and Tissue Characterization, Washington, Ultrasonic Imaging 15: 160

J.M Thijssen, A.F.W. van der Steen, C.L. de Korte, A.F. Deutman (1993) Ultrasonic characterization of the eye lens. First Annual Meeting of the European Community Ophthalmic Research Association: 30

A.F.W van der Steen (1993) Akoestische biomicroscopie. Ultrasonoor Bulletin 1993/2: 34-35

A.F.W. van der Steen, J.M. Thijssen, J.A.W.M. van der Laak, P.C.M. de Wilde, G.P.J. Ebben (1994) Quantitative correlation of acoustical and light microcopy features of liver tissue. 8th Congress of the European Federation of Societies for Ultrasound in Medicine and Biology, Innsbruck, European Journal of Ultrasound vol.1, Suppl. 1: S45

A.F.W. van der Steen, C.L. de Korte, J.M. Thijssen (1994) Spectral acoustical properties of human and porcine eye lenses. 8th Congress of the European Federation of Societies for Ultrasound in Medicine and Biology, Innsbruck, European Journal of Ultrasound vol.1, Suppl. 1: S55

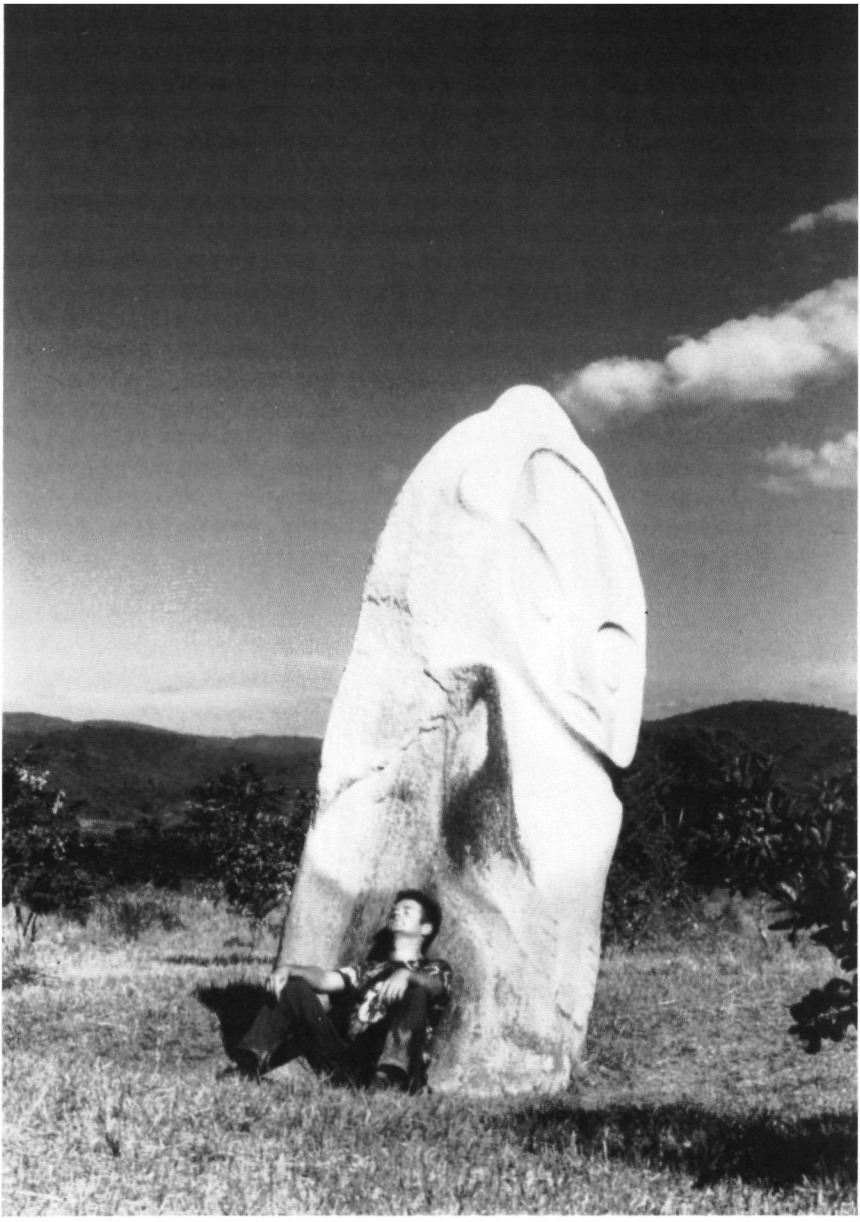

'Ziezoo'

(Nescio. De uitvreter. p.41)

Illustration at page 157 the author is taking a rest during an expedition to the Bada valley, central Sulawesi, Indonesia The easiest way to reach this valley is by Cessna, a five passenger aircraft that is operated by the Missionary Aviation Fellowship (MAF) Fourteen megalithic statues are scattered over this valley They represent either humans or animals, male or female, standing or lying Nothing is known about their origin or age The statue on the picture is called "Palindo" which is Poso language for "Entertainer"

photography Wilhelm Huber, september 1993

Stellingen

behorende bij het proefschrift

Acoustic biomicroscopy

door

Ton van der Steen

1. *In vitro* ultrageluidonderzoek is een essentieel gereedschap voor de modelvorming ten behoeve van weefselidentificatie met ultrageluid *in vivo*.
(dit proefschrift)

2. De paraffinecyclus dient te allen tijde vermeden te worden bij het prepareren van weefsels ten behoeve van akoestische microscopie. Het snijden van materiaal in diepgevroren toestand is wel goed bruikbaar.
(dit proefschrift)

3. Het is mogelijk op grond van *in vivo* meetbare akoestische parameters onderscheid te maken tussen vergruisbare en niet vergruisbare galstenen.
(dit proefschrift)

4. De variatie in ultrageluidverzwakking gedurende de hartcyclus levert een essentiële bijdrage aan de gemeten variatie in "integrated backscatter" uit het myocardium.
(dit proefschrift)

5. De akoestische eigenschappen van de ooglens variëren systematisch met de locatie in de lens.
(dit proefschrift)

6. Om op medisch-technologisch gebied tot hoogstaande resultaten te komen is multidisciplinair onderzoek een noodzaak. Goede communicatie is hierbij aanzienlijk belangrijker dan een hoog niveau aan vakkennis bij alle participanten.

7. Gezien de extreem geringe overeenkomst tussen promotie in het bedrijfsleven en op de universiteit zou het beter zijn als één van de twee organisaties een andere term zou gaan gebruiken. Vanwege de ver doorgevoerde traditionele identiteit binnen de universiteit (promotor, co-promotor, promotiecommissie, promotieplechtigheid, etc.) dient de verandering bij voorkeur in het bedrijfsleven plaats te vinden.

8. Van de maan af gezien zijn wij allen even groot.
(Multatuli)

9. Het is voor de mens onmogelijk de werking van zijn eigen hersenen volledig te begrijpen.

10. Het is geenszins bewezen dat hunebedden als graven gebouwd zijn.
("Eerste Nederlandse hunebeddengids" en "Het mysterie van de hunebedden" door Frits Bom, "Signalen uit het stenen tijdperk" door Erich von Däniken)

11. Ontwikkelingshulp waarbij niet geredeneerd wordt vanuit de cultuur en behoefte van het betreffende volk dient achterwege gelaten te worden.

12. Een goede eerste stap in de richting van het beëindigen van racisme is niet te stellen dat alle rassen gelijk zijn, maar te erkennen dat er culturele verschillen tussen volkeren zijn en zullen blijven. Slechts hierna kan de samenleving zijn culturen en rassen leren accepteren en waarderen.

13. De laatste stelling bij een proefschrift kan vaak beter weggelaten worden.

14.

Nijmegen, 4 februari 1994

ISBN 90 9006879 I